

Martin Roll Lied

Design of Mooring Systems in Extreme Sea States with focus on Viscous Drift Force Modelling

June 2019

NTNU
Norwegian University of
Science and Technology
Faculty of Engineering
Department of Marine Technology

Martin Roll Lied



Norwegian University of
Science and Technology

Design of Mooring Systems in Extreme Sea States with focus on Viscous Drift Force Modelling

Martin Roll Lied

Marine Technology

Submission date: June 2019

Supervisor: Kjell Larsen

Norwegian University of Science and Technology
Department of Marine Technology



MASTER THESIS SPRING 2019

for

Stud. tech. Martin Roll Lied

Design of Mooring Systems in Extreme Sea States with focus on Viscous Drift Force Modelling

Analyse av forankringssystemer i ekstreme sjøtilstander – fokus på modeller for viskøse driftkrefter

Background

The purpose of the mooring system is to keep a floating vessel safely at a required position. It normally consists of 8-16 mooring lines of heavy chain, steel wire ropes and/or synthetic polyester ropes connected to a seabed anchor.

During the past years, the requirements to the mooring and station keeping systems of mobile and permanent units have become more complex;

- The industry is moving into new frontiers (ultra-deep water down to 3000m depth and into arctic areas).
- There are more operations adjacent to other installations (flotel operations and tender support vessel operations).
- The new mobile units are becoming larger and many units are at the end of their lifetime.
- There are too many anchor line failures.

In addition, mooring failure rate is unacceptably high. Some incidents have been multiple line failures, leading to vessel drifting. The investigations show a variety of direct causes covering both inaccurate design, bad quality on mooring line components and lack of personnel competence related to operation of the system. A design issue is that today's analysis methods usually neglects the excitation related to viscous drift forces. This is considered a major shortcoming for the mooring design of slender semisubmersible platforms.

In spite of the advances in the numerical procedures for mooring analysis, there has been a number of incidents with mooring line failures over the recent years. For some of these incidents the mooring lines were overloaded during storms. This has uncovered a need to improve methods, procedures and standard industry practice in design prediction of nonlinear wave loadings in high and steep seas. Since 2015, the industry has started initiatives with the objective of improving design practice, one important initiative is the EXWAVE joint industry project aiming at proposing design guidelines. Phase II of that initiative was kicked-off in January 2019.

The overall objective of this master thesis is to increase the competence on extreme weather loads and load effects in mooring systems of semisubmersible platforms. Particular focus to be given on the hydrodynamic loading and the wave drift forces in extreme wave conditions.

Scope of Work

- 1) Review relevant literature and describe briefly mooring and station keeping concepts for mobile and permanent units. Focus on station keeping principles and main hardware components. Describe the selected semi (CAT D) in terms of main particulars and hydrodynamic properties.
- 2) Describe the design limit states for mooring systems with corresponding acceptance criteria outlined in rules and regulations. Compare design criteria for mobile and permanent units. Describe the time-domain analysis methods for mooring systems and how extreme vessel motions and line tension can be estimated. A special assessment and description of models for viscous wave drift loads in extreme sea states shall be included. The assessment shall cover both empirical formulas and theoretical models. In particular, findings from the EXWAVE project (phase I) and relevant papers shall be reported.
- 3) Based on the selected semi CAT D unit, the mooring system shall be determined based on compliance with the DNVGL regulation and an assumed location at the Heidrun field. A relevant empirical correction formula for viscous drift force to be included. The design shall be based on a time-domain analysis and the established model in SIMA/SIMO/RIFLEX.
- 4) Parameter variation and sensitivity analysis. The load effects in the mooring system shall be assessed due to a selected parameter variation and a variation of load models for viscous drift. Both empirical correction formulas and definition of a “slender elements” in SIMO shall be included. Extent to be agreed with the supervisor.
- 5) Conclusions and recommendations for further work.

General information

All necessary input data for the simulation case is assumed to be provided by Equinor.

The work scope may prove to be larger than initially anticipated. Subject to approval from the supervisor, topics may be reduced in extent.

In the project the candidate shall present his personal contribution to the resolution of problems within the scope of work.

Theories and conclusions should be based on mathematical derivations and/or logic reasoning identifying the various steps in the deduction.

The candidate should utilise the existing possibilities for obtaining relevant literature.

Report/Delivery

The thesis report should be organised in a rational manner to give a clear exposition of results, assessments, and conclusions. The text should be brief and to the point, with a clear language. Telegraphic language should be avoided.

The report shall be written in English and edited as a research report including literature survey, description of relevant mathematical models together with numerical simulation results, discussion, conclusions and proposal for further work. List of symbols and acronyms,

references and (optional) appendices shall also be included. All figures, tables and equations shall be numerated.

The original contribution of the candidate and material taken from other sources shall be clearly defined. Work from other sources shall be properly referenced using an acknowledged referencing system.

The report shall be submitted electronically (pdf) in Inspira, as specified by the department of Marine Technology. In addition, an electronic copy (pdf) to be sent to the supervisors.

Ownership

NTNU has according to the present rules the ownership of the project results. Any use of the project results has to be approved by NTNU (or external partner when this applies). The department has the right to use the results as if the work was carried out by a NTNU employee, if nothing else has been agreed in advance.

Thesis supervisor:

Prof. II Kjell Larsen, NTNU/Equinor

Deadline: June 11, 2019

Trondheim, January 29th, 2019

Kjell Larsen (sign.)

Martin Roll Lied (sign.)

Acknowledgement

This master thesis concludes the degree of Master of Science in Marine Hydrodynamics, a specialization in Marine Technology at the Norwegian University of Science and Technology in Trondheim. The thesis is conducted during the spring 2019 and is weighted 30 ECTS.

I would like to thank my supervisor, Professor II Kjell Larsen, for taking great interest in supervising me throughout this year. Your interest within the subject has inspired me, and our discussions with practical examples are invaluable. With weekly meetings and always being available when needed, your guidance has been substantial for keeping me in the right direction. Equinor is acknowledged through Kjell Larsen for providing input files for the model, relevant technical reports related to the model and relevant papers and technical reports related to the topic.

A special thanks is also given to PhD candidate Carlos Eduardo Silva de Souza for guidance in the SIMA software. His help with any questions regarding the software and analysis of the results obtained during this semester, has been greatly appreciated.

Furthermore, I would like to thank my fellow students and especially the students from our office, C1.084. With valuable discussions and countless hours in the office, you have made this year memorable.

Abstract

A theoretical background is presented within the topic of mooring of semi-submersibles. Hardware components and different types of station keeping systems are depicted and described. Regulations and standards related to position mooring is highlighted and utilized in design of a mooring system. The design process is thoroughly described in different steps related to the characteristics of the system. Design of a mooring system is a time-consuming process and countless hours have been spent in the SIMA software to establish a mooring system for further analysis.

Furthermore, three different load models for calculation of maximum axial force in mooring lines have been investigated. Two of the methods are based on wave drift forces from Newman's approximation, by utilizing quadratic current coefficients as input for calculation of the current forces. The last method calculates the viscous loads on the semi-submersible through the drag term in Morison's equation.

Eleven different cases have been analysed in the software SIMA. The 400 first seconds of the simulations for both the motions and forces are omitted as a part of the post-processing. The omitted section of the simulation is due to the initial conditions do not represent the desired sea state. According to the definitions given by DNVGL-OS-E301, all simulations performed are based on ultimate limit state with respect to 100 year significant wave height and wind speed, and 10 year current speed. In addition, all simulations are conducted in a collinear environment.

First, a comparison of the motions for all eleven cases is highlighted. The comparison is as the power spectrum of the sway motions for all the eleven cases, based on 15 wave seeds for each of the simulated case. For some of the cases only 14 seeds were completed. Furthermore, one case with slender elements and one case without slender elements is focused on to determine the effect of using slender elements.

All the eleven cases have significant energy peaks for both the low frequency and wave frequency sway motion. With one peak close to the period of the wave spectrum, and one significant peak in the low frequency region. The distinction for the frequencies of the sway motions are clear between the two contributions.

The sensitivity of drag coefficients between the different cases conducted are shown to give small variations in the contribution to most probable tension in the mooring line. In addition, the power spectrum of low frequency forces shows a small variation in magnitude between the different cases, where the viscous force contribution is not shown to be significant.

The deviation in motions for the different cases are not inconsistent, but for forces the obtained results are not coinciding with other obtained results. However, as the forces do not show the correlation to the obtained motions there is reason to doubt the obtained results for the motions as well as the forces that are calculated. The reason is believed to be due to a fault in how the current forces are calculated.

Sammendrag

En teoretisk bakgrunn er presentert innenfor temaet forankring av halvt-nedsenkbare plattformer. Forankringskomponenter og forskjellige typer forankringssystemer er avbildet og beskrevet. Regelverk og standarder knyttet til forankring er fokusert på og benyttet i utformingen av et fortankringssystem. Utformingsprosessen er grundig beskrevet i forskjellige trinn relatert til forankringssystemets egenskaper. Design av et forankringssystem er en tidkrevende prosess, og mange timer har blitt brukt i SIMA-programvaren for å etablere et forankringssystem brukt til videre analyse.

Videre er tre forskjellige lastmodeller for beregning av maksimal aksialkraft i forankringslinjer blitt undersøkt. To av metodene er basert på bølgedriftskrefter fra Newmans tilnærming, ved å benytte kvadratiske strømkoefisienter som bakgrunn for beregning av strømkrefter. Den siste metoden beregner de viskøse kreftene på halvt-nedsenkbare plattformer ved å bruke formuleringen av dragkrefter i Morison's ligning.

Elleve forskjellige tilfeller har blitt analysert i programvaren SIMA. De 400 første sekundene av simuleringene for både bevegelser og krefter blir utelatt som en del av etterbehandlingen. Den utelatte delen av simuleringen skyldes at de opprinnelige forholdene ikke representerer den ønskede sjøtilstanden. I henhold til regelverket i DNVGL-OS-E301, utføres alle simuleringer basert på 100 års signifikant bølgehøyde og vindhastighet og 10 års strømhastighet. I tillegg utføres alle simuleringer med kollinære bølge-, strøm- og vindbidrag.

Først er en sammenligning av bevegelsene for alle elleve tilfeller fremhevet. Sammenligning av energispekteret for svaibevegelser er gjennomført for alle de elleve tilfellene, basert på 15 frøtall for bølgene, for hvert av de simulerte tilfellene. For noen tilfeller ble bare 14 frøtall for bølgene fullført. Videre er et tilfelle med bruk av Morison's dragkraftbidrag og ett tilfelle ved bruk av strømkoefisienter fokusert på i forsøk på å bestemme effekten av å bruke Morison's dragkraftbidrag.

Alle de elleve tilfellene har betydelige energitopper for både lavfrekvente og bølgefrekvente svaibevegelser. Med en topp i nærheten av bølgeperioden i bølgespekteret, og en signifikant topp i lavfrekvensområdet. Forskjellen mellom frekvensene av svaibevisene er tydelig mellom de to bidragene.

Dragkoefisientenes sensitivitet ved to forskjellige tilfeller er utført. Det er vist å gi små variasjoner i bidraget til mest sannsynlige maksimale spenninger i forankringslinjen. I tillegg viser energispekteret for lavfrekvente krefter liten variasjon i størrelsesorden mellom de forskjellige tilfellene, hvor det viskøse kraftbidraget ikke er vist å være signifikant.

Avviket i bevegelser for de forskjellige tilfellene er ikke inkonsekvent, men for krefter er de oppnådde resultatene ikke sammenfallende med andre oppnådde resultater. Siden kreftene ikke viser forventet sammenheng til de oppnådde bevegelsene, er det grunn til å tvile på de oppnådde resultatene for bevegelsene, så vel som beregnede krefter. Grunnen antas å skyldes en feil i hvordan strømkrefter beregnes.

Contents

Acknowledgement	iv
Abstract	vi
Sammendrag	ix
1 Introduction	1
1.1 Theoretical background	1
1.2 Objective and motivation	3
2 Mooring systems	5
2.1 Hardware components	5
2.1.1 Chain	5
2.1.2 Synthetic fibre rope	6
2.1.3 Steel wire rope	7
2.1.4 Connecting links	7
2.1.5 Anchor types	8
2.2 Mooring and station keeping systems	11
3 Limit states	15
3.1 Design limit states	15
3.2 Overload check and design criteria	16
4 Theory	21
4.1 Rigid body motions	21
4.2 Equation of motion	23
4.2.1 Excitation forces	24
4.3 Inertia	27
4.4 Damping	28
4.5 Stiffness	30
4.6 Line characteristics and restoring forces	32
4.7 Analysis methods	33
4.7.1 De-coupled approach	35
4.7.2 Coupled approach	35
4.8 Morison's equation	36
4.9 Viscous drift forces	37
4.10 EXWAVE JIP	38

4.11	Load models	43
4.11.1	Potential wave drift coeff	43
4.11.2	Corrected wave drift coeff	43
4.11.3	Slender element method	44
4.11.4	Comparison and difference between the methods	45
5	Extreme value distribution	47
6	System description	49
6.1	Heidrun metocean design basis	49
6.2	Waves	50
6.3	Wind	51
6.4	The semi submersible	51
6.5	Design of the mooring system	53
7	Numerical simulation	61
7.1	Potential wave drift coefficients	62
7.2	Corrected wave drift coefficients	62
7.3	Slender modelling	63
7.3.1	Selecting drag coefficients	66
7.3.2	Base case C_D	67
7.3.3	EXWAVE JIP C_D	68
7.3.4	Low C_D	68
7.3.5	High C_D	68
7.3.6	One strip	69
7.3.7	No current	69
7.3.8	Mean wave elevation	69
7.3.9	No current and mean wave elevation	69
7.3.10	No slender	69
8	Results and discussion	71
8.1	Motions	72
8.2	Forces	79
9	Further work	87
10	Conclusion	89
	Bibliography	I
	Appendices	V
A	Properties of the Semi-submersible	V
B	Iterative design process	VI
C	Decay tests	VII
D	Quadratic current coefficients	IX
E	Wave drift coefficients	X
F	wave_drift_coeff.m	XI

List of Figures

2.1	Example of stud and studless chain together with design parameters for Ramnäs chain	6
2.2	Example of composition for synthetic fibre rope	6
2.3	Examples of steel wire ropes	7
2.4	Exemplification of transition components	7
2.5	Anchor Shackle and RF Connector	8
2.6	Illustration of drag and torpedo anchors	9
2.7	Illustration of anchor types	10
2.8	Alternative installation method for VLA	10
2.9	Examples of mooring systems	12
2.10	Turret mooring system	13
2.11	Illustration of dynamic positioning	14
3.1	T_{MPM} multiplied with safety factor $\leq MBS$	17
4.1	Coordinate system and rigid-body modes	22
4.2	Dynamic load factor	23
4.3	Mean wind velocity and wind gusts	26
4.4	Illustration of wave drift damping	29
4.5	Geometric and elastic stiffness illustrated in series	30
4.6	Taut-mooring line	30
4.7	Catenary mooring line	31
4.8	Forces acting on a mooring line element	32
4.9	Definition of the line characteristic	32
4.10	Horizontal restoring force	33
4.11	Separated and coupled analysis	35
4.12	Classification of wave forces	36
4.13	Illustration of cross-flow and wave-current interaction	38
4.14	Correction factor for viscous drift force from DNVGL-OS-E301 ed. July 2018	42
4.15	Illustration of how the drag forces are calculated with slender modelling	45
5.1	Measured axial force for an arbitrary time series, illustrates how to find global maxima for the time series	47
6.1	Heading direction of semi-submersible	50
6.2	Contour plot, Hs-Tp plane	51
6.3	RAO for all six DOF for 45 degrees heading	52

6.4	System overview	54
6.5	Decay for surge direction	57
6.6	Decay for sway direction	58
6.7	Pullout test	58
6.8	Sensitivity of line length	60
6.9	Convergence of mean standard deviation based on number of simulations N	60
7.1	Wave drift coefficients surge 45 deg	62
7.2	Wave drift coefficients sway 45 deg	63
7.3	Slender elements and modelling of the elements in SIMA, (a) geometry definition, (b) slender elements	63
7.4	Drag coefficients, rectangle with rounded corners	64
7.5	Determination of drag coefficients based on Appendix E, geometry 4 in DNVGL-RP-C205	65
7.6	Drag coefficients as a function of KC numbers	66
8.1	Realization of translational motions for case with corrected wave drift coefficients	72
8.2	Realization of translational motions for base case C_D	72
8.3	Power spectrum of sway motions for all cases	73
8.4	Realization of heave motions for cases with and without slender	74
8.5	Zoomed realization of heave motions	75
8.6	Statistics for LF sway motions, all cases	76
8.7	Statistics for LF surge motions, all cases	77
8.8	Selection of surge motion for arbitrary base case C_D realization	78
8.9	Power spectrum of surge motions for all cases	79
8.10	Realization of corrected wave drift coeff. axial force	80
8.11	Realization of base case C_D axial force	80
8.12	Gumbel distribution of T_{MPM}	82
8.13	Power spectrum of the low frequency force contribution	83
8.14	Power spectrum of the low frequency force contribution	85

List of Tables

2.1	Time dependent design criteria	11
3.1	Requirements to safety factors for permanent units	17
3.2	Requirements to safety factors for mobile units	17
3.3	Partial safety factors for ULS	18
3.4	Partial safety factors for ALS	18
4.1	Natural oscillation periods for semi-submersibles	24
4.2	Contributions from the different forces	24
4.3	Overview of mooring line failures between 2010-2013 on the Norwegian Continental Shelf	39
6.1	Principle parameters from Heidrun metocean design basis	49
6.2	Principle dimensions for the semi-submersible	52
6.3	Input parameters for 95-105mm	55
6.4	Results for 95-105mm	55
6.5	ULS check 95mm R5 studless chain	55
6.6	ALS check 95mm R5 studless chain	56
6.7	Base design, 95mm studless chain	56
6.8	Natural periods from decay	57
7.1	Slender coordinates	64
7.2	Slender base case C_D	67
7.3	Drag coefficients from EXWAVE jip	68
7.4	Drag coefficients for low C_D	68
7.5	Drag coefficients for high C_D	68
8.1	Results of design load for all simulations	81

Nomenclature

Abbreviations

<i>ALS</i>	Accidental Limit State
<i>CDF</i>	Cumulative Distribution Function
<i>DLF</i>	Dynamic Load Factor
<i>DNVGL</i>	Det Norske Veritas Germanischer Lloyd
<i>DOF</i>	Degree Of Freedom
<i>DP</i>	Dynamic Position
<i>FEM</i>	Finite Element Method
<i>FLS</i>	Fatigue Limit State
<i>HF</i>	High Frequency
<i>ISO</i>	International Standard Organization
<i>JIP</i>	Joint Industry Project
<i>LF</i>	Low Frequency
<i>MBS</i>	Minimum Breaking Strength
<i>MODU</i>	Mobile Drilling Unit
<i>NCS</i>	Norwegian Continental Shelf
<i>NPD</i>	Norwegian Petroleum Directorate
<i>PDF</i>	Prabability Distribution Function
<i>QTF</i>	Quadratic Transfer Function
<i>RAO</i>	Response Amplitude Operator

<i>SIMA</i>	Simulation and Engineering Analysis of Marine Operations and Floating Systems
<i>SIMO</i>	Simulation of Marine Operations
<i>StD</i>	Standard Deviation
T_{MPM}	Most Probable Maximum Tension
<i>ULS</i>	Ultimate Limit State
<i>WF</i>	Wave Frequency

Symbols

C_D	Drag coefficient
H_s	Significant wave height
<i>Hz</i>	Hertz
<i>KC</i>	Keulegan-Carpenter number
<i>Rn</i>	Reynolds number
S_f	Safety factor
T_p	Wave period
T_{env}	Environmental load
T_{pret}	Pre-tension load
Te	Tonne equivalent
Δ	Roughness number
β	Frequency ratio, heading angle
γ_F	Fatigue safety factor
γ_{SIMO}	Safety factor SIMO
γ_{env}	Environmental safety factor
γ_{pret}	Safety factor pre-tension
λ	Wave length
ξ	Damping ratio

ζ_a	Surface elevation
$^\circ$	Degrees
d_F	Fatigue damage ratio
d_c	Fatigue loads
d_i	Fatigue damage

Chapter 1

Introduction

Mooring systems are designed to maintain a stable position of a permanent or mobile floating unit in an oil field. The permanent or mobile unit is either connected to the seabed with drill pipe or risers, or in immediate vicinity to a unit which is connected to the seabed. Because of these restrictions, the motions of the unit must be controlled.

During the past years the requirements to mooring of permanent and mobile floating units have become more complex as a result of fatal accidents on the Norwegian Continental Shelf, NCS. In combination with more frequent extreme weather and associated extreme sea states, the industry has seen the necessity to change regulations regarding design of mooring systems.

In 2015, the EXWAVE joint industry project was initiated with the objective to improve methods and standard industry practice in prediction of extreme mooring line loads (DNV GL, 2017b). Phase II of the initiative was kicked-off in January 2019, and a recap of phase I with respect to drift forces is included in the thesis.

1.1 Theoretical background

The problem of potential drift has been extensively studied since the beginning of 1980's. Two different approaches for computation of mean and slowly varying potential drift force was established by Marou, Newman and Pinkster (Maruo, 1960)(Newman, 1967)(Pinkster, 1980). Marou and Newman used the principle of conservation of momentum surrounding the body, while Pinksters method directly integrates the pressure over the wetted body surface to solve potential drift cases. Both methods can give reasonable results as long as viscous forces are less dominant. For cases and structures where viscous forces dominate, Burns presented a study calculating viscous drift of a tension leg platform (Burns, 1983). The quadratic transfer function implemented in Morison's equation, presented by Burns, is found to be valid for current velocities larger than the maximum value of the water particle velocity. This article will be further discussed in Section 4.9.

Ferretti and Berta studied mean drift force and viscous drift force on a vertical cylinder with the use of Newman's formulation and thereof provided numerical solutions (Ferretti, C. Berta, M., 1980). The results were compared to results obtained by Morison's formulation (Morison *et al*, 1950). The study investigated the effect of current superimposed on the waves.

In 1984 a comparison between potential and viscous calculations regarding steady drift force on a vertical cylinder was conducted by (Chakrabarti, 1984). The effect of viscous drift forces was found to be at least a third-order term while potential drift force was found to be of second-order. Although the study investigated fixed cylinders, semi-submersibles experience similar challenges.

Over the last four decades the oil and gas industry on NCS has expanded into new territories. This has led to extra focus on the aforementioned topics towards oil and gas production. Norwegian researches have done a lot of studies within this field, which will be reflected by the selected studies for further outlining.

In 1997, Stansberg studied linear and non-linear system identification in model testing by investigating the quadratic transfer function (QTF) and its impact on the reconstructed response when compared to experimental tests. He identified very good correspondence for the quadratic transfer function and implemented the QTF in a proposed numerical model (Stansberg, 1997).

A related study, presented in 2001, investigated the interpretation and use of data from tests in irregular waves. The study was limited to irregular waves, which is normally used for verification of ocean structures. The deviation for the model when compared with experimental results, with respect to drift forces, damping and response of a moored semi-submersible was found to be 5-10% when current were not included. The conclusion was that data particular methods of data processing and interpretation are specially important when non-linear and complex processes in extreme sea states are investigated. For these cases, standard tools must be checked or calibrated to experiments and quadratic system analysis is shown to give realistic results (Stansberg, 2001).

Lie and Kaasen presented in 2008 basic models for slow-drift excitation and damping as a supplement to low-frequency potential loading. Their conclusions reinforce prior research within the field over the last two decades; viscous drag effects may have a large influence on the slow drift forces and response (Lie and Kaasen, 2008).

A study published in 2013 investigated wave drift forces and responses in currents. In addition, it included a brief review over studies conducted the past 20-25 years (Stansberg *et al.*, 2013). As outlined in the article, numerous studies on the topic have been completed. However, there has been little follow-up from the industry with respect to the results of the conducted studies. The conclusions encouraged to improve current engineering tools in order to predict the drift forces in a proper manner.

In the same period, between 2010 and 2013, there were a number of mooring line failures. This started a number of studies regarding these failures which made the industry aware of shortcomings in their models regarding maximum tension and associated motions (Kvitrud, 2014). A comprehensive description of recent studies and the proposed models on the topic will be further discussed in Section 4.9, after fundamental theory is clarified.

Literature explaining viscous drift forces is extensive, therefore this thesis has just covered a small part of the studies within the topic. Hopefully some of the main principles and challenges within the topic of viscous wave drift loads have been made clear from this review.

1.2 Objective and motivation

The overall objective of this master thesis is to increase the knowledge on extreme weather loads and load effects in mooring systems for semi-submersible platforms.

- Particular focus to be given on the hydrodynamic loading and viscous drift forces in extreme weather conditions.
- A mooring system is to be designed with catenary mooring and explained as a basis for further analysis.
- Different load models of the mooring system will be compared in order to evaluate their suitability with respect to the most probable maximum tension, T_{MPM} , in a mooring line and the corresponding motions of the semi-submersible.

The scope of work is formulated in the task included in the beginning of the thesis.

Chapter 2

Mooring systems

Mooring and station keeping systems for floating units are designed to keep the unit within a specific area. The mooring and station keeping systems have customized configurations dependent on the location and the surrounding environment. The components used in a mooring line vary from one mooring system to another, customized for each location. The mooring configuration gives the mooring systems certain attributes. A system typically consists of 8-16 mooring lines, with a combination of chain, synthetic fibre ropes and/or steel wire rope. In the following chapter hardware components and mooring and station keeping systems will be further elaborated and exemplified with illustrations. In addition some of the main parameters for the design of a mooring system will be described.

2.1 Hardware components

2.1.1 Chain

There are mainly two types of chain that are utilised for mooring lines. The types are studded chain illustrated to the left, and studless chain illustrated to the right in Figure 2.1. The properties of the chain used in this thesis are described in Ramnäs Bruk's product catalogue (Ramnäs Bruk, 2015). The dimension of the chain is defined by the diameter, D , as shown in Figure 2.1. Millimetre is used as the dimension for chain, and this will be evident in description of the mooring design later in this thesis. Studded chains are stronger and have better stability properties than studless chains, however studless chains may be used for permanent mooring to reduce the weight and cost of the total mooring system. Both chain types have high stiffness and good abrasion characteristics.

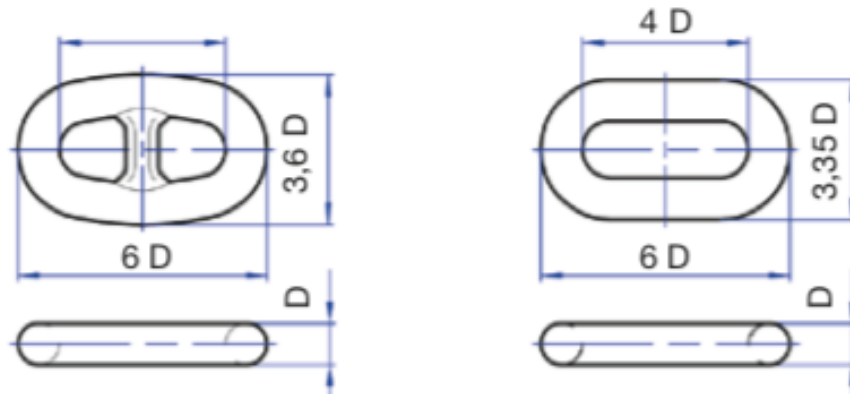


Figure 2.1: Example of stud and studless chain together with design parameters for Ramnäs chain (Ramnäs Bruk, 2015)

2.1.2 Synthetic fibre rope

Synthetic fibre ropes are a light and elastic alternative for mooring of marine structures. The weight of the synthetic fibre rope can often be negligible because of the weight of the rope and the buoyancy contribute almost equally. The low weight make the fibre ropes easy to handle, and can be the decisive factor when designing the mooring lines for a specific case.

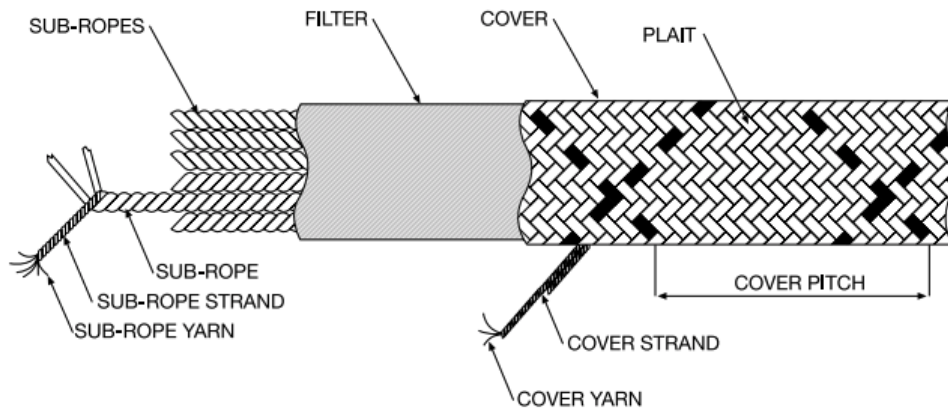


Figure 2.2: Example of composition for synthetic fibre rope (Bridon, 2013)

An example of the composition of the synthetic fibre rope is illustrated in Figure 2.2. Because of the low resistance to abrasion, synthetic fibre ropes are not allowed to touch the sea bed. Consequently, synthetic fibre ropes are often used single-handed in taut mooring, or as part of a catenary line with chain in the beginning and end of the mooring line.

2.1.3 Steel wire rope

The third widely used alternative for mooring of marine structures are the steel wire rope. Steel wire ropes can be designed as spiral strands, six-strands or multi strands as depicted to the left in Figure 2.3. To the right in the same figure, the estimated operating time is given for the different designs (Chakrabarti, 2005).

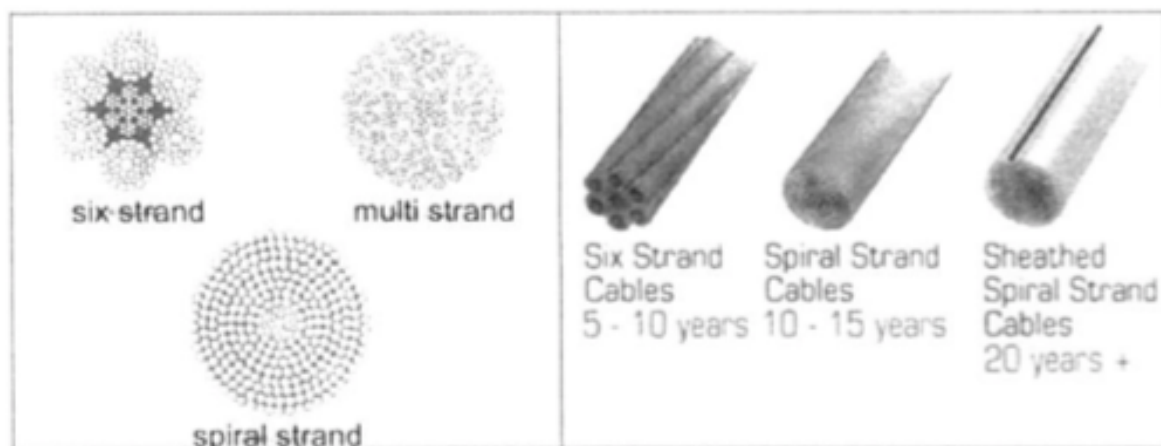


Figure 2.3: Examples of steel wire ropes (Chakrabarti, 2005)

The steel wire rope may be covered with a plastic sheath as shown to the far right in Figure 2.3, to give the steel wire better abrasion strength. Even though the abrasion resistance is improved with a plastic sheath around the strand, chain is often the preferred choice at the seabed when wire and chain are in the same mooring line configuration.

2.1.4 Connecting links

Mooring lines often consist of combinations between synthetic rope, steel wire rope and chain to give the mooring lines the desired characteristics for each individual case. Some of the transition components between the mooring line types and tools in the mooring line, are shown in Figure 2.4 and 2.5.



Figure 2.4: Exemplification of transition components (Ramnäs Bruk, 2015)

There are several types of shackles which can be used in a mooring line configuration based on the desired practical application. The RF connector for example, connects two pieces of mooring lines with terminations that have equal dimensions.

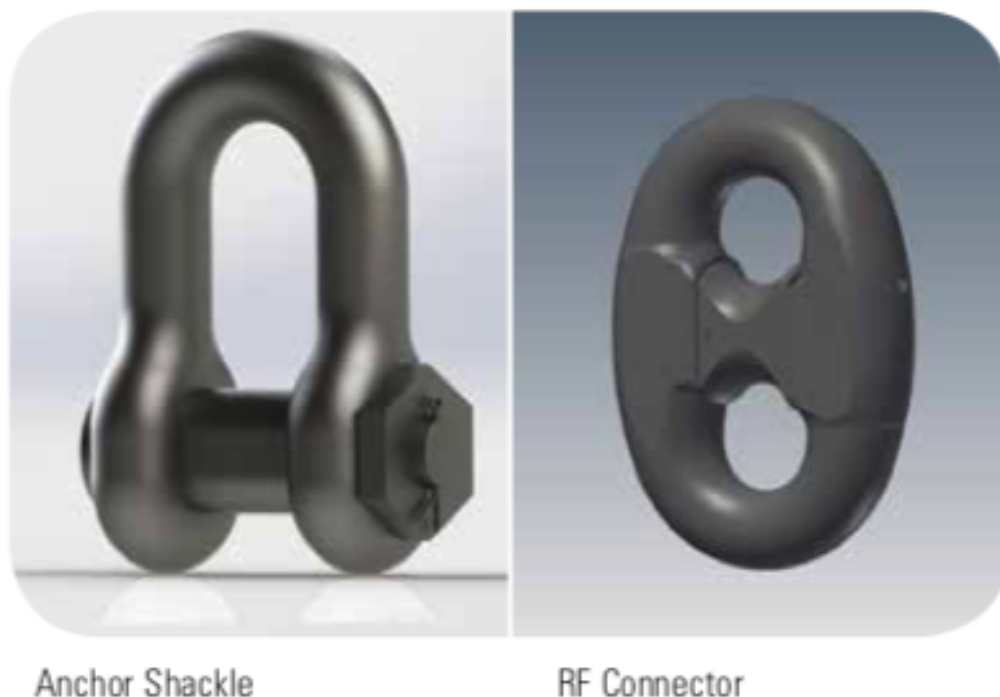


Figure 2.5: Anchor Shackle and RF Connector (Ramnäs Bruk, 2015)

2.1.5 Anchor types

At the end of a mooring line there is normally an anchor to safely keep the end of the mooring line fastened to the sea bottom. The most common anchor types are torpedo anchors, suction anchors, drag anchors and vertical loaded anchors. They will be described briefly in the following section.

Fluke anchor, also known as a drag anchor, is commonly used for mooring lines where the end of the mooring line lays in contact with the seabed. This is due to the anchor design has an adjustable pitch angle of the bottom component, called fluke area, which penetrates into the seabed. The fluke area is usually pitched depending on the type of soil. Consequently, the anchor does not withstand large vertical loads particularly well. An example of drag anchors are shown in Figure 2.6a.



(a) Drag anchors (Vryhof, 2017)



(b) Drop anchors (Bastos de Araujo et al., 2004)

Figure 2.6: Illustration of drag and torpedo anchors

Drop anchor, also known as a torpedo pile, is an anchoring type which can be used for mooring in deep water where other anchor types require a more complex installation. The definition of deep water is quite wide, but approximately above 1500 meters water depth is an adequate definition (Lavis, 2018). Torpedo piles are cost effective both in installation and fabrication, and leaves a small footprint in the soil when penetrating the seabed (Palm, 2016). The drop anchor is dimensioned to be exposed to horizontal forces. Possible drawbacks with this type of anchor is the chance for the pile to tilt in the soil which reduces its load capacity and the pile may miss its target when installing due to horizontal drift. The drop anchor is depicted in Figure 2.6b.

A suction anchor, shown in Figure 2.7a, has the shape as a closed cylinder which sucks down in the seabed. The way the suction action works is that a pump is attached to the anchor and pumps out the accumulated water while lowering the anchor. When the water is pumped out, vacuum is generated inside the cylinder and the anchor sucks into the soil. This anchor type is designed to withstand both horizontal and vertical loads. The fastening point is placed on the lower part of the construction to reduce eventual rotating motions of the anchor that can decrease its load properties. Suction piles are often used

for taut mooring where polyester fibre ropes are an essential part of the mooring line which requires an anchor that allows vertical loads. This is to ensure sufficient tension in the polyester fibre rope to prevent them from touching the seabed.



(a) Suction anchors (SPT Offshore, 2019)



(b) Vertical Loaded Anchor (Vryhof, 2017)

Figure 2.7: Illustration of anchor types

Vertical loaded anchor, as the name implies, is an anchor type approved for vertical loading. The anchor can be adjusted with a shear pin, showed in Figure 2.7b, to adjust for individual soil characteristics. Similar to the suction anchor, the vertical loaded anchors are a safe option for taut leg mooring of marine units. According to the producer of the anchor types illustrated in Figure 2.7b, the anchors are easy to install from one anchor handling vessel (Ruinen, 2004). One method for installation is illustrated in Figure 2.8.

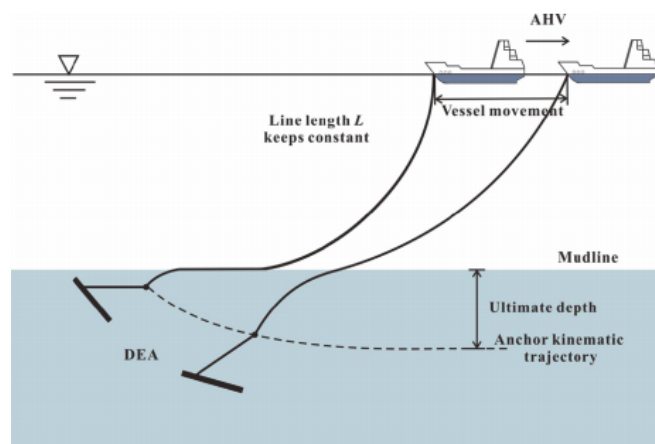


Figure 2.8: Alternative installation method for VLA (Wang et al., 2014)

2.2 Mooring and station keeping systems

The main requirement for the station keeping system of a semi-submersible is to limit the horizontal offset. This is to maintain a safe distance to other structures and maintain the integrity of connected risers and umbilicals. In order to limit the horizontal offset of the structure, it is important to understand how the forces and motions are related. Which will be further discussed in Chapter 4.

Today's challenging weather conditions and frequent storms, present several parameters when deciding on a station keeping system for a given case. Although developments within the marine industry have brought new station keeping concepts to the market, it is not clear which option is most suitable for the different cases. Some of the main factors that have to be considered when designing the mooring for a marine structure are:

1. Weight and elastic properties of the mooring lines will give different contribution to the stiffness, damping and the restoring force of the system.
2. The time perspective of the operation may give an indication of which alternative that is advantageous with respect to installation time for the anchors and system. The values presented in Table 2.1 are not definite time limits for each system.

	Long-term or permanent	Mobile mooring	Weather restricted mooring
Mooring period	> 5 years	< 5 years	months/weeks/days
Typical unit involved	Production vessel Storage unit	Drilling vessel Accommodation unit	Vessel involved in marine operations

Table 2.1: Time dependent design criteria (Larsen, 2018)

3. Water depth can be a critical factor when the mooring configuration shall be decided. E.g. the weight of chain at 3000 meters water depth will be both expensive and heavy.
4. The cost of different configurations is an essential parameter for the possible course of action.
5. The metocean prediction for the desired site is important with respect to wind, waves, current and directions for the aforementioned. Wave heights and wave periods are also predicted in the metocean design basis.
6. A hydrodynamic verification of the marine structure that the system is going to be designed with respect to. The hydrodynamic verification gives hydrostatics, natural periods, RAOs and mean wave drift forces for the structure. These will have significant influence in the design of the mooring system.

In the following the most common station keeping systems will be described.

Catenary mooring is a common station keeping system for mooring of both mobile and permanent units, numbered with 2 in Figure 2.9. Catenary mooring is a mooring system where most of the mooring line is chain or in combination with parts of steel wire rope. This method utilizes the weight of the mooring lines which impact the systems characteristics. Stiffness and damping are highly affected by the weight of the system, and will be further elaborated in Chapter 4. Catenary mooring works well by itself, but the system can be improved when it is combined with other components as thrusters or buoyancy elements. This depends on the assessment for each individual condition and will therefore not be further discussed. That said, a configuration with buoyancy elements is illustrated in Figure 2.9, numbered 3.

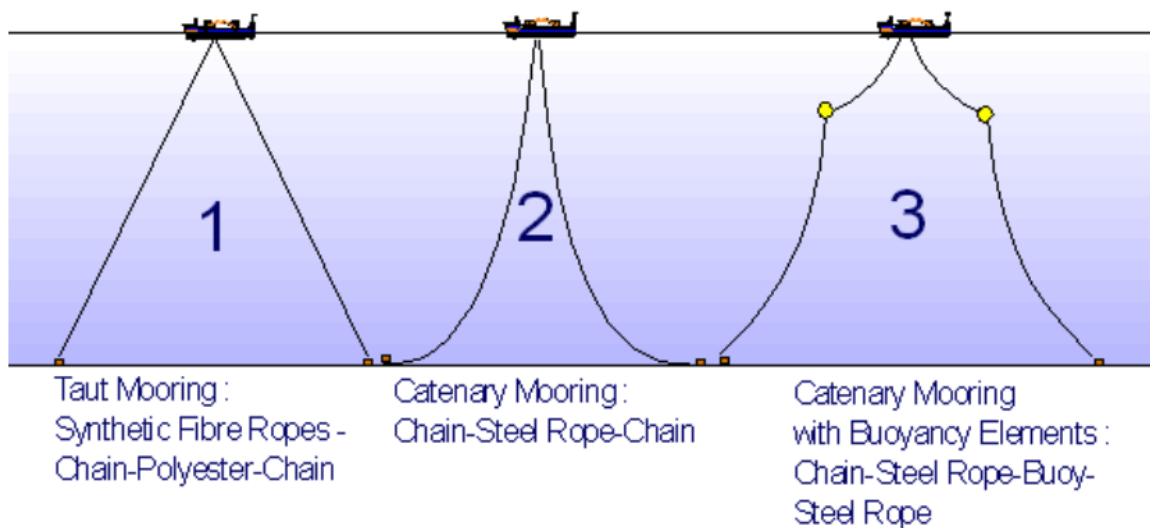


Figure 2.9: Examples of mooring systems (Larsen, 2018)

Taut mooring with synthetic fibre ropes are another mooring configuration which is used for both deep and shallow water. The system has low weight and high elasticity based on the properties of synthetic fibre ropes, and is a cheap alternative for mooring configuration. As seen from Figure 2.9, taut mooring requires less material than the catenary as the polyester ropes are tightened up. This makes the taut mooring a cheaper alternative than the catenary mooring.

Turret mooring is a station keeping principle with mooring lines gathered in either an internal turret, as illustrated in Figure 2.10, or an external turret. The mooring system is mostly used by vessels with a large waterline area and an asymmetric fore aft, to minimize the weather forces. The main principle is the projected area experiencing the full force of the weather is to be as small as possible. As mentioned before, this is to minimize the forces acting on the body. The internal turret is built as a part of the vessel, while the external turret is a component in fore or aft of the vessel.

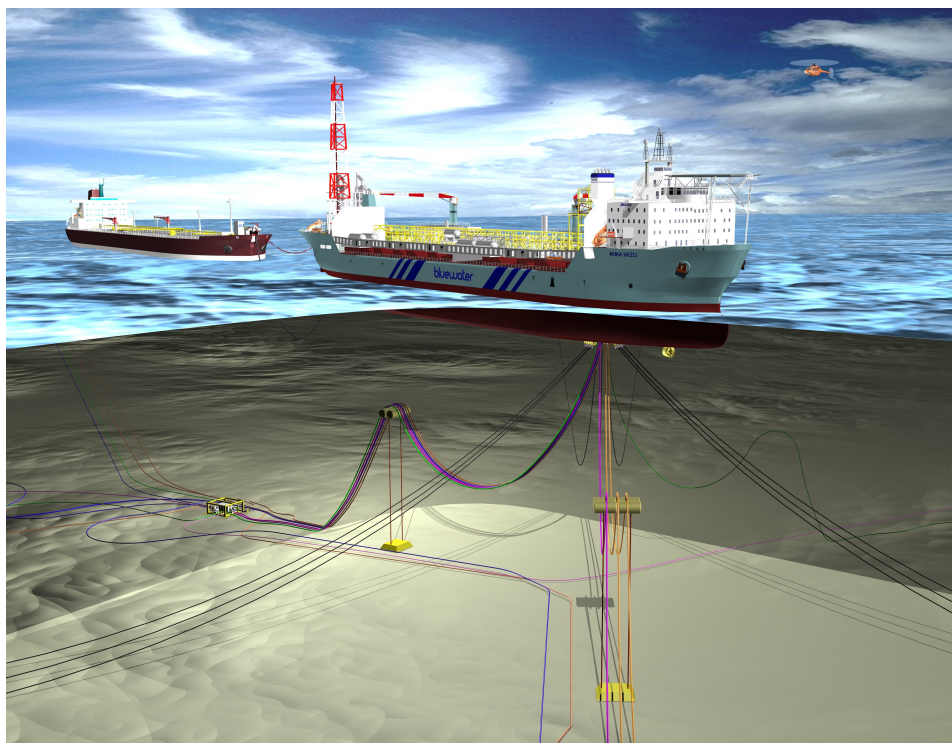


Figure 2.10: Turret mooring system (Bluewater, 2019)

Another offshore structure operating on the Norwegian Continental Shelf is the tension leg platform. Tension leg platforms limit vertical motions which is the desired outcome with this type of offshore structure. The tie-back drilling risers often have large axial stiffness, and the motions must be controlled with respect to this.

Catenary mooring with dynamic positioning, DP, included is a widely used mooring system in recent times. In addition to the catenary mooring as mention in previous section, the system is added a dynamic position controlled system. Dynamic positioning is a computer controlled position system which automatically aim to maintain the position of the floating unit. Propellers or thrusters provide the force to keep the vessels heading and position, based on position reference sensors, motion sensors, wind sensors and gyro compasses (The Nautical Institute, 2011).

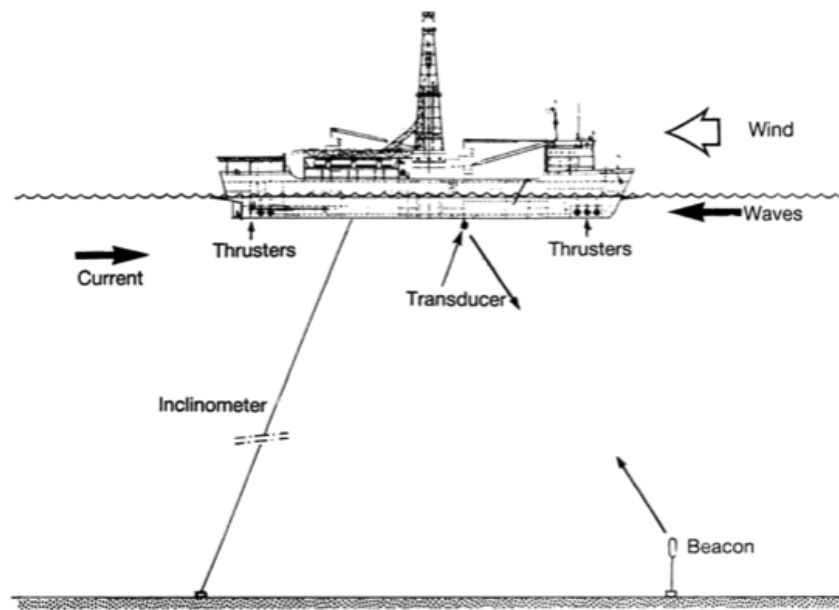


Figure 2.11: Illustration of dynamic positioning (Faÿ, 1990)

A mooring system can also be designed with only DP from propellers or thrusters. This is illustrated in Figure 2.11 for a undefined type of ship. To have a positioning system only based on propellers or thrusters requires a lot of power to withstand the environmental forces acting on the body. Due to the required power, full DP systems often operates over a short period. However, they are flexible and are easily manoeuvred to the desired location.

Chapter 3

Limit states

In the previous chapter different hardware components of the mooring system were focused on. Depending on where the offshore structure is located, different rules and regulations becomes relevant for the specific location. From the rules and regulations there are several design criteria that need to be fulfilled in order to get approved by a classification society, e.g. DNV GL or Bureau Veritas. In this section the rules and regulations for the NCS will be the basis for the design criteria, however international requirements will be mentioned as well. Different design limits and design criteria for mobile and permanent units will also be outlined and discussed according to DNVGL-OS-E301, *Position mooring* (DNV GL, 2018) and ISO19901-7, *Stationkeeping systems for floating offshore structures and mobile offshore units* (ISO, 2013).

3.1 Design limit states

The design of a single mooring line and a mooring system, is to resist estimated loads with a safety factor based on the limit state considered and will be further discussed later in this section. From DNVGL-OS-E301 Offshore standard (DNV GL, 2018) there are three design criteria given in terms of limit states formulation are defined as follows:

Ultimate Limit State

An Ultimate Limit State (ULS) to ensure that the individual mooring lines have adequate strength to withstand the load effects imposed by extreme environmental actions.

Accidental Limit State

An Accidental Limit State (ALS) to ensure that the mooring system has adequate capacity to withstand the failure of one mooring line, failure of one thruster or one failure in the thrusters' control or power systems for unknown reasons. A single failure in the control or power systems may cause that several thrusters are not working.

Fatigue Limit State

A Fatigue Limit State (FLS) to ensure that the individual mooring lines have adequate capacity to withstand cyclic loading.

In other words ULS is the design criteria to withstand the extreme environmental condition, without any failure of the mooring lines. ALS is the design criteria for having an intact system after one mooring line failure. FLS is the design criteria for the mooring line to withstand cyclic loading.

In the Norwegian, UK and a few other sectors, a 100-year return period is used as design basis for wind and waves. For currents a 10-year return period is used. The estimated return periods should give sufficient predictions of the weather to cover most cases. The 100-year return period corresponds with 10^{-2} annual probability value of exceedance. The environmental loads outlined in DNVGL-OS-E301 are wind loads, current loads, wave loads, wave drift forces, wave frequency motions and mean and low frequency motions. A short description of the different environmental loads and how they should be included in the limit state calculations follows.

Wave loads and current loads should be determined from wind tunnel tests, or numerical analysis if it can be validated with experimental tests for a similar unit (DNV GL, 2018). The mean wave drift force used for calculations is the steady component of the second order wave force. Mean drift force can be established from model basin test results or wave diffraction analysis from potential theory. Considering low-frequency wave forces, they may contain both potential and viscous effects. These viscous effects are not included in potential theory and must be taken into account for column-stabilized units such as semi-submersibles. When considering the mean wave drift coefficients, both current interaction effects and viscous effects are neglected in potential theory. Recently a study on the topic of mean wave drift force was conducted (Larsen K., Vigesimal T., Bjørkli R., Dalane D., 2018), the study presents a simplified empirical formula to include viscous and current effects given in Section 4.9.

Wave frequency motions shall be found by diffraction theory for large volume structures, and may be found with strip theory for slender structures. For column-stabilized units a combination of wave diffraction theory and Morison's equation should be used to calculate the wave frequency motions. Environmental actions due to waves, current and wind shall be included in the analysis of mean and low frequency motion response of the unit. This includes both mean, first and second order components from the loads.

3.2 Overload check and design criteria

The three design limit states are based upon the same design equation with the following basis:

$$\textit{Design capacity} - \textit{Design load effect} \geq 0 \quad (3.1)$$

For ULS and ALS, Equation 3.1 can be written as presented in Equation 3.2 according to (ISO, 2013). The most probable maximum tension multiplied with a safety factor should be less than or equal to the Minimum Breaking Strength (MBS). This is illustrated in Figure 3.1 and shows the correlation between the probability density functions for tension during the worst 100 year condition, and the probability density function for the tension strength in the mooring line. The largest tension in the mooring line is calculated from a 3 hour sea state.

$$T_{MPM} \cdot s_f \leq MBS \quad (3.2)$$

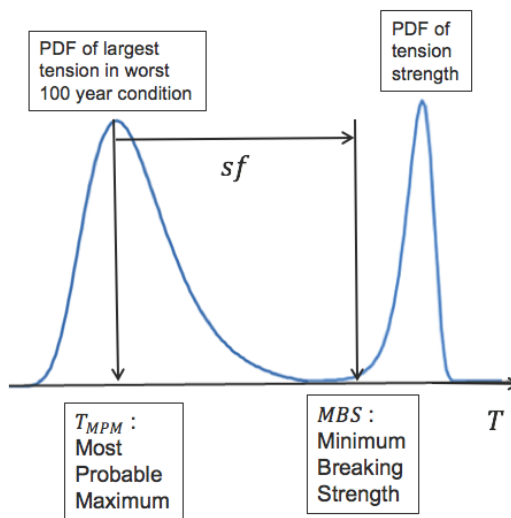


Figure 3.1: T_{MPM} multiplied with safety factor $\leq MBS$ (Larsen, 2018)

The Norwegian Continental Shelf has stricter requirements to the safety factors compared to international standards. For permanent and mobile units the safety factors are presented in Table 3.1 and 3.2 respectively (ISO, 2013).

Permanent oil storage or production units		
Weather condition	ULS	ALS
100 year return period	Norway: 2.2 International: 1.67	Norway: 1.5 International: 1.25
10 year return period	N/A	N/A

Table 3.1: Requirements to safety factors for permanent units (ISO, 2013)

Mobile drilling units		
Weather condition	ULS	ALS
100 year return period	Norway: 1.9	Norway: 1.3
5-10 year return period	International: 1.67	International: 1.25

Table 3.2: Requirements to safety factors for mobile units (ISO, 2013)

Permanent units have stricter safety factors than its mobile counterparts. According to Table 2.1 this is reasonable as the time perspective for permanent and mobile units are usually different.

In DNVGL-OS-E301 there are also some criteria related to safety factors and premises for design of mooring systems. The equation for safety factors are split up in partial safety

factors to differentiate between the safety factor for the pre-tension and pre-tension for the environmental loads action on the system. The design equation for both ULS and ALS are given below in Equation 3.3.

$$S_C - T_{pret} \cdot \gamma_{pret} - T_{C-env} \cdot \gamma_{env} > 0 \quad (3.3)$$

Present safety factors for permanent and mobile units are given in Table 3.3 and 3.4. The consequence classes are split into Class 1 and Class 2. The consequence classes applied in the ULS and ALS are defined as follows (DNV GL, 2018):

Class 1, where mooring system failure is unlikely to lead to unacceptable consequences such as loss of life, collision with an adjacent platform, uncontrolled outflow of oil or gas, capsize or sinking.

Class 2, where mooring system failure may well lead to unacceptable consequences of these types.

Partial safety factors for ULS			
		<i>Time domain analysis</i>	
Consequence class	Type of unit	Safety factor on pretension γ_{pret}	Safety factor on env. tension γ_{env}
1	Permanent	1.20	1.45
1	Mobile	1.20	1.35
2	Permanent & mobile	1.20	1.90

Table 3.3: Partial safety factors for ULS (DNV GL, 2018)

Partial safety factors for ALS			
		<i>Time domain analysis</i>	
Consequence class	Type of unit	Safety factor on pretension γ_{pret}	Safety factor on env. tension γ_{env}
1	Permanent	1.00	1.10
1	Mobile	1.00	1.05
2	Permanent & mobile	1.00	1.45

Table 3.4: Partial safety factors for ALS (DNV GL, 2018)

After considerations during this master thesis and by close dialogue with the supervisor, Kjell Larsen, the design in this task is based upon the rules and regulations given in DNVGL-OS-E301. In other words, the safety factors from DNV GL will apply for the mooring system design, and not the safety factors from ISO regulations. In addition, the design in the thesis is according to class 2 where a mooring system failure may well lead to unacceptable consequences as covered above.

For FLS, Equation 3.1 can be formulated in terms of the sum of the fatigue damage d_i . The total sum of fatigue loads, d_c , multiplied with a safety factor, γ_F , shall be smaller than one in order to fulfill the design criteria given in Equation 3.5 (DNV GL, 2018).

$$d_c = \sum_{i=1}^{i=n} d_i \quad (3.4)$$

$$1 - d_c \cdot \gamma_F \geq 0 \quad (3.5)$$

The value for the safety factor depends on the adjacent fatigue damage ratio, d_F . The definition of d_F are taken directly from DNVGL-OS-E301 and is as follows: *d_F is the adjacent fatigue damage ratio, which is the ratio between the characteristic fatigue damage d_c in two adjacent lines taken as the lesser damage divided by the greater damage. d_F cannot be larger than one.*

$$\begin{aligned} \gamma_F &= 5 \text{ when } d_F \leq 0.8 \\ \gamma_F &= 5 + 3\left(\frac{d_F - 0.8}{0.2}\right) \text{ when } d_F > 0.8 \end{aligned} \quad (3.6)$$

FLS is often presented in terms of an S-N curve (DNV GL) or T-N curve (ISO) curve which gives the component capacity against tension fatigue. FLS will not be further investigated in this thesis.

Chapter 4

Theory

The mooring system for a semi submersible is designed to withstand environmental loads with a certain safety factor, specified in Chapter 3. A mooring line's tension is calculated from the motion in the top end of the mooring line. The motions at the top of the mooring lines are a combination of the mean offset for the offshore structure and the dynamic motion of the structure. Static motion is the mean offset, while the dynamic motions are the sum of the wave, low and high frequency motions acting on the structure.

4.1 Rigid body motions

To understand the motions of a semi submersible, the rigid-body motions shown in Figure 4.1 must be clarified. The following sections will give an explanation to how the equation of motion for six degrees of freedom is solved in order to determine the desired mooring tensions.

Rigid-body motions of a floating structure can be divided into three translational motions and three rotational motions, as shown in Figure 4.1.

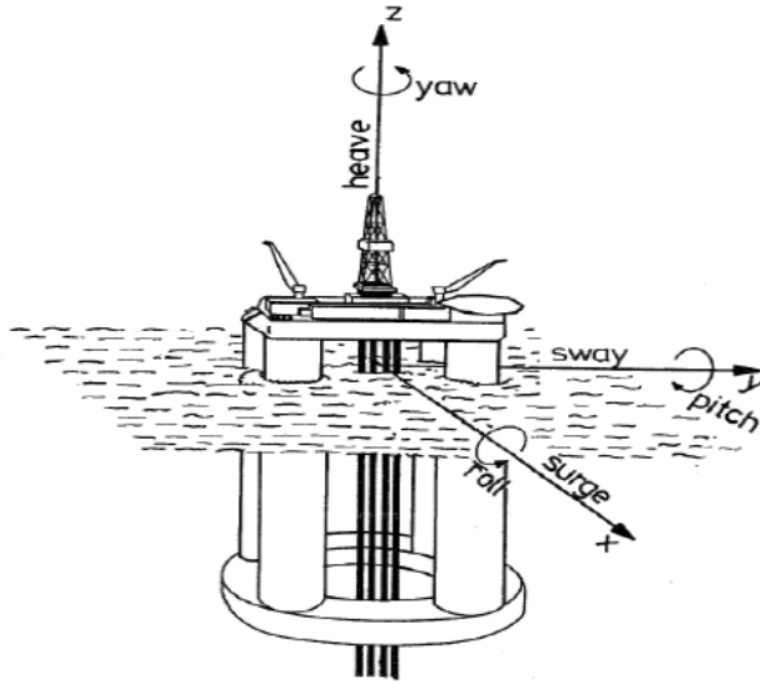


Figure 4.1: Coordinate system and rigid-body modes (Faltinsen, 1990)

The motions of an arbitrary position on the semi submersible can be expressed utterly by compact notation given in Equation 4.1, 4.2 and 4.3.

$$s = \eta_1 i + \eta_2 j + \eta_3 k + \omega \times r \quad (4.1)$$

where

$$\omega = \eta_4 i + \eta_5 j + \eta_6 k \quad (4.2)$$

and

$$r = xi + yj + zk \quad (4.3)$$

When inserting Equation 4.2 and 4.3 into Equation 4.1, the complete representation of the total motions are found. The combined translation and rotational contribution to total motion in terms of i, j and k are given in Equation 4.4.

$$s = \eta_1 i + \eta_2 j + \eta_3 k + \begin{vmatrix} i & j & k \\ \eta_4 & \eta_5 & \eta_6 \\ x & y & z \end{vmatrix} = (\eta_1 + z\eta_5 - y\eta_6)i + (\eta_2 + x\eta_6 - z\eta_4)j + (\eta_3 + y\eta_4 - x\eta_5)k \quad (4.4)$$

4.2 Equation of motion

The top end motion of a moored semi-submersible can be described by the equation of motion in all six degrees of freedom

$$(M + A(\omega))\ddot{r} + C(\omega)\dot{r} + D_l\dot{r} + D_q\dot{r} |\dot{r}| + K(r)r = Q(t, r, \dot{r}) \quad (4.5)$$

Where:

- M : Mass matrix
- $A(\omega)$: Frequency dependent added mass matrix
- $C(\omega)$: Frequency dependent potential damping matrix
- D_l : Linear damping matrix
- D_q : Quadratic damping matrix
- $K(r)$: Non-linear stiffness matrix
- r : Position vector
- \dot{r} : Velocity vector
- \ddot{r} : Acceleration vector
- $Q(t, r, \dot{r})$: Excitation force vector

The focus for this thesis will be translation in surge, accordingly only x-direction will be of interest and Equation 4.5 can be redefined as:

$$(M + A(\omega))\ddot{x} + C(\omega)\dot{x} + D_l\dot{x} + D_q\dot{x} |\dot{x}| + K(x)x = Q(t, x, \dot{x}) \quad (4.6)$$

Dynamic load factor (DLF) give the relation between the load frequency and the natural frequency of the system as illustrated in Figure 4.2.

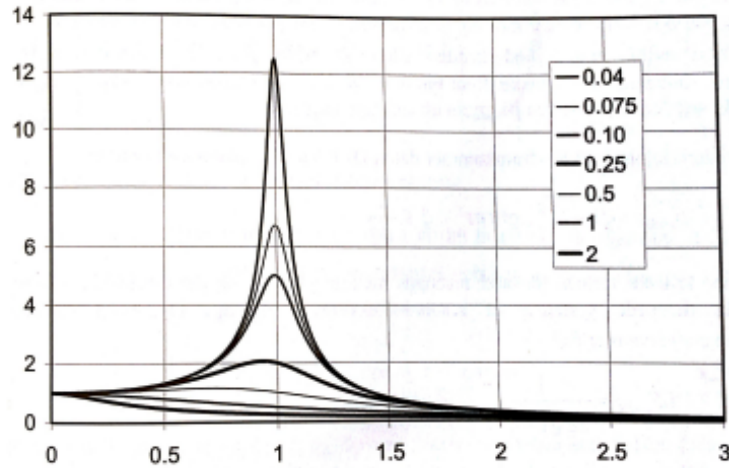


Figure 4.2: Dynamic load factor (Larsen, 2014)

Dynamic load factor, also known as DLF, is the unit on the y-axis and the frequency ratio β given by $\frac{\omega}{\omega_0}$ is the unit on the x-axis. The values in the legend are different

damping ratios ξ , given by $\frac{c}{2m\omega_0}$. If the curves are evaluated at a frequency ratio of 1.0, the damping ratios conform with the height of the peak. Low damping ratios result in higher DLF peaks, hence, damping of the system is critical to reduce the motions. The formula for dynamic load factor is given as follows (Larsen, 2014):

$$DLF = \frac{1}{\sqrt{(1 - (\frac{\omega}{\omega_0})^2)^2 + \omega^2 \frac{c^2}{k}}} = \frac{1}{\sqrt{(1 - (\beta)^2)^2 + (2\xi\beta)^2}} \quad (4.7)$$

For semi-submersibles the natural oscillation period is within the following magnitude (DNV GL, 2017b):

Natural oscillation periods for semi-submersibles						
Response	Surge	Sway	Heave	Roll	Pitch	Yaw
Oscillation period [s]	> 100	> 100	20-50	30-60	30 - 60	> 100

Table 4.1: Natural oscillation periods for semi-submersibles

4.2.1 Excitation forces

The total contribution to excitation forces in the equation of motion originates from

$$Q(t, x, \dot{x}) = q_{wa} + q_{wi} + q_{cu} + q_{thr} \quad (4.8)$$

Excitation regimes

The forces have dissimilar contributions to the total excitation force, primarily in terms of mean offset, wave frequency, WF, and low frequency, LF, which are the important top end motions for mooring system design. For that reason, high frequency motions with a period between 2-5s will be neglected in this thesis.

Excitation regimes			
	Mean	Wave Frequency, 5-30s	Low Frequency, 30-300s
Waves	Mean wave drift forces due to 2 nd order wave loads	1 st order forces	2 nd order difference forces
Wind	Mean wind speed	-	Wind gust
Current	Mean current speed	-	-
Thrusters	Mean thruster force	-	Dynamic thruster forces

Table 4.2: Contributions from the different forces (Larsen, 2018)

The forces were mentioned in Section 3.1, but they need a more thorough explanation to be understood correctly and this will be presented in the following.

From the excitation regimes presented in Table 4.2, the eigenperiods for the semi-submersible can be in the same order of magnitude as the load frequencies. The region where the load period is close to the natural period is called resonance region and

large undesirable motions can be excited. Therefore, the damping of the system is very important to counteract resonant motions (Faltinsen, 1990).

Wave forces

Wave forces can be divided into first order wave forces and second order wave forces.

- **First order wave forces**

Wave frequency forces represent linearised 1st order wave forces which are proportional to the wave amplitude. First order wave forces can be divided into excitation loads and radiation loads, and are obtained through potential theory.

- **Second order wave forces**

The non-linear wave force contribution originates from 2nd order wave loads, proportional to the square of the wave amplitude. For moored semi-submersibles, second order wave forces of interest is the mean wave drift forces and low-frequency loads. The formula for the mean wave drift loads can, according to (Faltinsen, 1990) be expressed as:

$$\overline{F}_i^s = 2 \int_0^\infty S(\omega) \left(\frac{\overline{F}_i(\omega; \beta)}{\zeta_a^2} \right) d\omega \quad i = 1, \dots, 6 \quad (4.9)$$

Low-frequency loads may be of lower magnitude than mean wave drift forces, however the effect of low-frequency forces is important due to load frequencies close to the natural frequencies of the system (Larsen, 2014). The general formula for low frequency loads is presented in Equation 4.10. T_{jk}^{ic} are the second-order quadratic transfer functions (QTF) for the slowly varying forces. The QTFs are independent of the sea state, but are functions of the two frequencies ω_k and ω_j (Faltinsen, 1990). QTF is based on cross-bi-spectral analysis and will not be further discussed in this thesis. Both the general formula for mean value of low-frequency loads and the general formula (4.10) with Newman's approximation applied, can be found in *Sea loads on ships and offshore structures* (Faltinsen, 1990).

$$F_i^{SV} = \sum_{j=1}^N \sum_{k=1}^N A_j A_k [T_{jk}^{ic} \cos\{(\omega_k - \omega_j)t + (\epsilon_k - \epsilon_j)\} + T_{jk}^{is} \sin\{(\omega_k - \omega_j)t + (\epsilon_k - \epsilon_j)\}] \quad (4.10)$$

Furthermore, high-frequency (HF) loads do contribute, but this is negligible for moored structures with large volume like semi-submersibles. Natural frequencies for semi-submersibles are significantly lower than high-frequency loads which point to an inertia dominated system with small impacts from high-frequency forces.

Wind forces

q_{wi} includes mean value from mean wind velocity and low-frequency forces excited by wind gusts, illustrated in Figure 4.3.

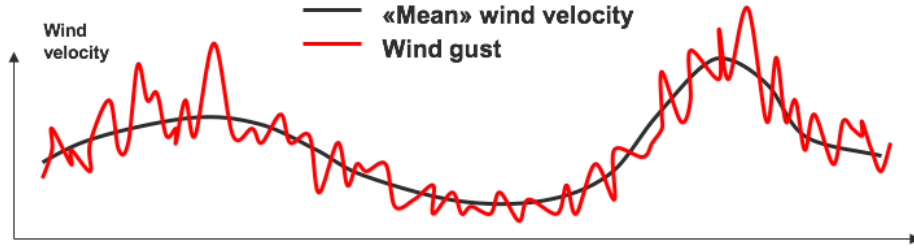


Figure 4.3: Mean wind velocity and wind gusts

The wind force contribution is formulated as

$$q_{wi}(t) = C_{wi} \cdot (U(t) - \dot{x}_{LF})^2 \quad (4.11)$$

where the time dependent wind velocity

$$U(t) = \bar{U} + u(t) \quad (4.12)$$

and the wind force coefficient

$$C_{wi} = \frac{\rho_{air}}{2} \cdot C_D \cdot A \quad (4.13)$$

where:

- ρ_{air} : Air density
- C_D : Global drag coefficient
- A : Area projected to wind
- \bar{U} : Mean wind velocity
- $u(t)$: Dynamic wind gusts

\dot{x}_{LF} , the low frequency floater velocity, and $u(t)$ is assumed to be relatively small compared to the mean wind velocity, $\bar{U} \gg \dot{x}_{LF}$ and $\bar{U} \gg u(t)$. Equation 4.11 is then written in terms only consisting of terms including \bar{U}

$$q_{wi}(t) \approx C_{wi} \cdot \bar{U}^2 + 2 \cdot \bar{U} \cdot u(t) - 2 \cdot C_{wi} \cdot \bar{U} \cdot \dot{x}_{LF} \quad (4.14)$$

The first term in the force contribution is the constant mean force, the second term is the low frequency excitation force and the last term is the low frequency damping force. The wind force coefficient must be established from wind tunnel tests for different headings (DNV GL, 2018), as mentioned in Chapter 2.

Current forces

The contribution to the total force from q_{cu} , is the force given by mean current velocity and the current force coefficient, based on metocean data for the location. Current gusts and current turbulence are neglected.

$$q_{cu}(t) = C_{cu} \cdot (\bar{V} - \dot{x}_{LF}) | \bar{V} - \dot{x}_{LF} | \quad (4.15)$$

$$C_{cu} = \frac{\rho_{water}}{2} \cdot C_D \cdot A \quad (4.16)$$

where:

- ρ_{water} : Density water
- C_D : Global drag coefficient
- A : Area projected to wind
- \bar{V} : Mean current velocity
- \dot{x}_{LF} : Floater velocity

$\bar{V} - \dot{x}_{LF}$ is the relative velocity from the mean current and the low frequency motion. The relation between \bar{V} and \dot{x}_{LF} is assumed to be $\bar{V} \gg \dot{x}_{LF}$ and the squared \dot{x}_{LF} term is therefore neglected in the final current force.

$$q_{cu}(t) \approx C_{cu} \cdot (\bar{V}^2 - 2\bar{V}\dot{x}_{LF}) \quad (4.17)$$

The first term in the force contribution is the constant current force and the second term is the low frequency damping force. The current force coefficient must be established in the same manner as for wind loads.

Thruster forces

Thrusters are not included in this thesis, but their possible contribution should be mentioned. q_{thr} is the mean thruster force and/or the dynamic force dependent on automatic or manual control for the thruster system. Thrusters may give a large contribution to both forces and damping based on how the thruster system is arranged pertaining to the waves, wind and current.

4.3 Inertia

Both the inertia terms, M and $A(\omega)$ are related to the acceleration of the semi submersible. The gravitational mass M is directly related to the weight of the structure from steel, equipment etc., while the added mass $A(\omega)$ is frequency dependent and will be further discussed in Section 4.7, Analysis methods.

4.4 Damping

Damping for a semi-submersible is important to reduce the resonant low-frequency motion and therefore reduce the response of the system. So far, both wind and current are shown to contribute to the low frequency damping for a semi-submersible. Other important damping contributors are viscous loads on the floater hull, wave drift damping, drag forces on mooring lines and risers and damping from propellers and thrusters.

Viscous loads on floater hull

Viscous force on the columns and pontoons is the main source of damping for a semi-submersible (Lie et al., 2007). Viscous effects can be divided into skin friction effects and viscous effects due to the pressure distribution around the structure (Faltinsen, 1990).

Drag forces on mooring lines and risers

Drag forces on mooring lines originate from the horizontal top end motions of the semi-submersible. When the semi-submersible moves in a direction, the drag contribution will increase and thus contribute to the damping force and reduce the motion. The mooring line damping can contribute with between 30-40% of the total damping (Lie et al., 2007).

Low frequency wind damping

According to Equation 4.14, the negative term on the right hand side of the force contribution will often operate as a damping term. When the low frequency velocity of the structure is larger than zero, this velocity will give a contribution to the total damping of the system. Otherwise, this term will give a contribution to the total force acting on the system.

Low frequency current damping

The reasoning given for the wind damping above, holds for current damping as well. The negative term on the right hand side of Equation 4.17, remains negative when the low frequency structure velocity is larger than zero. Meaning, this will give a damping contribution to the system.

Wave drift damping

Wave drift damping is often based on wave drift damping coefficients obtained in the frequency domain. For a sea state characterized with a wave spectrum $S(\omega)$, the constant wave drift damping can then be estimated by:

$$\bar{C} = 2 \int_0^{\infty} C(\omega)S(\omega)d\omega \quad (4.18)$$

This will not be further investigated in the thesis, but it is worth to mention where the term originates from when it is implemented in SIMA. The contribution to wave drift

damping is caused by the waves, and is illustrated by Figure 4.4 taken from (Faltinsen, 1990).

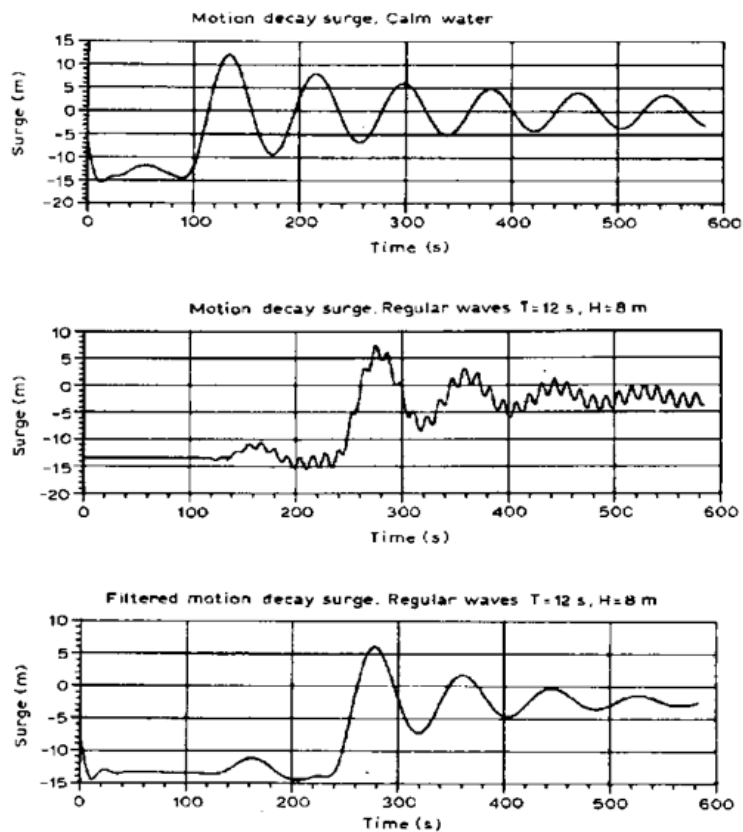


Figure 4.4: Illustration of wave drift damping (Faltinsen, 1990)

Here you can see the change in decay time between the upper and the lower graph, where the upper is decay in calm water and the lower is filtered decay in regular waves. The surge motions decay is significantly faster when waves are present.

Thruster damping

Thrusters can contribute with damping either as a constant force or by a motion controlled force acting pertaining to measured wind, waves and current. This contribution will be dependent on how the thrusters are configured.

4.5 Stiffness

The total stiffness for a system, K_T , is given by the elastic and geometric stiffness. The total contribution for one mooring line is given in Equation 4.19 and illustrated in Figure 4.5.

$$\frac{1}{K_T} = \frac{1}{K_G} + \frac{1}{K_E} \quad (4.19)$$

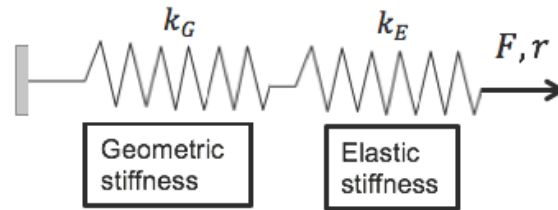


Figure 4.5: Geometric and elastic stiffness illustrated in series

The total stiffness provides the restoring force that is important to control the low frequency motions and mean offset of the system.

Elastic stiffness

Elastic stiffness originates from the line axial elongation in the mooring line and is of specific interest for taut-leg mooring when the polyester ropes provides the dominating stiffness component for the system.

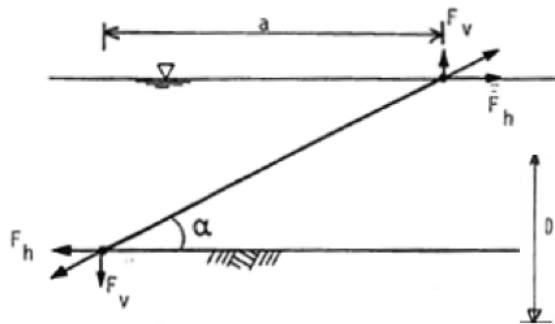


Figure 4.6: Taut-mooring line (Larsen, 2018)

The moment equilibrium of the mooring line according to Figure 4.6 is

$$F_h \cdot D = F_v \cdot a \quad \rightarrow \quad F_h = \frac{F_v \cdot a}{D} \quad (4.20)$$

F_h gives the restoring force in horizontal direction. This may also be written in terms of the linear correlation to the horizontal displacement in surge direction, x , and the stiffness K

$$F_h = F \cdot \cos \alpha = K \cdot x \cdot \cos \alpha \quad (4.21)$$

Geometric stiffness

The contribution to the geometric stiffness is originating from the weight and the change of geometry of the mooring line for catenary moorings systems. Based on the moment equilibrium for geometric stiffness, the combination of change in suspended weight and moment arm will contribute to a non linear restoring force when the semi-submersible is displaced from the equilibrium position. This is illustrated in Figure 4.7 and expressed in Equation 4.22

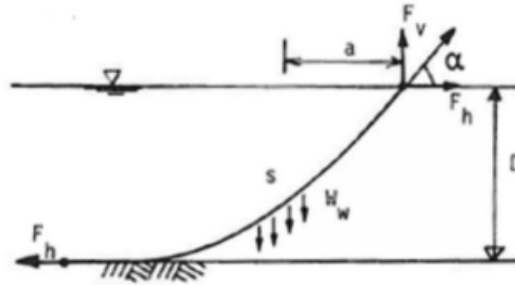


Figure 4.7: Catenary mooring line (Larsen, 2018)

$$F_h \cdot D = W_w \cdot a \quad \rightarrow \quad F_h = \frac{W_w \cdot a}{D} \quad (4.22)$$

For a single mooring line element shown in Figure 4.8, the tangential forces acting on the element are given by Equation 4.23 and 4.24. A more thorough explanation and derivation of the expression can be found in (Larsen, 2015) and (Faltinsen, 1990).

$$dT = [w \cdot \sin \varphi - F(1 + \frac{T}{EA})] \cdot ds \quad (4.23)$$

$$Td\varphi = [w \cdot \cos \varphi + D(1 + \frac{T}{EA})] \cdot ds \quad (4.24)$$

where:

- ds : The static equilibrium of a segment of length with zero tension
- D : Mean hydrodynamic force per unit length in normal direction
- F : Mean hydrodynamic force per unit length in tangential direction
- A : Cross sectional area of the mooring line
- E : Elastic modulus
- T : Line tension

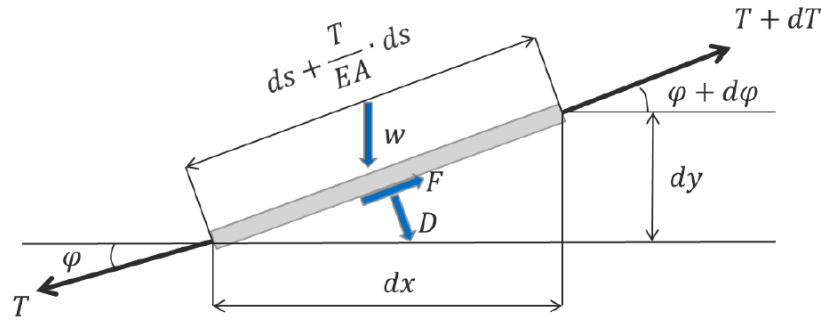


Figure 4.8: Forces acting on a mooring line element (Larsen, 2015)

4.6 Line characteristics and restoring forces

One of the primary aspects within mooring systems, is the relation between the tension in the line and the horizontal offset. In order to establish an equation for the total horizontal offset, Equation 4.23 and 4.24 can be rewritten by assuming $\frac{T}{EA} \ll 1$ and thereby the term is neglected. The complete derivation of the total line characteristics can be found in (Larsen, 2015).

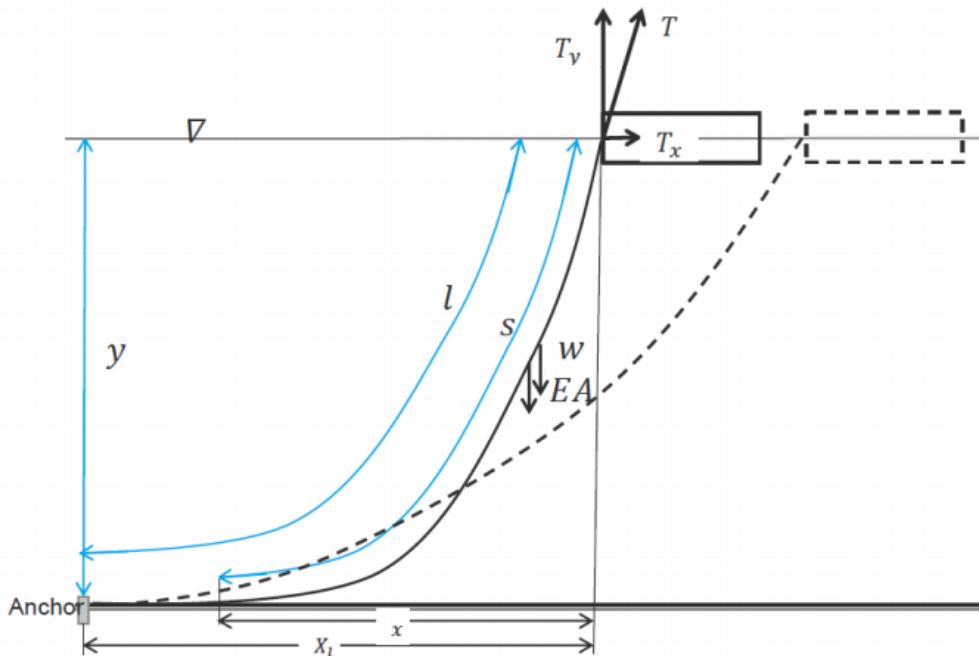


Figure 4.9: Definition of the line characteristic (Larsen, 2015)

When assuming $\frac{T}{EA} \ll 1$ and deriving said equation, the result is Equation 4.25 which gives the total horizontal length from anchor to offset position in x-direction.

$$X_l = l + \frac{T_x}{w} \cdot \cosh^{-1} \left(1 + \frac{w \cdot y}{T_x} \right) - \sqrt{y \cdot \left(y + \frac{2T_x}{w} \right)} \quad (4.25)$$

It is important to mention that the concept may not be suited for large water depths as the weight of the mooring system increases substantially.

Restoring force

The restoring force is found by summing up the surge contributions given by Equation 4.26 corresponding to the illustration in Figure 4.10.

$$F_{Restoring, Surge} = \sum_{i=1}^n T_{xi} \cos \psi_i \quad (4.26)$$

This equation will give the total restoring force in surge direction exerted by the summation of all the horizontal offsets from equilibrium position. The summation is over the number of anchor lines i , and ψ_i is the angle between T_{xi} and surge direction x in the coordinate system.

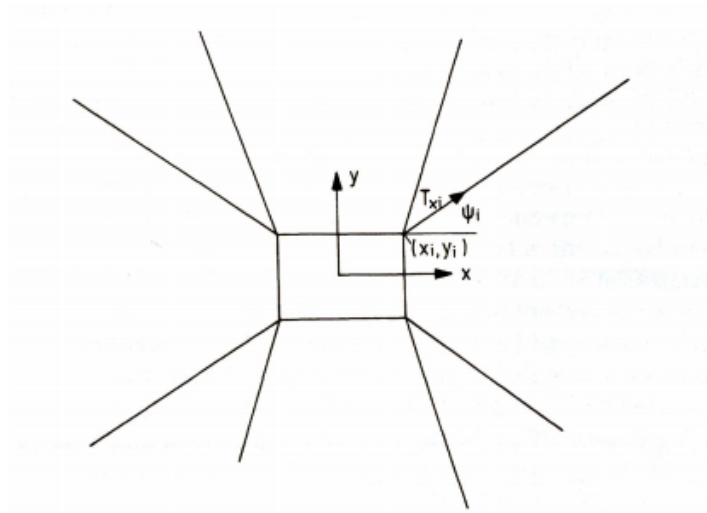


Figure 4.10: Horizontal restoring force (Faltinsen, 1990)

4.7 Analysis methods

When solving the equation of motion there are two different approaches to find the top end motions.

The first approach is by representing a Gaussian process with a frequency spectrum, where the spectrum show the energy of the process as function of the frequency. With this method, all terms must be linearised and is done with use of the linear principle of superposition (Larsen, 2014). Linear principle of superposition uses either direct linearisation or an iterative linearisation to solve non-linearities. When representing in

the frequency domain, the method includes separation of LF and WF motions and forces. Besides forces and motions, non-linear stiffness and damping terms must be linearised as well. Frequency domain will not be further discussed in the thesis.

The other approach is by numerical integration in the time domain. When this approach is used, both LF and WF motions are solved simultaneously and all non-linearities are directly taken into account. Evaluating Equation 4.6, $A(\omega)$ and $C(\omega)$ are frequency dependent. The terms have to be correctly transformed from frequency dependent to time domain in order to receive the correct inputs for the equation of motion.

As mentioned both $A(\omega)$ and $C(\omega)$ are frequency dependent terms which can be solved in WAMIT, a potential theory software solving the coefficients in the frequency domain. In time domain the frequency dependent terms are represented in a retardation function for further calculations in SIMA. The retardation function are presented below. Both SIMO and RIFLEX software's operate in the time domain.

In time domain, analysis of a stochastic process is described through a time realization and the corresponding response. According to section 2.2.8 in DNVGL-OS-E301, a number of simulations (10-20) must be performed for a 3 hour sea state to get a representative selection with respect to uncertainty. This will be investigated later in the thesis. The maximum tension in the mooring line for each simulation should be used in a statistical model to evaluate the result for any specific condition.

To obtain the time dependent equation of motion, Equation 4.27, the frequency dependent equation of motion given in Equation 4.6 needs to be transformed from frequency to time domain.

$$(M + A_\infty)\ddot{x} + \int_0^t h(t - \tau)\dot{x}(\tau)d\tau + D_l\dot{x} + D_q\dot{x} | \dot{x} | + K(x)x = Q(t, x, \dot{x}) \quad (4.27)$$

By Fourier transforming the obtained $A(\omega)$ and $C(\omega)$ by WAMIT, the retardation function can be established as showed in Equation 4.28 including Equation 4.29 and 4.30. It represents the memory effect of the floater motions. A complete explanation of the retardation function can be found in (Yuan et al, 2017).

$$h(\tau) = \frac{2}{\pi} \int_0^\infty C(\omega) \cos \omega\tau d\omega = -\frac{2}{\pi} \int_0^\infty \omega A(\omega) \cos \omega\tau d\omega \quad (4.28)$$

$$A(\omega) = -\frac{1}{\omega} \int_0^\infty h(\tau) \sin \omega\tau d\tau \quad (4.29)$$

$$C(\omega) = \int_0^\infty h(\tau) \cos \omega\tau d\tau \quad (4.30)$$

4.7.1 De-coupled approach

There are mainly two different ways to calculate the response and forces for a mobile unit in time domain. In the de-coupled approach, also known as separated approach, the mooring system is calculated separately from the module. To include forces from the mooring and riser systems in the vessel motion analysis, the mooring and risers are included quasi-statically using non-linear position dependent forces (Ormberg and Larsen, 1998)(DNV GL, 2017b). This way of calculating the motions includes some simplifications. The damping of the system, which is important for calculating low frequency motions, must be included by a linear damping force. Damping can often be difficult to estimate and the input is given as a linear coefficient which does not necessarily represent the physical phenomenon. Another simplification is the way the current effects are included in the calculations. The current forces from mooring and risers are also included as coefficients. With coefficients to represent both damping and stiffness from the mooring and risers, the calculated motions and line tensions may be inaccurate (Ormberg and Larsen, 1998). This is due to separated calculations for the motions with regard to the centre of gravity of the model. Therefore mooring behaviour and mooring tensions are calculated with the obtained motions from step one as depicted in Figure 4.11. In other words, coupling and interaction effects may not be included in a proper manner.

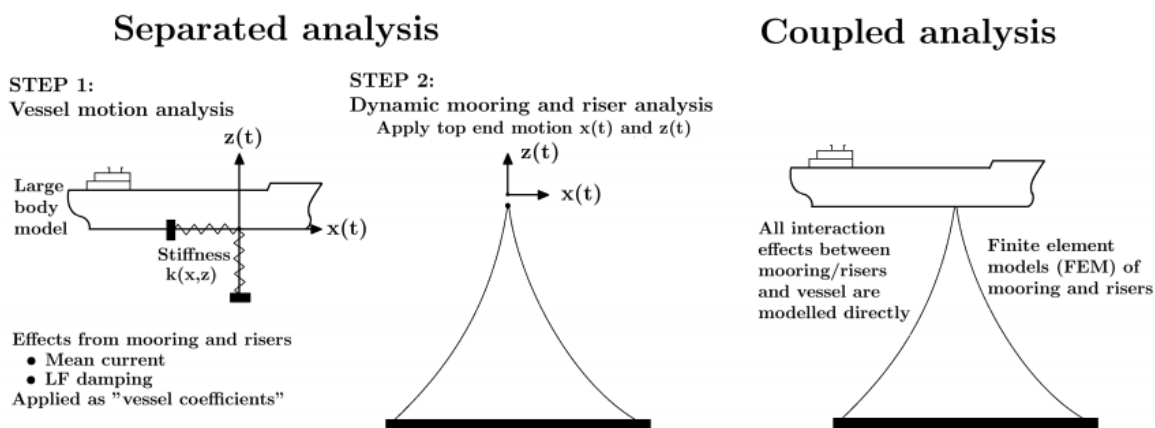


Figure 4.11: Separated and coupled analysis (Ormberg and Larsen, 1998)

4.7.2 Coupled approach

The coupled approach simultaneously calculates the floater motions and the mooring line dynamics in one complete model. With this approach coupling effects, interaction effects and load effects from mooring and risers are all modelled directly in the simulations (Ormberg and Larsen, 1998). Both of the approaches are illustrated in Figure 4.11.

4.8 Morison's equation

Forces acting on a structure are classified based on the ratio between the characteristic lengths of the structure, wave height and wave length. The basis for the explanation will be a circular structure with diameter, D , the incoming wave length, λ and the incoming wave height, H . The interaction between the waves and the body is classified after what load is most dominant. When $\lambda/D < \approx 5$, diffraction loads are important. Diffraction loads occur when the waves are relatively short compared to the structure diameter and are excited by the body. When $\lambda/D > \approx 5$ the structure is relatively small compared to the incoming wave length, the long-wave approximation can be used. In other words, both mass forces and viscous forces can give a force contribution to the loads acting on the structure.

Dependent on the steepness of the incoming wave, the distinction between the dominant loads are $H/D \approx 10$. Meaning, the mass loads are in general dominant for $H/D < \approx 10$, and these loads are proportional to the acceleration squared. When $H/D > \approx 10$ and λ/D is sufficiently large, the viscous loads that are proportional to the velocity squared, become dominant. An illustration of wave force classification is given in Figure 4.12.

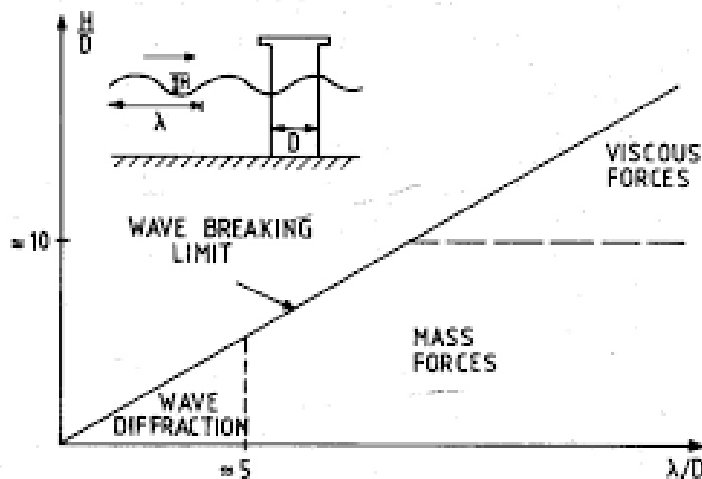


Figure 4.12: Classification of wave forces

Morison's equation (Morison *et al*, 1950) is typically used to calculate wave loads on a structure when the viscous forces can be large. The total horizontal force dF acting on a strip of length dz of a rigid cylinder can be written as

$$dF = \rho \frac{\pi D^2}{4} dz C_M a_1 + \frac{\rho}{2} C_D D dz |u|u \quad (4.31)$$

4.9 Viscous drift forces

Viscous drift forces consist primarily of three contributions where all contribute to the total drag force. These three can be split into two categories. Viscous drift force due to larger projected area and viscous drift force due to higher total velocity. These are both due to the effect of waves and current. In the following, the viscous drift forces will be of focus and effects contributing to these forces. For simplicity the equations presented will be given in unit lengths.

The general formulation of the drag force from Equation 4.31 is rewritten in unit lengths as

$$f_D = \frac{\rho}{2} C_D D |u|u \quad (4.32)$$

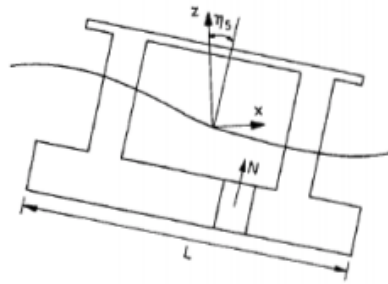
where ρ is the density of water, C_D is the drag coefficient, D is the diameter of the cylinder and u is the horizontal particle velocity component written on compact form. The horizontal particle velocity is fully described by $u = u_0 \cos \omega t$, which gives an oscillating particle velocity.

The first contribution to viscous drift forces is referred to as free-surface effect. A rigid cylinder is normally not the case for structures at larger water depths, and free-surface effects need to be considered. Drag force decays with $e^{\frac{4\pi z}{\lambda}}$ which indicates that the force is concentrated in the free surface zone (Pettersen, 2007). When the free surface condition is taken into account an extra term is presented in the calculation of drag force in Equation 4.33. \dot{x} is the horizontal velocity of the cylinder with respect to the incoming wave velocity, u .

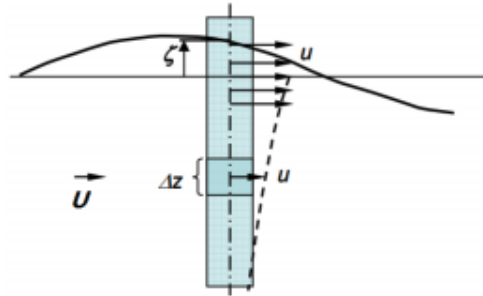
$$f_D = \frac{\rho}{2} C_D D |u - \dot{x}|(u - \dot{x}) \quad (4.33)$$

Both u and \dot{x} are products of cosine, with $u = u_0 \cos \omega t$ and $\dot{x} = \omega x_0 \cos(\omega t - \epsilon)$. Here ϵ is the phase angle with respect to the incoming wave. An extra description of free-surface modelling together with the other contributions from viscous drift forces will be explained in Section 4.11.

The second contribution from viscous drift forces is the net force acting in the direction of the wave, as a result of the larger subjected area contributing to drag force in the crest rather than the trough (Burns, 1983). This is illustrated in Figure 4.13a for a large volume semi-submersible with large wavelength compared to cross-sectional dimensions (Greco, 2012). The physical interpretation from this effect, based on the illustration, is the pitch motion that arise from difference in crest and trough which results in a force component acting in surge direction. Both columns and pontoons give a contribution which are proportional to the wave amplitude cubed. The mathematical expressions for each of the cases can be found in (Greco, 2012) p.103-104.



(a) Cross-flow (Faltinsen, 1990)



(b) Wave-current interaction (Wang, 2016)

Figure 4.13: Illustration of cross-flow and wave-current interaction

The third contribution, named wave-current interaction, comes from adding up the wave induced water particle velocity and current velocity when they contribute in the same direction. The drag force, which is proportional to velocity squared, will give a larger contribution when wave particle velocity and current velocity coincide. Equation 4.32 is then rewritten in terms of water particle velocity u , and current velocity U

$$f_D = \frac{\rho}{2} C_D D |u + U| (u + U) \quad (4.34)$$

Accordingly, the net velocity component gives a smaller contribution to the drag force when the current velocity acts in the opposite direction of the wave velocity (Burns, 1983).

4.10 EXWAVE JIP

A study published in 2014 investigated recently mooring line failures and the corresponding root of the failures (Kvitrud, 2014). The failures reported in this paper occurred between 2010 and 2013 and is given in Table 4.3.

After the study published by Kvitrud in 2014 regarding mooring line failures, the industry realized the necessity to review and improve existing methods, procedures and industry standards. In Table 4.3 you can see that overload is the most common reason for the mooring line failures. From a hydrodynamic perspective and the regulations outlined

in DNVGL-OS-E301, overload is of specific interest given that load effects should be accounted for in the design criteria presented in Section 3.2.

	Fatigue	Overload	Mechanical damage	Manufacturing errors	Sum
Chains	3	3		1	7
Fibre ropes			3		3
Steel wires		2 (+2)	1		3 (+2)
Kenter link	1				1
Socket connection				1	1
Sum	4	5 (+2)	4	2	15 (+2)

Table 4.3: Overview of mooring line failures between 2010-2013 on the Norwegian Continental Shelf (Kvitrud, 2014)

This was the start of the EXWAVE Joint Industry Project (JIP) managed by DNV GL, in close cooperation with Sintef Ocean and Statoil (Equinor) and a couple of other companies contributing as well. The JIP lead to a number of studies and recommendations (DNV GL, 2017b) and these will be further clarified in the following.

The first study on the topic were presented on the Offshore Technology Conference in Houston in 2015 (Stansberg et al., 2015). *Challenges in Wave Force Modelling for Mooring Design in High Seas* investigated wave-current interaction, viscous wave drift forces and large and nonlinear wave-frequency vessel motions. Recommendations for actions and further developments for improved predictions in industry practice was given by proposing a temporary empirical correction formula for both potential flow and viscous effects. The correction formula was given as:

$$f_D = \frac{F_d(\omega, U, H_s)}{A^2} = [f_{d,pot} \cdot (1 + C_p \cdot U) + B(G \cdot U + H_s)] \quad (4.35)$$

where:

$f_{d,pot}$ = Second order mean wave drift coefficients from first-order potential theory in zero current

A = Wave amplitude

C_p = Potential-flow wave-current interaction coefficient chosen to be 0.25

$B = B' * d_{sum_s}$ (viscous drift) where $B' = k * p$; $d_{sum} = \sum d_j$ (sum of column diameters)

k = The wave number $\frac{2\pi}{\lambda}$ λ = Wave length

$p = \exp[-1.25(kD_0)^2] \left[\frac{kN}{(m^3)} \right]$, D_0 = Diameter of main columns

$G = 10$ (With dimensions time,[s])(This comprises the viscous wave-current interaction part, found empirically)

In the following years the formula has been compared to experimental tests and numerical calculations using potential flow. Several studies in the topic have been conducted, a short summary of the different articles follows.

OMAE2017-62550: Simulation of low frequency motions in severe sea states accounting for wave-current interaction effects

(Ommani B., Fonseca N., Stansberg C. T., 2017)

The paper compares model tests with two numerical methods for estimating drift forces on a semi submersible. An alternative approach to overcome some of the limitations in today's practice when calculating drift forces is introduced along with the experimental results.

Today's practice for estimating drift forces is based on the assumption that wave drift forces can be computed from zero current wave drift force coefficients for a stationary floater. In addition, simplified correction models for slow drift velocity effects and current effects are used in the calculations.

The "new" method used in the paper is the semi-empirical model which considers wave-current interactions effects and corrects the potential flow wave drift force coefficients proposed by (Stansberg et al., 2015). The different wave directions and a wave drift damping model is also taken into account. Furthermore, results from the semi-empirical method is compared to a potential flow method.

The conclusion of the paper shows a clear underestimation of the slow drift motions with the use of the zero current potential wave drift force coefficients. The semi-empirical formula obtained results closer to the experimental tests, when considering the mean drift coefficient in severe sea states with current. However, low frequency response seems to be overestimated with the same formula.

A significant improvement in prediction of the slow drift motion with the use of a drift force interpolation method is proposed in the paper. The method is validated with model tests.

OMAE2017-62319: Viscous Drift Force and Motion Analysis of Semi-Submersible in Storm Sea States Compared With Model Tests

(Yang et al., 2017)

The study compared experimental tests with simulation models and presented a simplified formula for current and viscous effects on drift forces for non-collinear wave-current conditions. The formula is the following:

$$f_d^{(pot)}(\omega, U_c) = (1 + C_p U_c) f_d(\omega_e, 0) \quad (4.36)$$

The first term is pure potential flow accounting for the effect of current on the mean drift force and the second term accounts for the viscous effects.

Storm sea states were of interest, and are still of interest when analysing the design limit states. Due to the desired maximum conditions, the formula was modified to account for waves and current in extreme cases with their maximum values.

$$f_{d,i}^{(visc)}(\omega, U_c, H_s) = \tilde{B}(\omega) \cdot (G \cdot U_c \cos \beta_{cw} + H_s) \begin{pmatrix} \cos \beta \\ \sin \beta \end{pmatrix} \quad (4.37)$$

One of the conclusions of the study is the presented formula for current and viscous effects for wave drift coefficients for non-collinear wave-current conditions. The modified wave drift coefficient was not applied in the numerical simulations conducted in the study, however, this is done in later studies on the topic.

OMAE2018-78595: Analysis of Semi-submersible under Combined High Waves and Current Conditions Compared with Model Tests

(Yang et al., 2018)

A follow-up to the study presented the year before, to verify modified wave drift forces in the numerical simulation tool SIMO. The focus was numerical prediction of low frequency surge motion of a semi-submersible combining high waves and current. Results matched reasonably well for low frequency motions, when the simulation results are compared with experimental tests.

Another conclusion worth emphasizing is that for the time domain, the viscous effect on low frequency motion can either be modelled by a Morison's model or the simplified formula presented.

OMAE2018-77873-draft: LOW FREQUENCY EXCITATION AND DAMPING OF FOUR MODUS IN SEVERE SEA STATES WITH CURRENT

(Fonseca et al., 2018)

A study where four different Mobile Drilling Units, MODUs, were tested in the ocean basin facility at SINTEF Ocean in Trondheim. The semi-empirical formula was used to calculate wave drift coefficients, which were compared with experimental tests and MULDIF simulations. MULDIF is a linear three-dimensional frequency domain potential theory code, developed by Sintef Ocean (Sprenger et al., 2017). Three different current states were run: $U_c = 0 \frac{m}{s}$, $U_c = 0.82 \frac{m}{s}$ and $U_c = 1.58 \frac{m}{s}$. H_s and T_p were equal for the compared tests.

One of the semi-submersibles used in the study has nearly the exact same geometry as the one used in this thesis, and the results obtained for "Semi C" in the article is of specific interest.

The conclusions from the study with respect to semis with larger column diameter are the following:

- Drift forces at the low frequency range results from a combination of potential flow and viscous drift
- Current effects tend to increase the wave drift forces at the low frequency range (0.08-0.11Hz). The increase is significantly noticeable for the semi-submersibles with larger columns.
- EXWAVE semi-empirical formula tends to underestimate the empirical wave drift coefficients for semi-submersibles with larger columns in the range between 0.07-0.09Hz, for all currents.

OMAE2018-77178: MOORING OF SEMI SUBMERSIBLES IN EXTREME SEA STATES – SIMPLIFIED MODELS FOR WAVE DRIFT FORCES AND LOW FREQUENCY DAMPING

(Larsen K., Vigesimal T., Bjørkli R., Dalane D., 2018)

This study is the last in the series of recently conducted studies leading to the EXWAVE semi-empirical correction formula included in DNVGL-OS-E301. The formula is split into surge and sway direction separately and is shown in Figure 4.14 together with complementary explanation for the included terms.

Guidance note:

In a sea state characterized by significant wave height H_s , peak period T_p and current u_c , the wave drift coefficient for a column stabilised unit in x and y direction (per unit wave amplitude, A) may be taken as:

$$f_{D,x}(\theta, u_c, H_s) = f_{D,pot}^x(\omega, \theta) \left(1 + C_p u_c \cos \theta_{rcd}\right) + B \left(G \cdot u_c \cos \theta_{rcd} + H_s\right) \cos \theta$$

$$f_{D,y}(\theta, u_c, H_s) = f_{D,pot}^y(\omega, \theta) \left(1 + C_p u_c \cos \theta_{rcd}\right) + B \left(G \cdot u_c \cos \theta_{rcd} + H_s\right) \sin \theta$$

where $f_{D,pot}^x$ = mean wave drift coefficient in surge without current from potential theory [kN/m²]

$f_{D,pot}^y$ = mean wave drift coefficient in sway without current from potential theory [kN/m²]

C_p = wave-current interaction coefficient [s/m]. C_p is in the range 0.2-0.4. For column-stabilised units $C_p=0.25$. For ship shaped units, a higher value is recommended.

ω = wave frequency

θ = wave direction

θ_{rcd} = relative direction between waves and current

u_c = current velocity

H_s = significant wave height

$$B = B' \cdot D_{sum} \left[\text{kN/m}^3 \right]$$

$$B' = k \cdot \exp \left[-1.25 \cdot (k \cdot D_0)^2 \right] \left[\text{kN/m}^3 \right]$$

$$k = 2\pi/\lambda = \text{wave number} \left[\text{m}^{-1} \right]$$

$$\lambda = \text{wave length} \left[\text{m} \right]$$

$$D_{sum} = 4 \cdot D_0 \left[\text{m} \right]$$

$$D_0 = \sqrt{A_{wp}/\pi} \left[\text{m} \right]$$

A_{wp} = total waterplane area, [m²]

$G = 10$ [s].

Figure 4.14: Correction factor for viscous drift force from DNVGL-OS-E301 ed. July 2018 (DNV GL, 2018)

To obtain the presented results, the cross-bi-spectral analysis presented in earlier studies (Stansberg, 1997; Stansberg, 2001), is used to estimate the quadratic transfer function, QTF, in order to extract empirical wave drift coefficients. A brief description was also presented in Section 4.2.

Conclusions from the study with respect to the semi-submersible corresponding to the selected CatD C340 model (Semi C), are:

- Underestimation of wave drift forces by potential flow predictions at the low frequency range
- The EXWAVE semi-empirical formula tends to underestimate empirical wave drift coefficients between $0.07\text{-}0.09Hz$ for all currents.
- Current effects tend to increase wave drift forces at the low frequency range ($0.08\text{-}0.11Hz$).
- Viscous effects increases with increasing wave height and ocean current level
- Recommended to use a total damping level of 40-70% in system mooring design for semi-submersibles. Exception: thoroughly calibrated numerical models.
- Damping from viscous forces on the hull and mooring are the main contributors to LF damping in surge and sway

4.11 Load models

Three different alternatives for modelling LF wave excitation and damping have been utilized in this thesis. The first method is wave drift forces based on Newman's approximation, referred to as potential wave drift coeff. in the thesis. The second method is wave drift forces based on Newman's approximation in combination with corrected wave drift coefficients including current contributions and viscous effects, referred to as corrected wave drift coeff. The third method is wave drift forces based on Newman's approximation, however viscous loads are modelled using the drag term in Morison's equation. This method is referred to as slender element method.

4.11.1 Potential wave drift coeff

This method is based on Newman's approximation where the current force is modelled through quadratic current coefficients. The downside with this method is that viscous and current interaction effects on wave drift forces are neglected.

4.11.2 Corrected wave drift coeff

The theory for the correction formula method was elaborated in the previous section, with corrected potential wave drift coefficients to account for wave-current interaction and viscous effects. Same as for the potential wave drift coeff., this method includes the current contribution from given quadratic current coefficients as input for SIMA. The damping related to current coefficients originates from the relative velocity between the incoming current velocity and semi-submersible motions as elaborated in Chapter 4 (SINTEF Ocean, 2018b). However, wave drift damping is modelled by either linear or quadratic damping matrices.

4.11.3 Slender element method

Slender element method differs from both potential wave drift coeff. and corrected wave drift coeff. load modelling by introducing slender elements to account for the viscous forces and current contribution up to the actual wave surface. This is a load contribution related to the drag term in Morison's equation. By introducing slender elements, second order waves are considered by integrating wave forces up to the wave surface.

Free surface effects and wave-current interaction will together give the total contribution from current forces for slender elements. As mentioned in Section 4.2, the force contribution from currents introduces additional force and damping terms. This is one of the main reasons why motions of a mooring system is non-linear and hard to predict without simulations or experimental tests.

$$f_D = \frac{1}{2} \rho C_D D |(\bar{u} + U(z)) - (\dot{x}_{LF} + \dot{x}_{WF})| ((\bar{u} + U(z)) - (\dot{x}_{LF} + \dot{x}_{WF})) \quad (4.38)$$

Slender modelling includes contributions from the mean current velocity, \bar{u} , wave particle velocity, $U(z)$, and both LF and WF velocities of the semi-submersible, \dot{x}_{LF} and \dot{x}_{WF} , shown in Equation 4.38. WF contributions with regard to force calculation is found in the local centre of gravity for each of the slender elements strips, while others are related directly to the global centre of gravity. This can be seen in Figure 4.15, and the total contribution from forces and damping due to slender modelling is given in Equation 4.39 and 4.40.

$$F_{Di} = \int_z \frac{1}{2} \rho C_D(z) D dz |(\bar{u} + U(z)) - (\dot{x}_{LF} + \dot{x}_{WF}^{loc})| ((\bar{u} + U(z)) - (\dot{x}_{LF} + \dot{x}_{WF}^{loc})) \quad (4.39)$$

$$F_{Dtot} = \sum_{i=1}^N F_{Di} \quad (4.40)$$

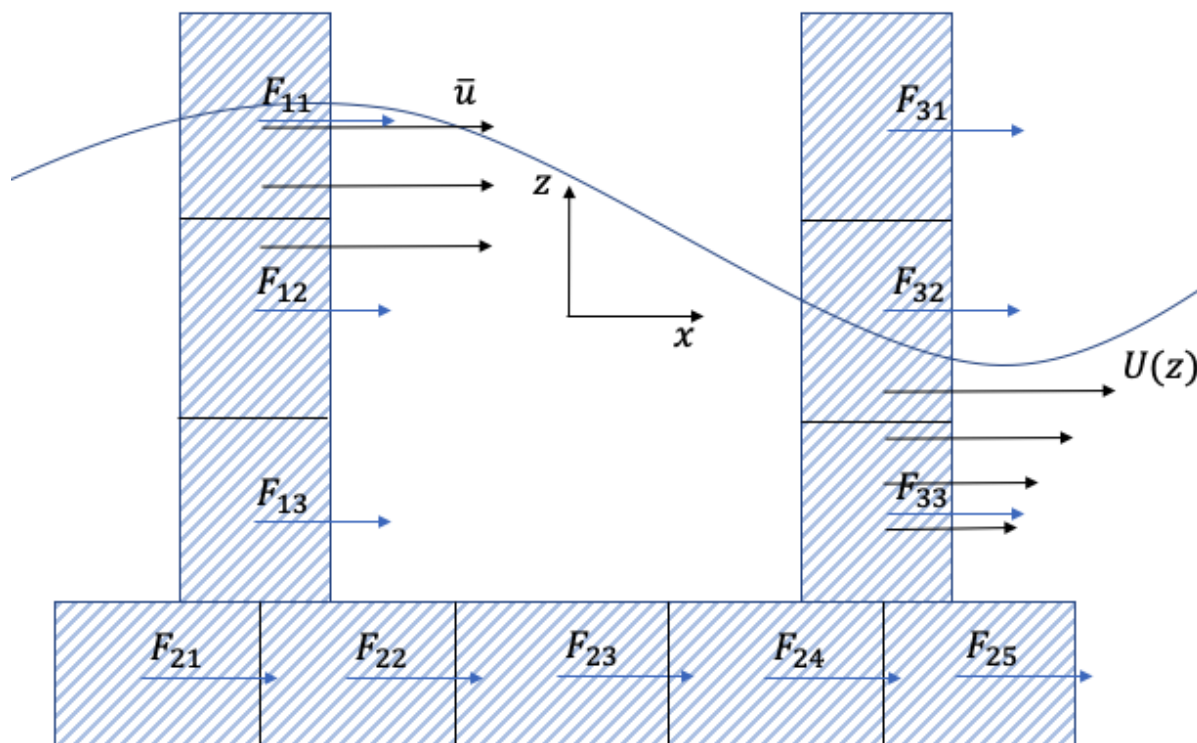


Figure 4.15: Illustration of how the drag forces are calculated with slender modelling

Equation 4.39 includes both wave induced water particle velocity, current velocity and wave and low frequency structure velocities. This is the complex equation that is solved for slender modelled structures with a number of strips per element.

4.11.4 Comparison and difference between the methods

The main difference between the two first methods and slender element modelling method, are how the forces and damping from current contribute to the systems motion. The two first methods base the force and damping from current by quadratic current coefficients which includes the current by its relative velocity component. However, they do not consider viscous hull damping on the structure. In SIMA, the quadratic current coefficients are formulated similarly as shown in Equation 4.41, where \bar{u} is the current velocity and cu signifies current.

$$K_{cu} = \frac{F_{cu}}{\bar{u}^2} \quad (4.41)$$

On the other hand, slender modelling includes the drag force and damping caused by the slender elements motion in the water which then affects the motions of the system. The formulations given in Equation 4.38 and 4.39, are the reformulated drag terms in Morison's equation presented in Section 4.8.

Chapter 5

Extreme value distribution

In design of mooring systems the most probable maximum tension, T_{MPM} , in the most heavily loaded mooring line is of specific interest (DNV GL, 2018). To calculate T_{MPM} for a mooring line, extreme value distributions of the global maxima are applied.

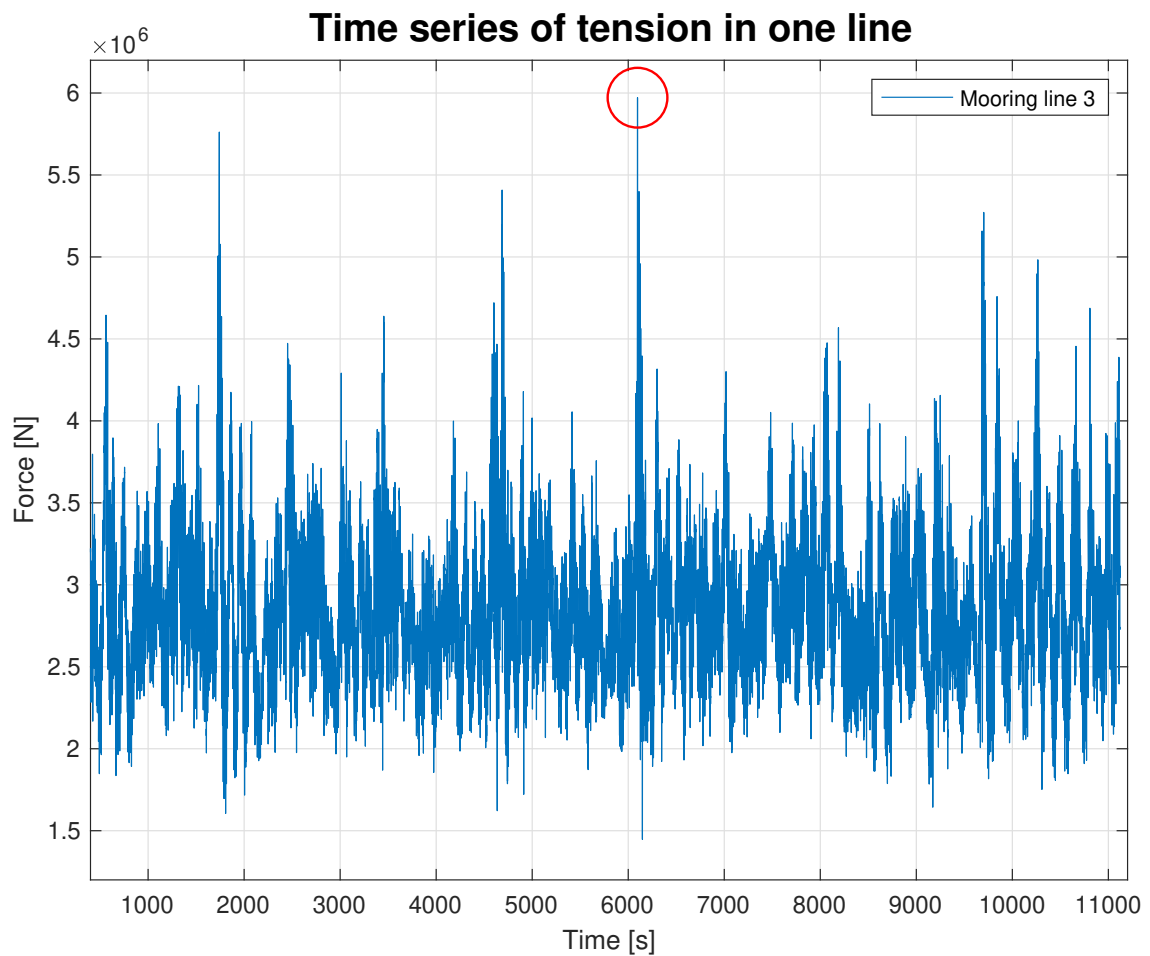


Figure 5.1: Measured axial force for an arbitrary time series, illustrates how to find global maxima for the time series

The individual maxima for each time series of the tension in the most heavily loaded mooring line is found as:

$$Y = \max\{x_1, x_2, x_3, \dots, x_n\} \quad (5.1)$$

The sample of the global maxima for each time series, $y_1, y_2, y_3, \dots, y_n$, are commonly presented by a Gumbel distribution which is suited for extreme value distributions (Leira, 2014). The cumulative distribution function and probability distribution function for Gumbel distributions follows Equation 5.2 and 5.3, respectively.

$$F_y(y) = \exp\{-e^{-\alpha(y-u)}\} \quad -\infty < y < \infty \quad (5.2)$$

$$f_y(y) = \alpha \exp\{-\alpha(y-u) - e^{-\alpha(y-u)}\} \quad (5.3)$$

Where α and u is the moment estimators, and y is the input parameter.

$$\alpha = \frac{1}{\hat{s}_y} \frac{\pi}{\sqrt{6}} = \frac{1.28255}{\hat{S}_y} \quad (5.4)$$

$$\begin{aligned} u &= \hat{\mu}_y - \hat{s}_y \frac{\sqrt{6}}{\pi} 0.57722 \\ &= \hat{\mu}_y - \hat{s}_y \cdot 0.45 \end{aligned} \quad (5.5)$$

The mean and standard deviation of the maxima sample are found by these basic equations.

$$\hat{\mu}_y = \frac{1}{N} \sum_{i=1}^N Y_i \quad (5.6)$$

$$\hat{s}_y = \sqrt{\frac{1}{N-1} \sum_{i=1}^N |Y_i - \hat{\mu}_y|^2} \quad (5.7)$$

Section 2.2.8 in DNVGL-OS-E301, states the following: *For the Gumbel distribution the most probable maximum, MPM, is given by*

$$MPM = \mu - 0.45\sigma \quad (5.8)$$

where μ and σ are mean and standard deviation of the peaks (i.e. the maximum observed from each simulation)(DNV GL, 2018). This formula is the exact same formula as presented in Equation 5.5 for the moment estimator, together with the other moment estimator α which is related to the spread of the distribution.

Chapter 6

System description

In this chapter the system description will be explained together with how the base design was established. The system design is based on Heidrun metocean design basis and the metocean study is the background with regard to wave height, wave period, weather direction, current and wind. The limitations and constraints during the system design will be elucidated in order to clarify possible inaccuracies in the obtained design and results.

6.1 Heidrun metocean design basis

For this thesis, the Heidrun metocean design basis is used, where in Table 6.1 below, the most relevant design parameters are presented.

Main parameters		
Significant wave height	16	[m]
Conditional spectral peak period	18.2	[s]
Wind speed	36	[m/s]
Surface current	1.05	[m/s]
Approximate water depth	350	[m]
Water depth used for design	341	[m]
Weather direction used in design	135	°

Table 6.1: Principle parameters from Heidrun metocean design basis (Statoil, 2004)

The parameters presented are based on the 100-years return period for waves and wind, together with 10-year return period for current. These values correspond to the environmental criteria (DNV GL, 2018) covered in Chapter 3.

To evaluate the worst weather condition possible, a collinear environment is applied for heading $\beta = 135^\circ$. Illustration of the headings are given in Figure 6.1 on the next page. Both waves, wind and current act in the same direction according to environmental loads outlined in section 2.5.5 in DNVGL-OS-E301.

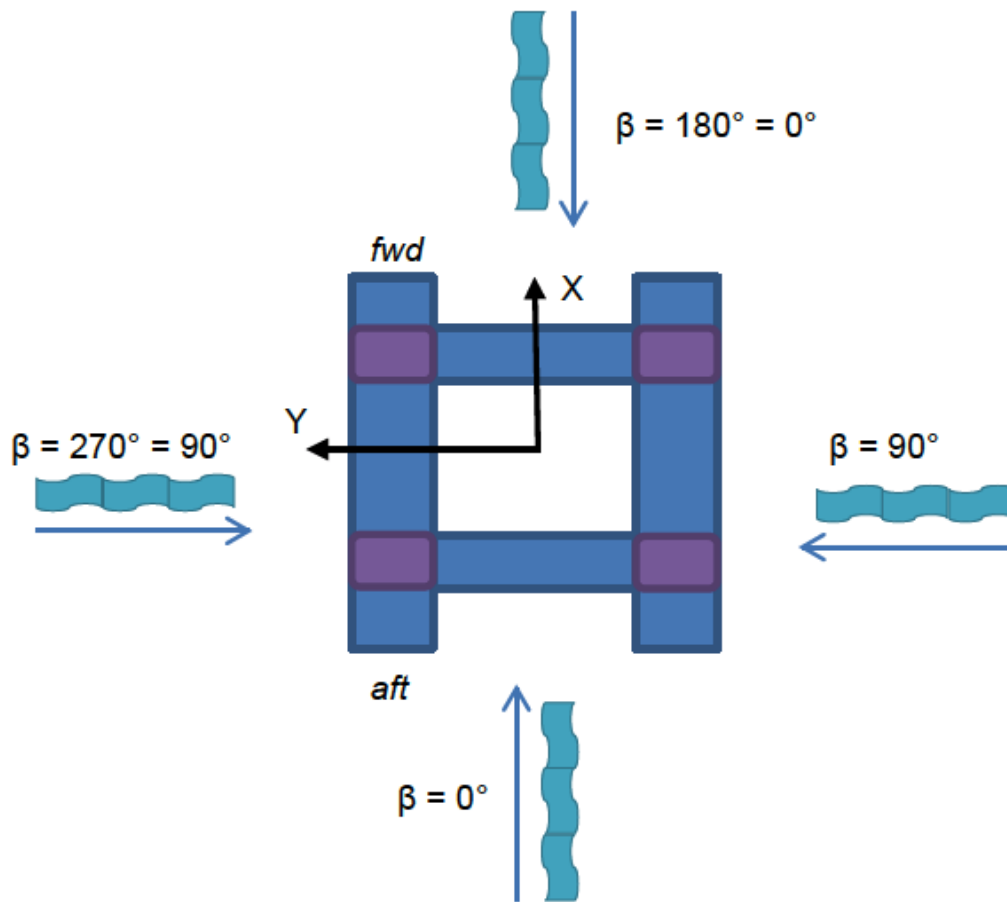


Figure 6.1: Heading direction of semi-submersible (Statoil, 2015)

6.2 Waves

The wave spectrum for the generated waves is a Jonswap spectrum where the input is as follows; significant wave height, peak period, spreading exponent and number of directions in spreading function. These are summarised in Table 6.1. Both spreading type and number of directions was set to default in SIMA, which are 2 and 11 respectively.

The sea state with the highest significant wave height, H_s , and the associated wave period, T_p , may not give the largest axial force in the mooring line. Optimally, a study with combinations of H_s and T_p from the contour plot and the corresponding maximal axial force in the mooring line should be carried out. Due to shortcomings in the design process which will be elaborated in Section 6.5, the significant wave height and wave period is based on the peak of the 100-years contour plot given from Figure 6.2.

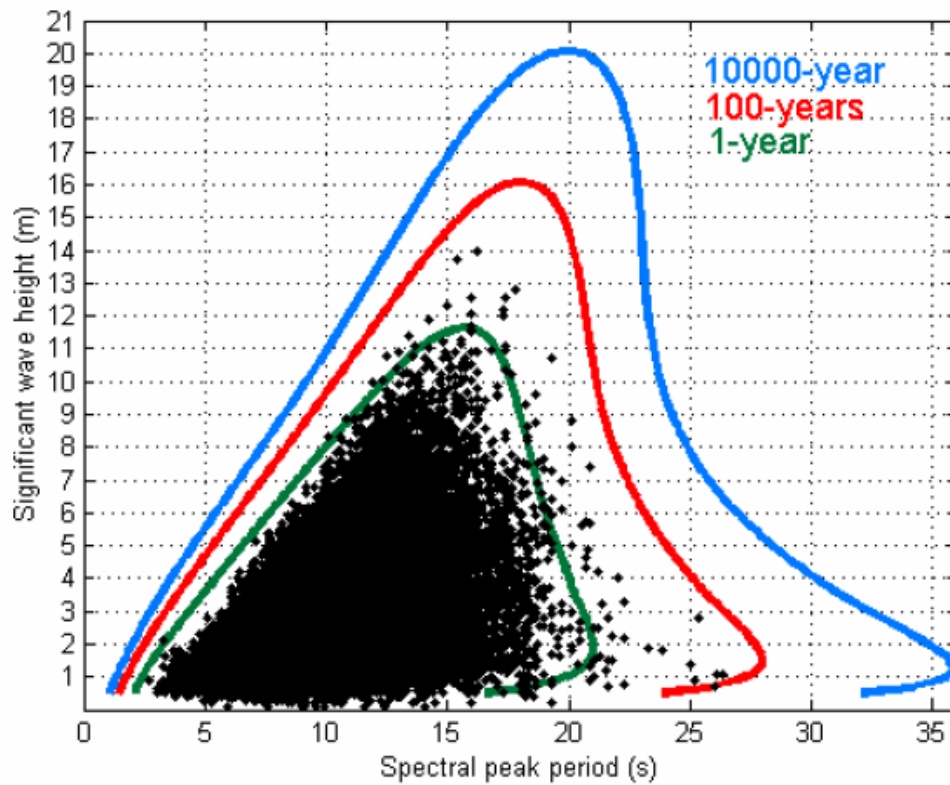


Figure 6.2: Contour plot, H_s - T_p plane (Statoil, 2004)

6.3 Wind

The wind input for the model is according to Table 6.1, with a wind speed of $36 \frac{m}{s}$. The direction for the wind is $\beta = 135^\circ$ as defined in the section above. In SIMA, the wind velocity is presented described by a spectrum called NPD wind spectrum. NPD stands for the Norwegian petroleum directorate, and the spectrum is according to the required input given by DNVGL-OS-E301 (DNV GL, 2018). With use of NPD, the mean one hour wind speed profile at height Z is:

$$\bar{V}_Z = \bar{V}_{10} \left[1 + C \ln \left(\frac{Z}{10} \right) \right] \quad (6.1)$$

where

$$C = 0.0573 \sqrt{1 + 0.15 \bar{V}_{10}} \quad (6.2)$$

6.4 The semi submersible

The model used in the thesis is a Cat D #3 semi-submersible, drilling rig. For the design of mooring system and simulations in this thesis, the rig is considered a pro-

duction rig. The reason is stated in Section 6.5. The semi-submersible consist of 2 pontoons, 4 columns and 2 blisters between the two pontoons. The main dimensions of the semi-submersible are presented in Table 6.2 and the hydrodynamic properties based on WAMIT calculations for the semi-submersible can be found in Appendix A.

Rig dimensions		
Pontoon length	114.4	[m]
Beam outside pontoon	76.7	[m]
Beam of pontoon	16.25	[m]
Height of pontoon	9.75	[m]
Column LxB (incl. blister)	18.85 x 16.25	[m ²]
Survival draught	19.15	[m]
Displacement	54770	[Te]
Water plane area	1202	[m ²]

Table 6.2: Principle dimensions for the semi-submersible

The semi-submersibles motions relative to the incoming waves are of given from a first order motions transfer function, RAO. The RAOs for the semi-submersible in 45 degrees heading is presented in Figure 6.3.

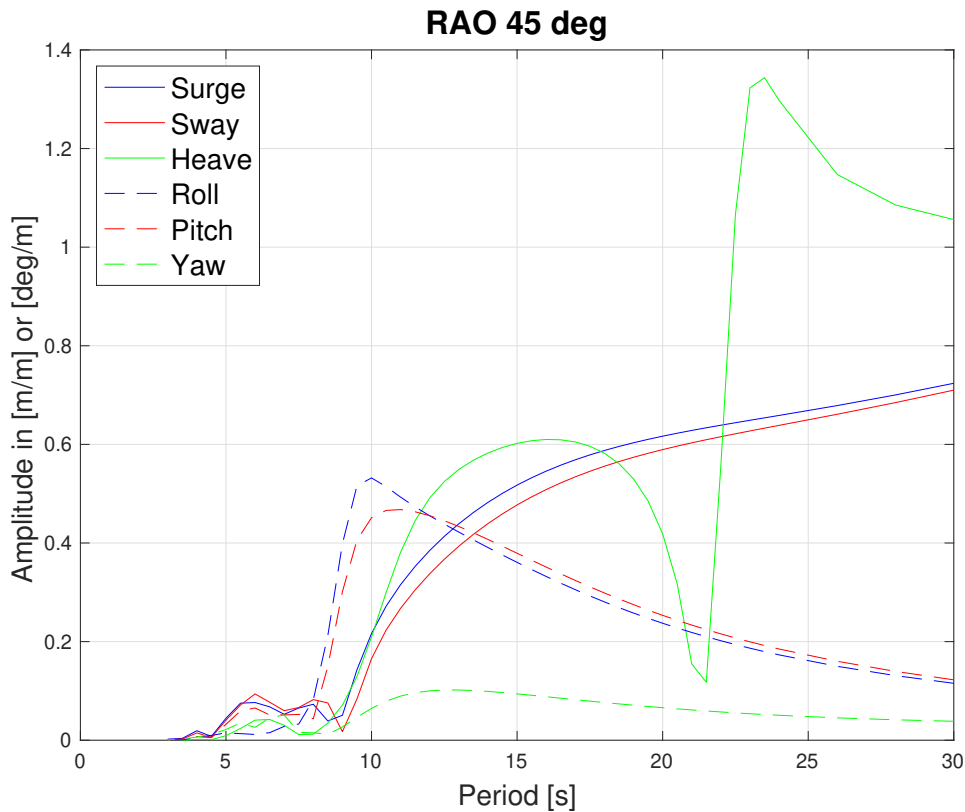


Figure 6.3: RAO for all six DOF for 45 degrees heading (Statoil, 2015)

6.5 Design of the mooring system

The design of the mooring system is an iterative process where the goal is to fulfil the requirements in DNVGL OS-E301. For this thesis the mooring system is designed with respect to the ULS partial safety factors given from Chapter 2. For each dimension of the chain, both the diameter, break load, weight, E-modulus changes. These changes have major impact on the characteristics of the system. In terms of design, a change in diameter for example, affects the pre tension of the mooring lines and ballast weight on the semi-submersible to correspond to the weight of the suspended chain in water.

The design process started in SIMO with the basis from the project thesis conducted during the autumn 2018 (Lied, 2018). The mooring system consisted of 12 mooring lines in four groups of triples in each corner of the semi-submersible, with 84mm R5 chain specified with a breaking load of 858Te. During the project thesis no model was designed, only validation of the existing model.

An agreement was reached with the supervisor Kjell Larsen about the semi-submersibles designation which changed from a drilling unit to a production unit. This gave the basis with respect to safety factors when it comes to design for permanent units instead of mobile units. In addition, SIMO is a software for motion study and station-keeping of multi-body systems which does not consider finite element method calculations (SINTEF Ocean, 2018b). Based on the aforementioned and operational standard given from section 4.2.2 in DNVGL-OS-E301, an extra 20% safety factor was added to each of the partial safety factors for the results obtained from SIMO. This gives an extra SIMO safety factor, $\gamma_{simo} = 1.2$.

The design of a new mooring system lead to several changes to the system arrangement. The chain changed from R5 to R4 as a basis for the design and number of mooring lines were increased from 12 to 16. An overview of the updated system is presented in Figure 6.4. The cluster centre is quartered to the production unit. In addition, there is a 5° angle between each of the mooring lines in each cluster. When designing with respect to ULS in SIMO, the design equation (Equation 3.3) is rewritten as given in Equation 6.3.

$$S_C - T_{pret} \cdot \gamma_{pret} \cdot \gamma_{simo} - T_{C-env} \cdot \gamma_{env} \cdot \gamma_{simo} > 0 \quad (6.3)$$

An overview of the iterative design process with respect to ULS and ALS is given in Appendix B. The input for each of the chain diameters are mostly obtained from Ramnäs Bruk Product Catalogue (Ramnäs Bruk, 2015) together with values given by instructions in DNVGL-OS-E301. A few other chain diameters were tested, but were rejected because of either a too large margin to the ULS design criteria or was unable to satisfy the design criteria.

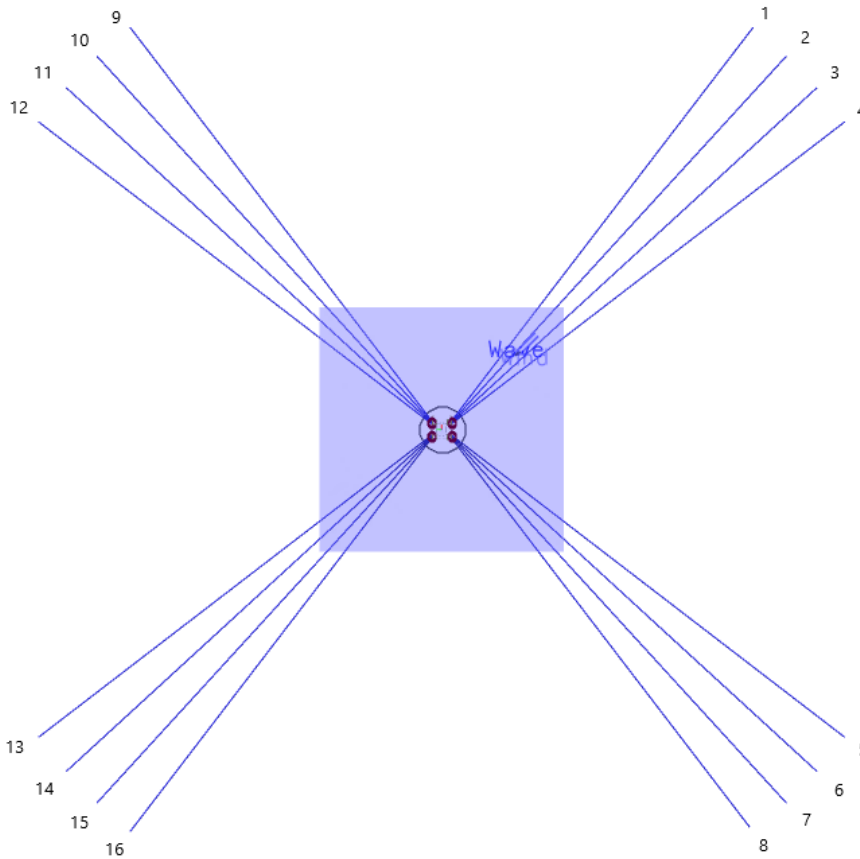


Figure 6.4: System overview

Due to non-linearities for the mooring lines, it is not easy to estimate which combination satisfies the regulations given from DNVGL-OS-E301. Therefore, an iterative process was utilized to obtain a design able to satisfy the ULS criteria with low margin. The results for the mooring system design in SIMO resulted in 16 mooring lines with 95mm studless R4 chains with a breaking strength of 918Te.

The next step in the design process was to export the model into RIFLEX. RIFLEX is a software that solves non-linear relations between global deformations and stress resultants in time domain (SINTEF Ocean, 2018a). In SIMO, the additional safety factor of 1.2 mentioned earlier, was used on both environmental loads and pretension loads. When designing in SIMO, the mooring lines were designed by chain dimensions as input. This is not possible in RIFLEX and the chain is therefore modelled as one continuous tubular object with a diameter equal the combined cross sectional area of two bars (Orcina Ltd, 2019). In addition, shackles and transitional components are not included in the model.

Table 6.4 is the results from the ULS check, where the diameter of 95mm did not fulfil the design criteria when similar loads were simulated in RIFLEX. This led to a new round of iterations. First, a 100mm was designed and analysed, and continued on to 105mm as the latter did not satisfy the partial safety factors in the offshore standard. The design parameters are shown in Table 6.3 and subsequent forces and design criteria are given in Table 6.4. Utilizing a diameter of 105mm was less optimal with regard to ULS design criteria than both 95mm and 100mm.

Diameter	95	100	105	[mm]
Chain type	R4	R4	R4	-
Break load	9001	9864	10754	[kN]
Pre tension	900.1	986.4	1075.4	[kN]
Weight in air	181	200	221	[kg/m]
Ballast	1.3e7	1.37e7	1.58e7	[N]
E-modulus	5.213e10	5.2e10	5.188e10	[Pa]
Total mooring line length	2000	2000	2000	[m]

Table 6.3: Input parameters for 95-105mm

Diameter	95	100	105	[mm]
Tabulated break load	9001	9864	10754	[kN]
Max axial force, simulated in RIFLEX	5800	6085	6910	[kN]
Environmental load	4900	5100	5830	[kN]
Results design equation	-1390	-1010	-1620	[kN]

Table 6.4: Results for 95-105mm

Due to the focus in this thesis, which are viscous models and not the design of an optimal mooring system. A decision with respect to chain grade was made to have a realistic design which fulfils the regulations. Together with supervisor Kjell Larsen, there was agreement of increasing the chain type from R5 chain instead of R4. Due to the increase in break load, the 95mm studless chain was utilized. With regard to chain grade, R5 was chosen due to a higher break load. Where for R5 the break load is 10512kN, while 9001kN for R4 (Ramnäs Bruk, 2015).

Consequently, a change from R4 to R5 chain did not result in any noticeable difference with respect to translations of the semi-submersible. With this configuration the maximum translation of the semi-submersible in sway direction was above 30% of the water depth, thus, the pre-tension of the semi-submersible increased from 10% to 15%. Resulting max translations are given in Table 6.5 alongside ULS check calculations.

ULS check		
Diameter	95	[mm]
Tabulated break load	10512	[kN]
Max axial force, simulated in RIFLEX	5971	[kN]
Environmental load	4355	[kN]
Result design equation	298	[kN]
Suspended mooring line length	1623.8	[m]
Total mooring line length	2000	[m]
Max translation surge	-48.5	[m]
Max translation sway	59.9	[m]

Table 6.5: ULS check 95mm R5 studless chain

The mooring line length of 2000m satisfies the criteria outlined in section 4.8.3, permissible line length in the offshore standard (DNV GL, 2018). This criteria states that maximum line length can be "*suspended line length at a line tension equal to the breaking strength of the line plus 500m*".

A check for ALS is also required, where the results are presented in Table 6.6. For the ALS check the most loaded mooring line, line 3, is removed. As shown in the table, the result of the design equation is below zero. But if the value is presented in terms of the utility factor (DNV GL, 2018), which is to be less than 1, the value is 1.00067. In percentage this equals 0.067% and hence, negligible.

ALS check		
Diameter	95	[mm]
Tabulated break load	10512	[kN]
Max axial force, simulated in RIFLEX	7750	[kN]
Environmental load	6140	[kN]
Result design equation	-265	[kN]
Max translation surge	-55.8	[m]
Max translation sway	67.9	[m]

Table 6.6: ALS check 95mm R5 studless chain

The final base design, presented in Table 6.7, has the following parameters.

Diameter	95	[mm]
Chain type	R5	-
Break load	10512	[kN]
Pre tension	1616	[kN]
Weight in air	181	[kg/m]
Ballast	1.3e7	[N]
E-modulus	6e10	[Pa]
Axial stiffness	8.506e8	[N]
Total mooring line length	2000	[m]

Table 6.7: Base design, 95mm studless chain

With the dimensions set, a direction check is run to ensure that the worst case scenario is investigated. It is important to mention that only one wave seed in the direction check was tested. For this case the waves, wind and current were applied from 0, 45 and 90 degrees in RIFLEX. 45° referred to in this situation is the same direction as $\beta = 135^\circ$ illustrated in Figure 6.1. The most critical direction was 45 degrees, the same direction as the first design was based on.

Weather direction	0	45	90	[°]
Line with maximum axial force	9	3	4	-
Max axial force, simulated in RIFLEX	4409	5971	4989	[kN]

To verify systems characteristics, decay tests were performed for all six DOF. This is done by applying a constant force or moment corresponding to the DOF, before removing said force or moment. The natural oscillation of the system is then measured. The obtained results are presented in Table 6.8, and the plots for surge and sway are shown in Figure 6.5 and Figure 6.6. The other four decay plots can be found in Appendix C.

Decay tests		
Response	Natural period	-
Surge	230.3	[s]
Sway	283.2	[s]
Heave	22.5	[s]
Roll	55.1	[s]
Pitch	50.8	[s]
Yaw	128.1	[s]

Table 6.8: Natural periods from decay

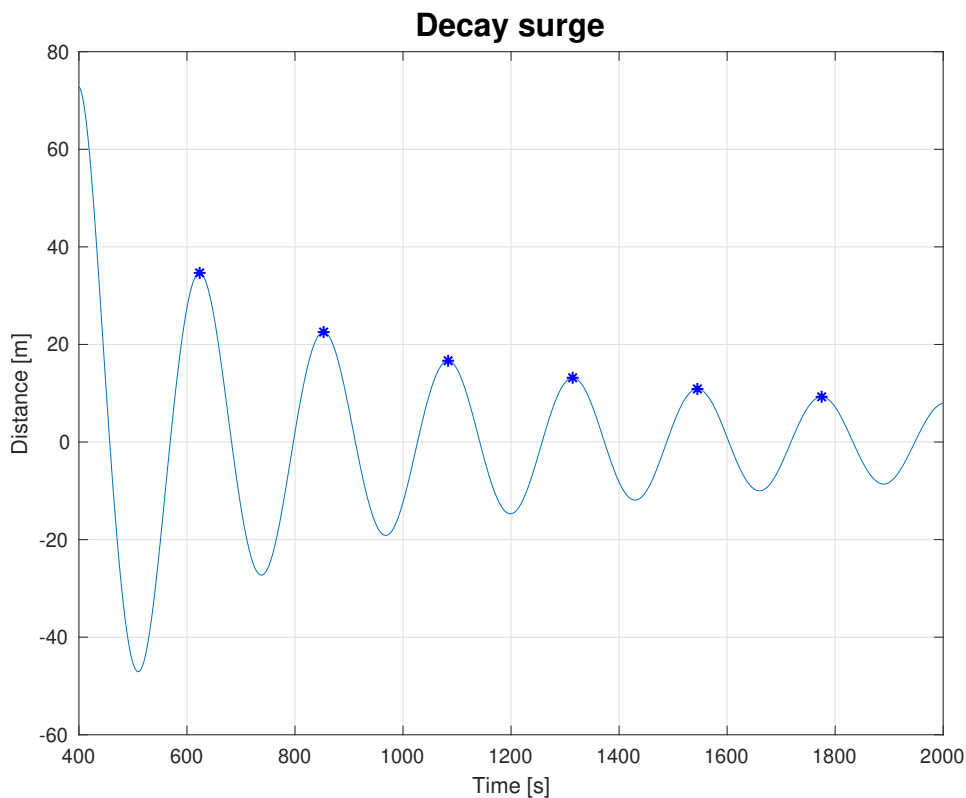


Figure 6.5: Decay for surge direction

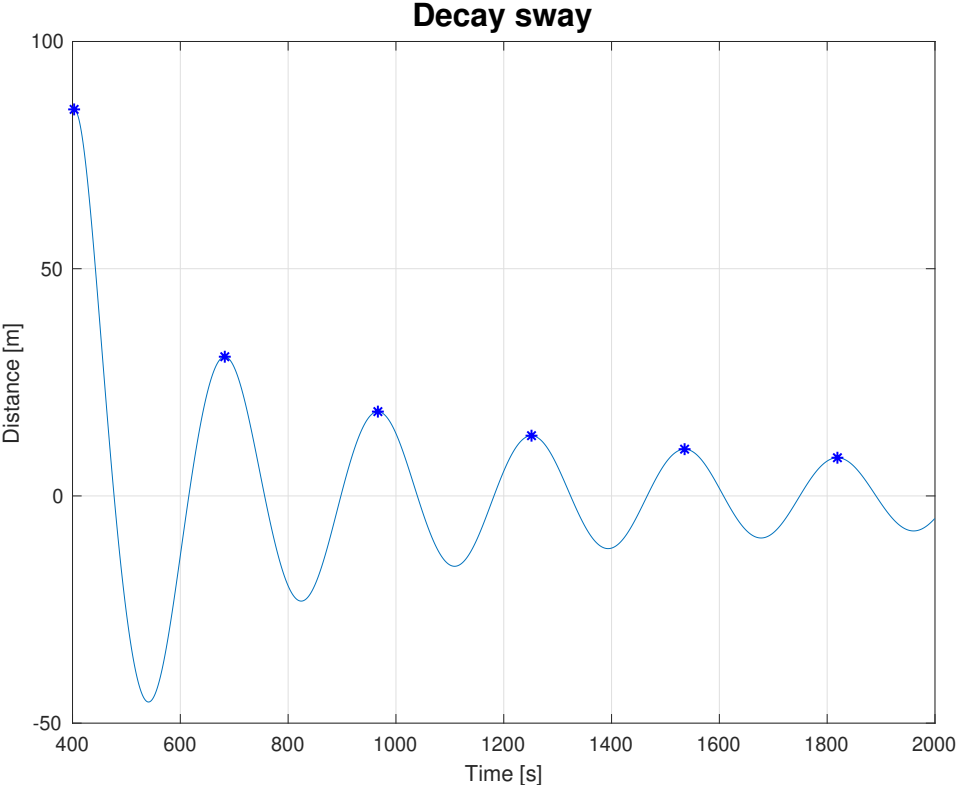


Figure 6.6: Decay for sway direction

To find the mooring systems stiffness, pullout tests were conducted for both surge and sway direction. The results are given in Figure 6.7 and in the following section.

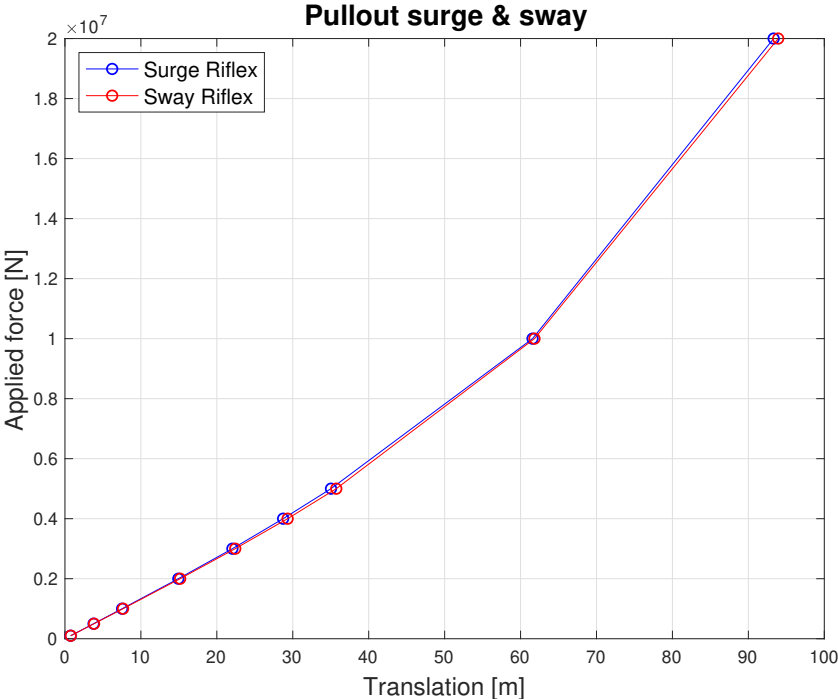


Figure 6.7: Pullout test

The formula for mooring system stiffness is the following for surge and sway direction. Where x and y are displacement in surge and sway, respectively. While $F_{x,y}$ is the force in surge and sway, respectively.

$$K(x, y) = \frac{F_{x,y}}{x, y} \quad (6.4)$$

From the obtained values the last value is omitted for calculation of mooring system stiffness. This is both due to non linearities with larger applied forces, and the semi-submersible is not designed to have larger translations than 60m according to ULS check.

Mooring system stiffness for surge and sway was found to be $139 \frac{kN}{m}$ and $137 \frac{kN}{m}$, respectively. This gives a critical damping of $6260 \frac{kNs}{m}$ for surge and $6230 \frac{kNs}{m}$ for sway. When this is compared to the model input in SIMA the system has a higher stiffness and higher mooring system damping than the input in the model. The model values are calculated by assuming viscous hull damping and mooring system damping are of equal magnitude (Larsen K., Vigesimal T., Bjørkli R., Dalane D., 2018), where viscous hull damping is calculated by $2 \cdot K_{cu} \cdot \bar{V}_{cu}$. Consequently, the contribution for both viscous hull damping and mooring system damping is $4 \cdot K_{cu} \cdot \bar{V}_{cu}$. Furthermore, wind damping is calculated by $2 \cdot K_{wi} \cdot \bar{V}_{wi}$. Wave drift damping in surge and sway is assumed to be approximately 30% of the viscous hull damping (Larsen K., Vigesimal T., Bjørkli R., Dalane D., 2018).

The total damping in surge and sway is found to be $2067 \frac{kNs}{m}$ and $4013 \frac{kNs}{m}$, respectively. This is equivalent to 33% of critical damping in surge direction and 64% of critical damping in sway direction. The formula for critical damping is $C_{cr} = 2 \cdot \sqrt{(M + A)} \cdot K_m$. With a change in pretension for the model of nearly 100%, the results may not be too surprising. From a paper presented in 2018, the total damping increased by 70% when the pretension was increased by 70% (Larsen K., Vigesimal T., Bjørkli R., Dalane D., 2018). Critical damping is closely related to the mooring system stiffness and therefore increases when the stiffness of the system increases. On the other hand, quadratic coefficients are independent of the system stiffness and thus, not affected by the change in critical damping. A result of this may give a relatively small damping ratio between the surge damping and the critical damping in surge.

To verify the system and ensure its robusticity, two sensitivity cases were performed. The first case was conducted for 2000m and 2200m length of the mooring lines. The results differed 3% in T_{MPM} when increasing the mooring line from 2000m to 2200m. An intuition was that T_{MPM} should be reduced when the mooring line length was increased. This was disproved and the difference in T_{MPM} is assumed to be negligible. Further simulations are completed with mooring line lengths of 2000m.

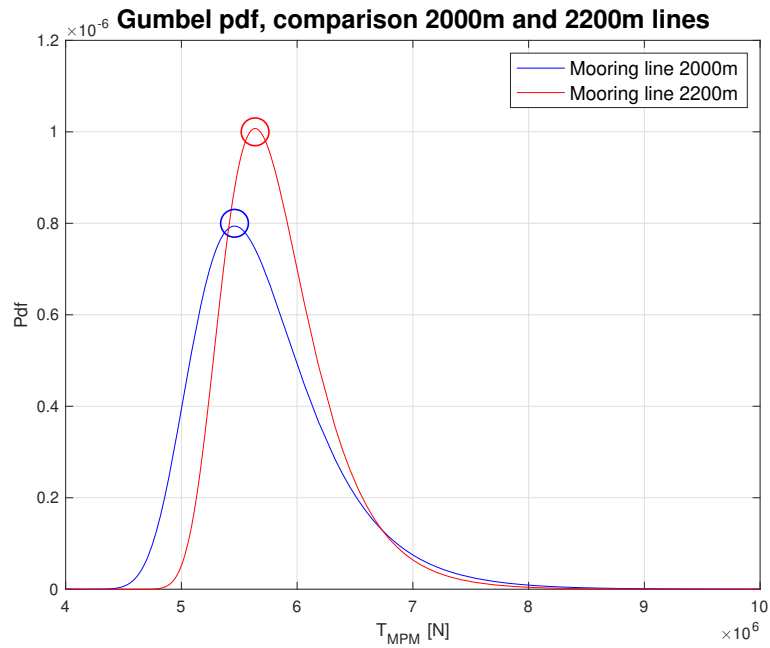


Figure 6.8: Sensitivity of line length

Another sensitivity case of interest is the number of wave seeds for the simulations. When the number of wave seeds are compared in terms of standard deviation for N number of simulations. Figure 6.9 is a comparison between the individual standard deviations and mean standard deviation for the N th number of the simulations. The change in standard deviation from 10 to 20 simulations is assumed to be negligible and a number of 10-20 simulations corresponds to section 2.2.8 in DNVGL-OS-E301 (DNV GL, 2018).

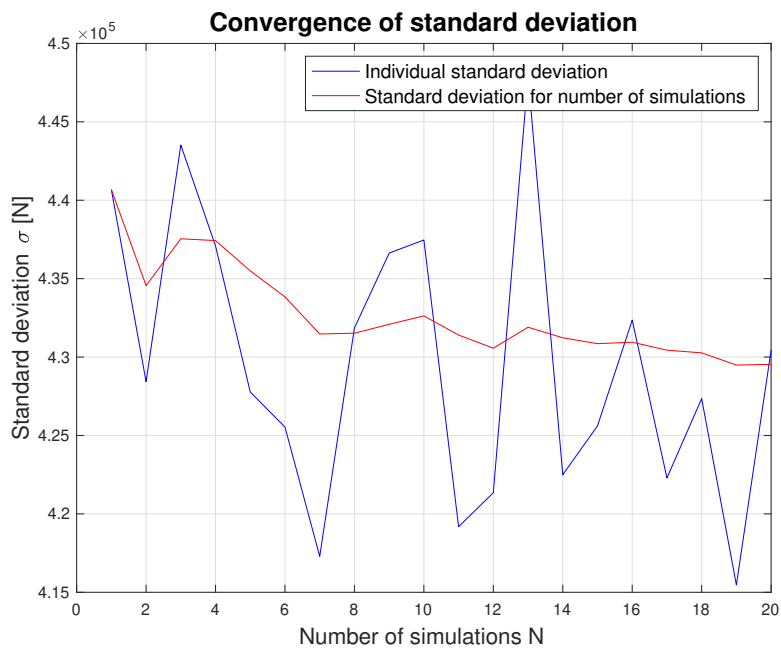


Figure 6.9: Convergence of mean standard deviation based on number of simulations N

Chapter 7

Numerical simulation

In this chapter the different simulation cases will be presented. There are a total of eleven cases with slightly different input parameters for some of them. The goal by simulating the different cases is to compare the results and to quantify the effects from different parameters. The results will be presented in the next chapter and the eleven cases which have been performed are the following:

- (a) Potential wave drift coefficient
- (b) Corrected wave drift coefficient
- (c) Base case C_D
- (d) EXWAVE C_D
- (e) Low C_D
- (f) High C_D
- (g) One strip C_D
- (h) No current
- (i) Mean wave elevation
- (j) No current and mean wave elevation
- (k) No slender elements

All simulations are conducted with 15 different wave seeds, corresponding to the number of simulations required in DNVGL-OS-E301 (DNV GL, 2018). The simulations are conducted in SIMA for a coupled SIMO-RIFLEX model, referred to as RIFLEX.

7.1 Potential wave drift coefficients

The basis for the analysis is the mooring system that was designed and presented in Chapter 6. This case is based on the model presented in Section 4.11. This way of executing the mooring system design was the industry practice until the EXWAVE JIP introduced the semi-empirical correction formula. The quadratic current coefficients utilized for both potential and corrected wave drift coefficients can be found in Appendix D.

7.2 Corrected wave drift coefficients

One of the concluding marks from phase I in the EXWAVE JIP, is the semi-empirical correction formula for viscous effects and current interaction effects was introduced. The formula was incorporated in DNVGL-OS-E301 (DNV GL, 2018) in the revised edition from July 2018 and is presented in Chapter 4. Potential wave drift coefficients and corrected wave drift coefficients is presented in Figure 7.1 and Figure 7.2 for surge and sway respectively. The calculation of the corrected wave drift coefficients follows the procedure presented in Section 4.10, Figure 4.14. Similar figures for surge 0 degrees and sway 90 degrees can be found in Appendix E. When evaluating the wave drift coefficients the deviation for the larger time periods implies that the contributions from the wave drift forces will be larger for periods in the range from 10s and above.

Input for the correction formula can be found in Appendix E, were the setup of the file is written in a format to match the wave drift coefficient input file in SIMA.

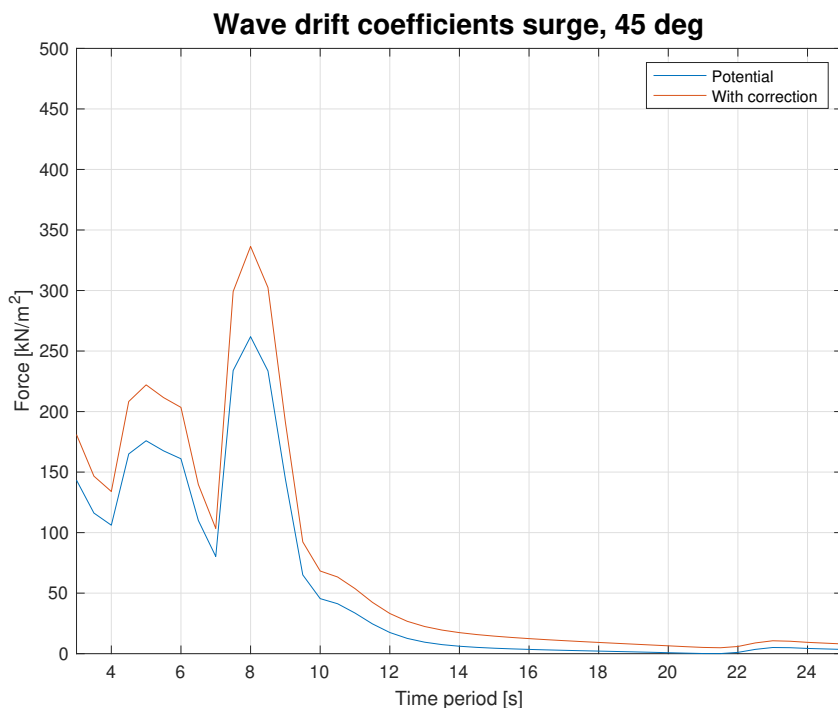


Figure 7.1: Wave drift coefficients surge 45 deg

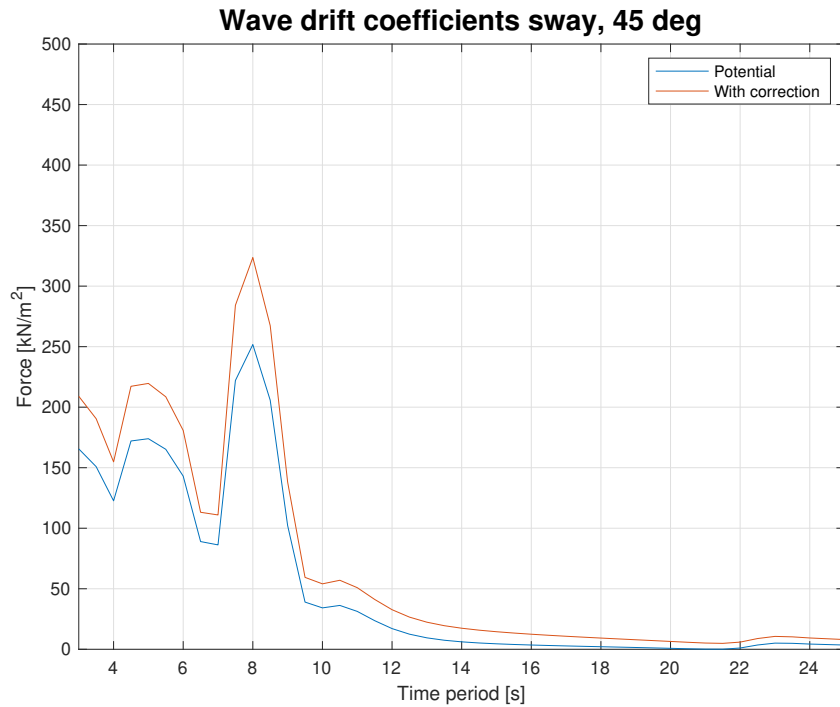


Figure 7.2: Wave drift coefficients sway 45 deg

7.3 Slender modelling

In the following section slender modelling for the semi-submersible is illustrated in Figure 7.3b with coordinates in Table 7.1. The slender elements are placed in the geometrical centre of the pontoon, column or blister given from Figure 7.3a. Pontoons, columns and blisters are denoted p,c and b respectively. These classifications are important when determining each elements drag coefficient.

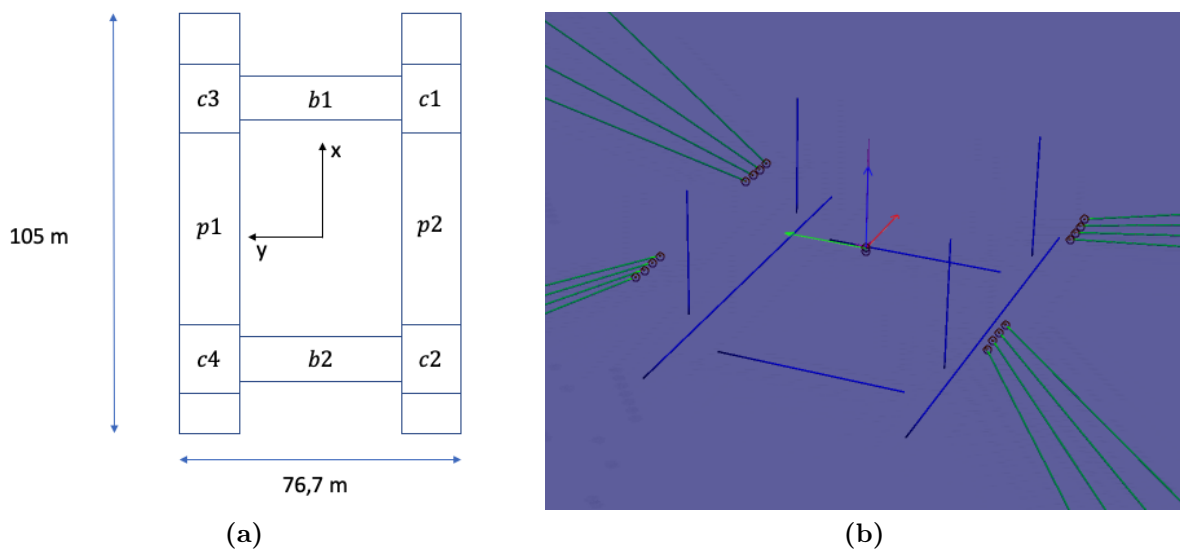


Figure 7.3: Slender elements and modelling of the elements in SIMA, (a) geometry definition, (b) slender elements

Coordinates for slender elements							
Slender element	End point 1 [m]			End point 2 [m]			Element length local x direction [m]
	x	y	z	x	y	z	
Column 1	30	-30	20.6	30	-30	-9.4	30
Column 2	-30	-30	20.6	-30	-30	-9.4	30
Column 3	30	30	20.6	30	30	-9.4	30
Column 4	-30	30	20.6	-30	30	-9.4	30
Pontoon 1	52.5	30	-14.275	-52.5	30	-14.275	105
Pontoon 2	52.5	-30	-14.275	-52.5	-30	-14.275	105
Blister 1	32	-22	-16	32	22	-16	44
Blister 2	-32	-22	-16	-32	22	-16	44

Table 7.1: Slender coordinates

All the cases including slender elements, except from the case named one strip, have the following number of strips per slender element:

- Columns consist of 10 strips
- Pontoons consist of 10 strips
- Blisters consist of 3 strips

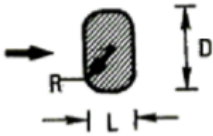
Geometry	Drag coefficient, C_D							
4. Rectangle with rounded corners 	L/D	R/D	C_D	L/D	R/D	C_D		
	0.5	0	2.5	2.0	0	1.6		
			0.021			2.2	0.042	1.4
			0.083			1.9	0.167	0.7
			0.250			1.6	0.50	0.4
	1.0	0	2.2	6.0	0	0.89		
			0.021			2.0	0.5	0.29
			0.167			1.2		
			0.333			1.0		
	$Re \sim 10^5$							

Figure 7.4: Drag coefficients, rectangle with rounded corners (DNV GL, 2017a)

In Figure 7.5, the method for choosing drag coefficients according to DNVGL-RP-C205, *Environmental conditions and environmental loads*, is shown for the different slender components (DNV GL, 2017a).

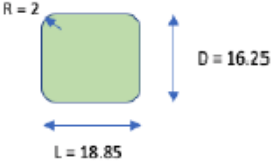
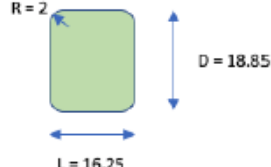
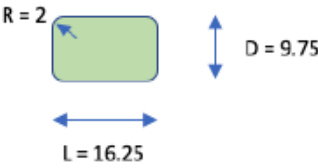
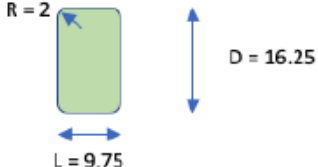

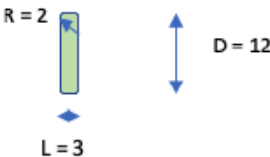
Element	Cross-section	L/D	R/D	CDs
Columns		≈ 1	0,12 \rightarrow 0,167	C _{dy}
		≈ 1	0,11 \rightarrow 0,167	C _{dz}
Pontoons		≈ 2	0,21 \rightarrow 0,167	C _{dy}
		$\approx 0,5$	0,12 \rightarrow 0,167	C _{dz}
Blisters		≈ 2	0,66 \rightarrow 0,5	C _{dy}
		$\approx 0,5$	0,167 \rightarrow 0,25	C _{dz}

Figure 7.5: Determination of drag coefficients based on Appendix E, geometry 4 in DNVGL-RP-C205

The values in Figure 7.5 are based on the geometry of the slender elements presented in Figure 7.3 and Table 7.1. It should be mentioned that the pontoon slender elements are modelled with straight edges, hence, the length of the pontoons are calculated with 105m instead of 114.4m. For columns and pontoons the choice of L/D and R/D is straight forward, but for blisters the choice of L/D has a large impact on the drag coefficient. The drag coefficients in Figure 7.4 shows the difference in outcome for blister drag coefficients if L/D is rounded up to $L/D = 6$ instead of rounded down to $L/D = 2$.

Although the choice of drag coefficients seems to be straight forward based on the geometry, this is not necessarily true.

7.3.1 Selecting drag coefficients

When deciding the drag coefficient for an applicable case there are some considerations that should be included. Drag coefficients are dependent on Reynolds number, Rn , Keulegan-Carpenter number, KC , and the roughness number, Δ .

$$C_D = C_D(Rn, KC, \Delta) \quad (7.1)$$

For simplicity in the numerical simulations, Rn and Δ are assumed to be constant and the drag coefficients will be adjusted with respect to the KC number.

In DNVGL-RP-C205 the drag force is defined as described in Chapter 4.9, in drag force per unit length

$$f_D = \frac{\rho}{2} C_D D |u|u \quad (7.2)$$

The definition of KC number for infinite water depth can be written in terms of surface elevation, ζ_a and the diameter, D , of the cylinders for a semi-submersible (Hildebrandt et al., 2009).

$$KC = \pi \cdot \frac{H}{D} = 2\pi \cdot \frac{\zeta_a}{D} \quad (7.3)$$

For circular cylinder drag coefficients with a KC number lower than 10 will roughly follow a straight line from zero to $C_D = 2$ (Larsen, 2018). With KC numbers in the area of 4-10 for the semi-submersible, it is reasonable to select drag coefficients in this region from Figure 7.6.

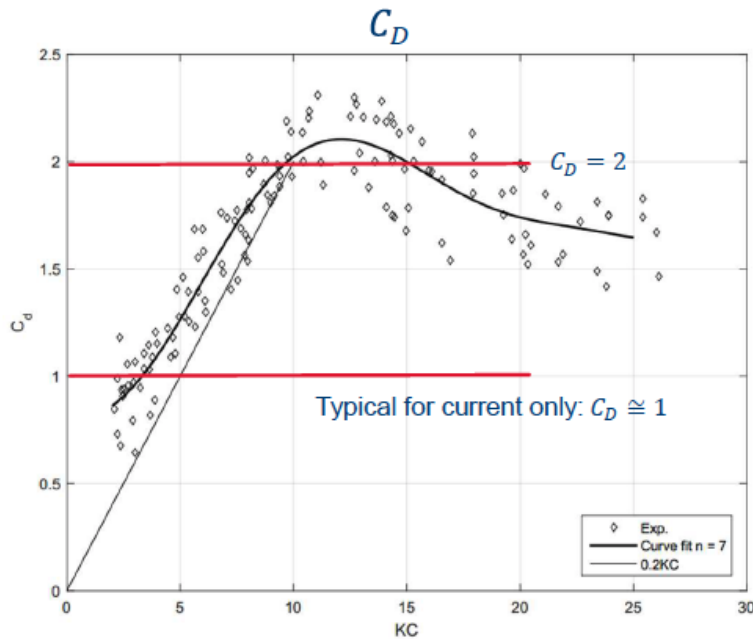


Figure 7.6: Drag coefficients as a function of KC numbers (Larsen, 2018)

The input to SIMA for the quadratic drag terms is defined as

$$C_2 = \frac{1}{2}\rho C_D D \quad (7.4)$$

With the local x-direction defined out of the plane for the cross sections illustrated in Figure 7.5.

7.3.2 Base case C_D

For the base case C_D of the slender modelling, the drag coefficients are based on the current coefficients which were included in the model for this semi-submersible. Despite the attempt to fit the drag coefficients to the current coefficients included in the model, the basis from Figure 7.5 and KC number is taken into account.

$$A_{Dsurge} \cdot C_D = 4 \cdot A_{col} \cdot C_{Dcol} + 2 \cdot A_{pon} \cdot C_{Dpon} + 2 \cdot A_{blis} \cdot C_{Dblis} \quad (7.5)$$

$$C_{quad,surge} = A_{Dsurge} \cdot C_D \cdot 0.5 \cdot \rho \quad (7.6)$$

Utilizing the formulas presented in Equation 7.5 and 7.6 the following values were obtained for $C_{quad,surge}$ and $C_{quad,sway}$;

Comparison quadratic drag SIMA and slender				
Quadratic drag SIMA		Quadratic drag slender		
Surge	Sway	Surge	Sway	
4.08e5	8.19e5	4.95e5	1.99e6	$[Ns^2/m^2]$

The relative deviation in sway is clear, whether or not this effect is substantial will be investigated in the results. With respect to the presented evaluations, the drag coefficients for base case is presented in Table 7.2.

Drag coefficients base case				
	C_{dy}	C_{dz}	C_{2y}	C_{2z}
Columns	1.2	1.2	9993.8	11593
Pontoons	0.7	1.6	3497.8	13325
Blisters	0.4	1.0	1383	5535

Table 7.2: Slender base case C_D

7.3.3 EXWAVE JIP C_D

The drag coefficients for this simulation is based on the recommended coefficients presented in the *Handbook on low-frequency wave forces and response - guidelines and recommendations* (DNV GL, 2017b). The geometry is assumed to be close to similar to the semi-submersible examined in this thesis and therefore it is of interest to simulate the drag coefficients obtained from this study.

Drag coefficients EXWAVE JIP				
	C_{dy}	C_{dz}	C2y	C2z
Columns	1.1	1.1	9161	10627
Pontoons	1.0	1.2	4997	9993.8
Blisters	1.0	1.0	1537.5	6150

Table 7.3: Drag coefficients from EXWAVE jip

7.3.4 Low C_D

For the low C_D case, the drag coefficients for columns and pontoons are reduced compared to base case C_D . The selected values are still within the same area of magnitude related to KC numbers, but in the lower range of C_D 's.

Drag coefficients low C_D				
	C_{dy}	C_{dz}	C2y	C2z
Columns	1.0	1.0	8328.1	9660.6
Pontoons	0.4	1.2	1998.8	9993.8
Blisters	0.4	1.0	1383	6150

Table 7.4: Drag coefficients for low C_D

7.3.5 High C_D

Based on the same arguments as for the low C_D , the high C_D case is in the upper range for applicable drag coefficients related to KC number. The drag coefficients for this case is for most of the elements the double of the base case C_D and it is interesting to see how this will affect the models behaviour.

Drag coefficients high C_D				
	C_{dy}	C_{dz}	C2y	C2z
Columns	2.2	2.2	18322	21253
Pontoons	1.6	2.2	7995	18322
Blisters	2.2	1.4	3382.5	8610

Table 7.5: Drag coefficients for high C_D

7.3.6 One strip

The configuration for this simulation uses the same drag coefficient input as the base case. However, the number of strips per element is reduced to one. This is to quantify the effect with regard to second order waves with integration of wave forces to wave surface.

7.3.7 No current

Another case of interest is to remove the current input and see how it affects the motions of the semi-submersible and tension in the mooring lines.

7.3.8 Mean wave elevation

For the case with mean wave elevation the base case C_D is used, but for calculations in the wave zone the mean water level is basis for the calculations instead of second order waves with integration of wave forces to wave surface.

7.3.9 No current and mean wave elevation

For this case the current is removed and the calculation is based on mean wave elevation, thus, second order wave with integration of wave forces to wave surface are not included.

7.3.10 No slender

This is a case without any slender elements and no quadratic current coefficients. The case is carried out based on curiosity to see how this affects the simulation. Which may tell something about the impact of the slender elements both with respect to forces and damping of the system.

Chapter 8

Results and discussion

For the motions presented in this chapter, a time step of 0.5s are saved from the analysis. The simulation time for each wave seed is 11200 seconds. For the forces presented in this chapter, all simulations are performed with a time step of 0.05s. Similar to the motions, a simulation time of 11200 seconds is conducted. The 400 first seconds of the simulations for both the motions and forces are omitted as a part of the post-processing, except from the realizations presented in Figure 8.1, 8.2, 8.10 and 8.11. The omitted section of the simulation is due to the initial conditions do not represent the desired sea state.

In this chapter semi-submersible motions and most probable maximum tension in the most loaded mooring line for each of the simulated cases will be presented. According to the definitions given by DNVGL-OS-E301, all simulations presented in this chapter are based on ULS with respect to 100 year significant wave height and wind speed, and 10 year current speed. All simulations are conducted in a collinear environment with a weather direction as defined in Section 6.1.

Results of the eleven cases will be given next. Aspects and considerations of the results will be discussed alongside with the presented results.

First, a comparison of the motions for all eleven cases is highlighted. The comparison is presented in Figure 8.3 as the power spectrum of the sway motions for all the eleven cases, based on 15 wave seeds for each of the simulated case. For some of the cases only 14 seeds were completed and hence, the presented values does not follow the formulated order in Chapter 7. These are the one strip and no current case. Furthermore, one case with slender elements and one case without slender elements is focused on to determine the effect of using slender elements.

8.1 Motions

The trend for all cases are highlighted with one realization from modelling without slender elements (corrected wave drift coefficients) and a case with slender elements (base case C_D). Corrected wave drift coefficient case is chosen due to its deviating statistical results presented in Figure 8.6 and base case C_D has similar statistical results for nearly all cases with slender elements. Realizations of the sway translational motions for the corrected wave drift coefficients is presented in Figure 8.1 and the slender base case C_D is presented in Figure 8.2.

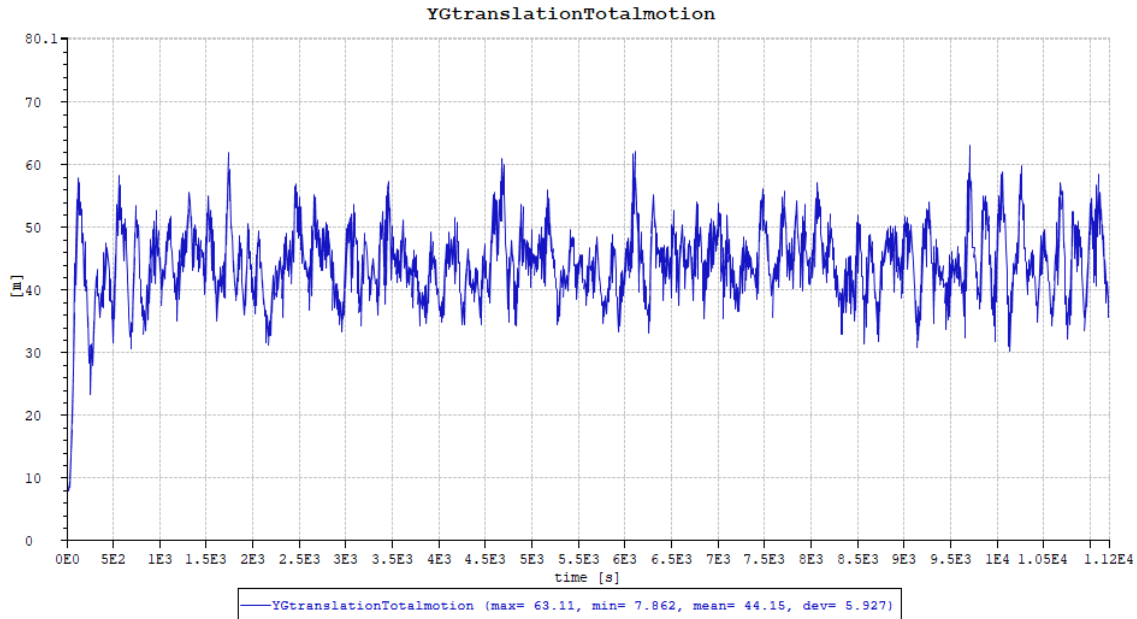


Figure 8.1: Realization of translational motions for case with corrected wave drift coefficients

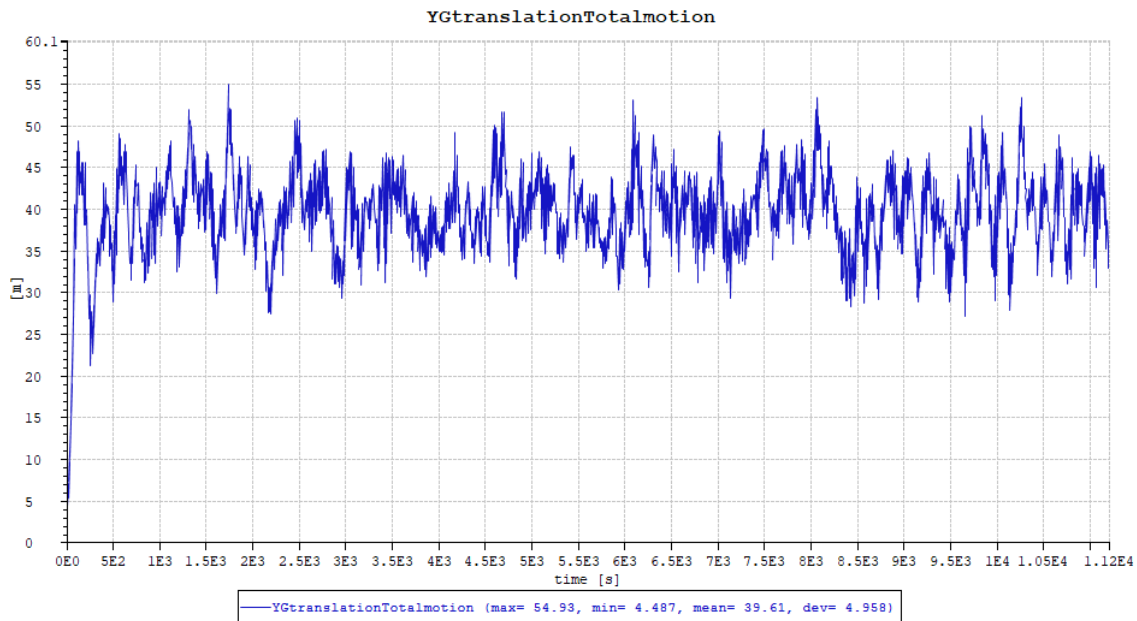


Figure 8.2: Realization of translational motions for base case C_D

By comparing translational motions in Figure 8.1 and Figure 8.2, there is a close correlation between the motions and the majority of the peaks. Nonetheless, there are variations in the motions resulting in larger mean translation for the case without slender elements. With a mean of 44m for the corrected wave drift coefficients and 40m for the base case C_D , the deviation in displacement is 10% between the two cases. Statistics for the LF sway motions are presented in Figure 8.6. There is reason to believe the deviation in mean value is related to the effect of modelling slender elements instead of the quadratic current coefficients. This is based on the case with corrected wave drift coefficients where linear and quadratic damping in surge and sway are not modified. Another consideration is the result of semi-empirical formula which increases the wave drift forces based on current interaction and viscous effects. Therefore, with increasing forces in combination with an unmodified damping the translational motions may increase relatively more than they should.

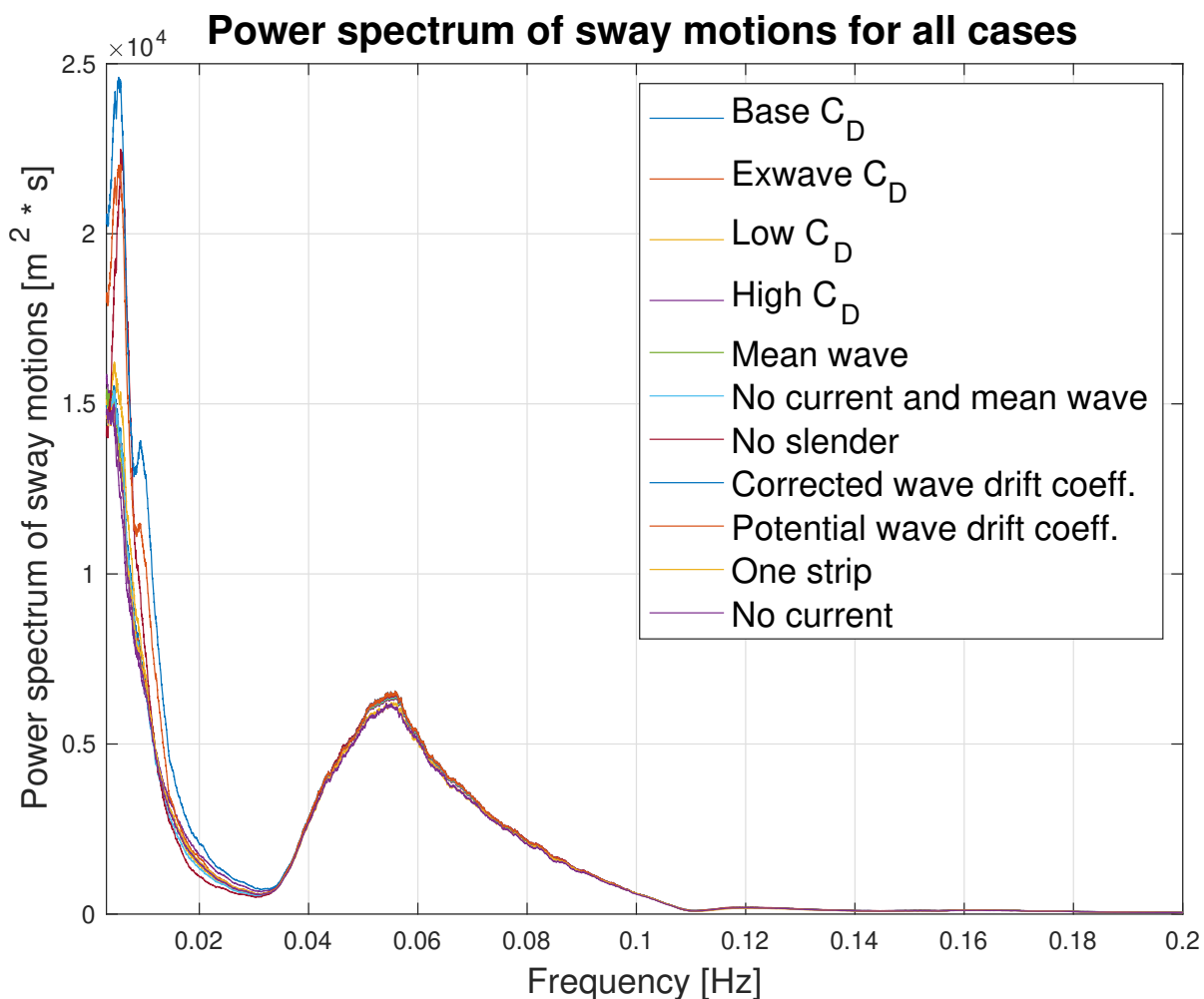


Figure 8.3: Power spectrum of sway motions for all cases

When the sway motions of the two cases are compared in a power spectrum, it can be seen that both the cases have a significant energy peak for both the LF and the WF contribution given in Figure 8.3. In combination with the realizations of the translational motions it can be seen that the erratic behaviour of the base case C_D does not affect the

mean offset for the semi-submersible. In fact, the opposite occurs and the base case C_D has a lower mean drift than the other case.

In addition, it is also observable that the power spectrum is reasonably similar for all cases, with one peak close to $T_p = 18.2s$ at $0.055Hz$ and one peak for the low frequency region above $30s$. Low frequency contributions on the corrected wave drift and potential wave drift coefficient seem to experience a higher peak than the other cases which. This may be related the damping of the system which has formulary discussed earlier in the section.

From Figure 8.4 and 8.5 the difference in heave motion is illustrated for the same cases as mentioned above, base case C_D and corrected wave drift coefficients. The standard deviation is $2.16m$ and $2.56m$ for base case C_D and corrected wave drift coefficient respectively. The reason for the difference in heave motions is believed to originate from the viscous hull damping when the slender elements experience heave translations. Which is due to the additional drag which originates from the drag coefficients defined in the slender modelling. Whereas the corrected wave drift coefficients are only defined in surge, sway and yaw.

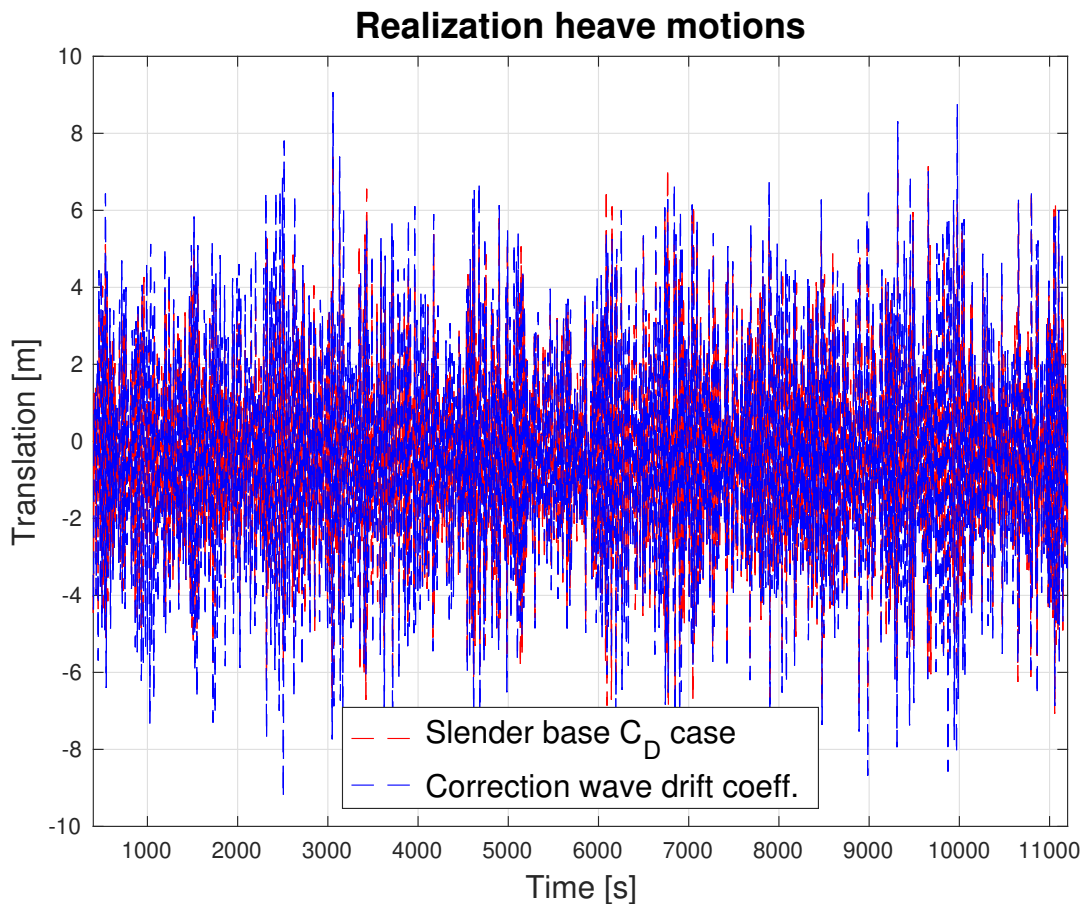


Figure 8.4: Realization of heave motions for cases with and without slender

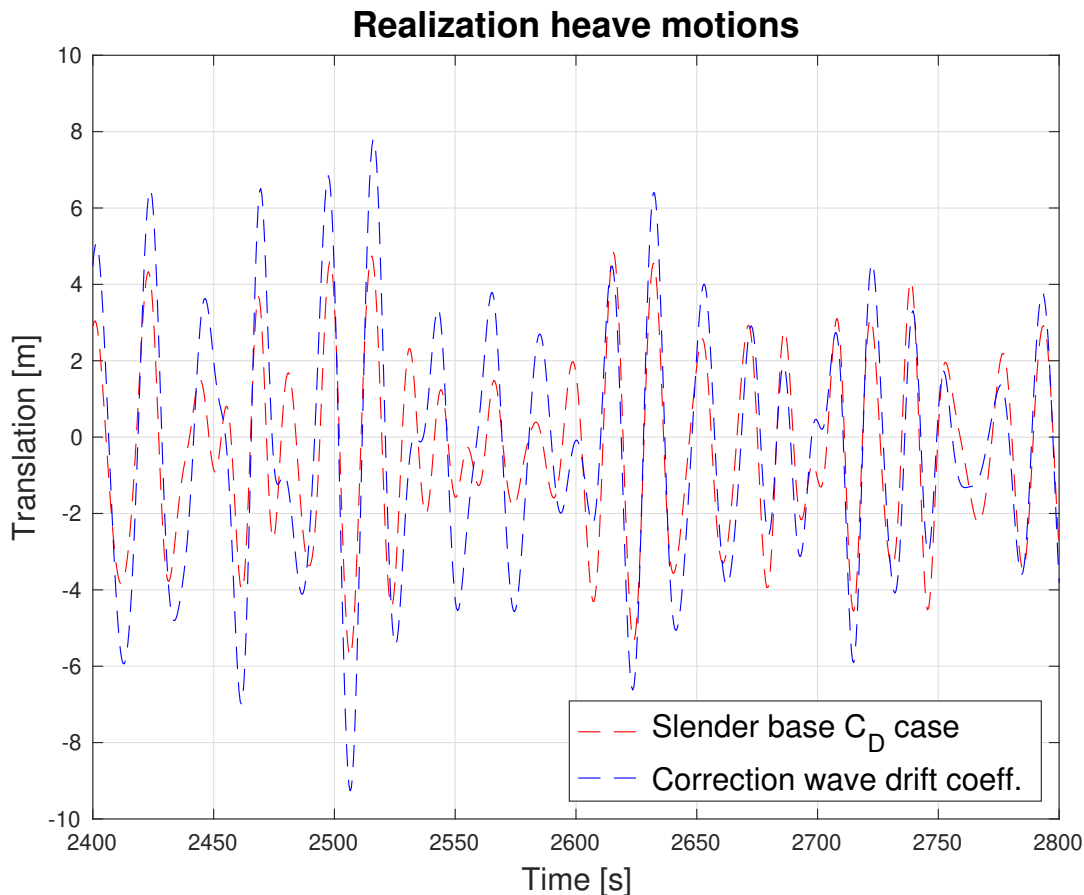


Figure 8.5: Zoomed realization of heave motions

The effect of added drag can also be shown in the statistics of the sway motions in Figure 8.6. The maximum values for the cases with quadratic current coefficients experience larger extreme sway translations than the other cases simulated. This is also believed to be contributed to the reduced damping as formulary discussed. Thus, the semi-submersible is able to move further when LF and WF waves occur in unison. In addition, the quadratic current coefficient in sway is up to three times as large as its surge counterpart for directions between $40\text{-}50^\circ$. This can be viewed in Figure D1 in Appendix D. Therefore requiring more restoring force to bring the semi-submersible back into mean drift position.

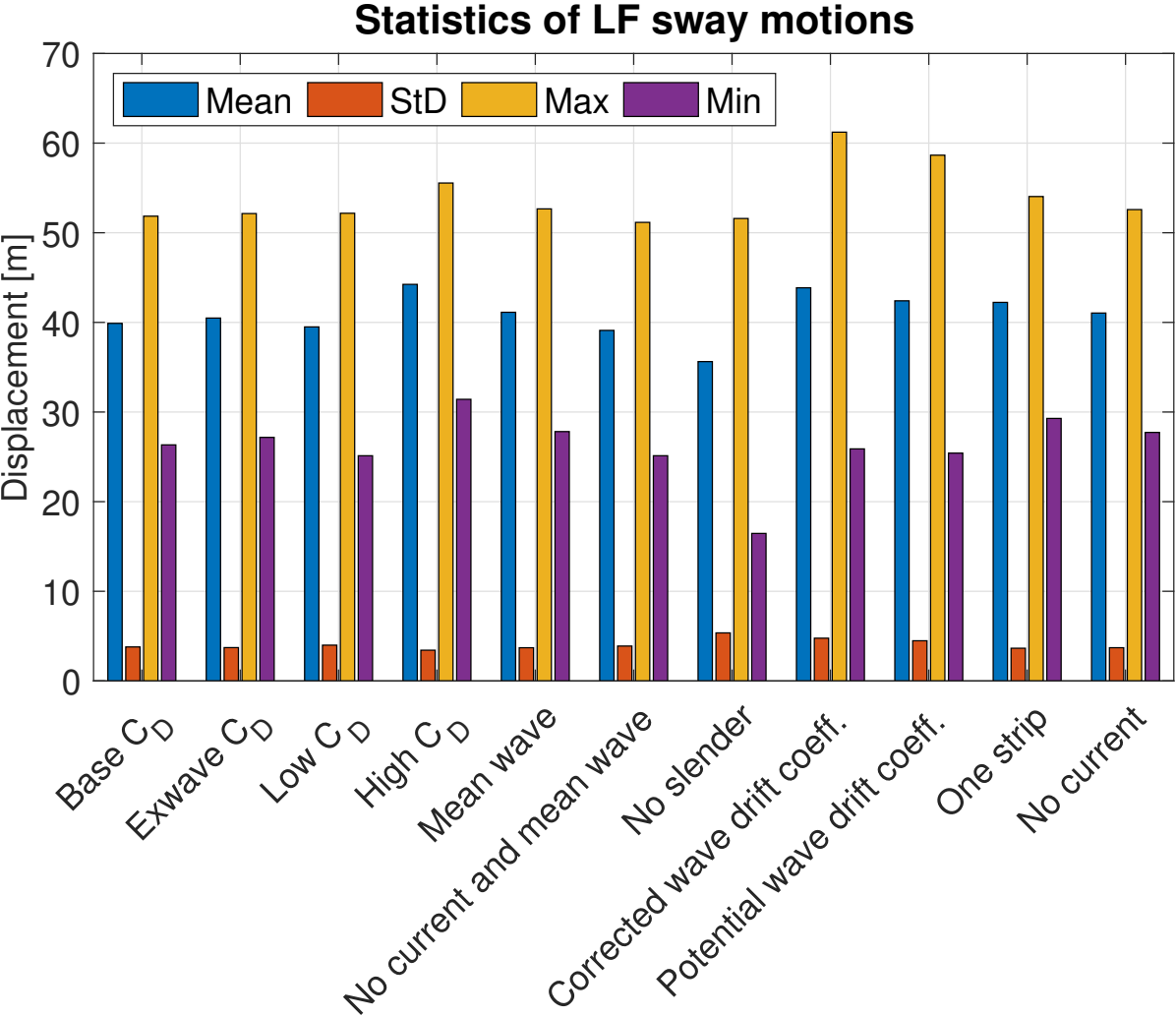


Figure 8.6: Statistics for LF sway motions, all cases

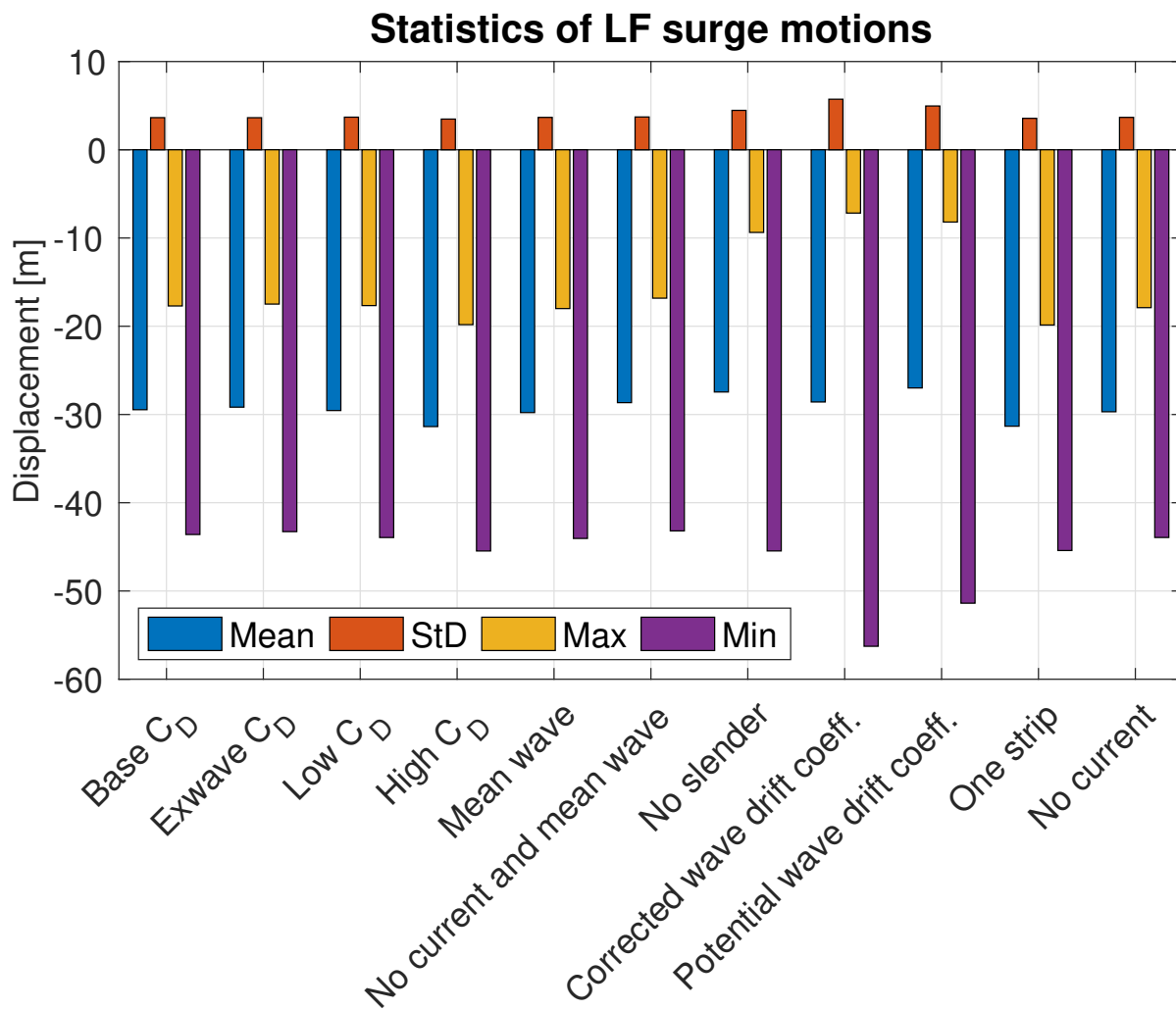


Figure 8.7: Statistics for LF surge motions, all cases

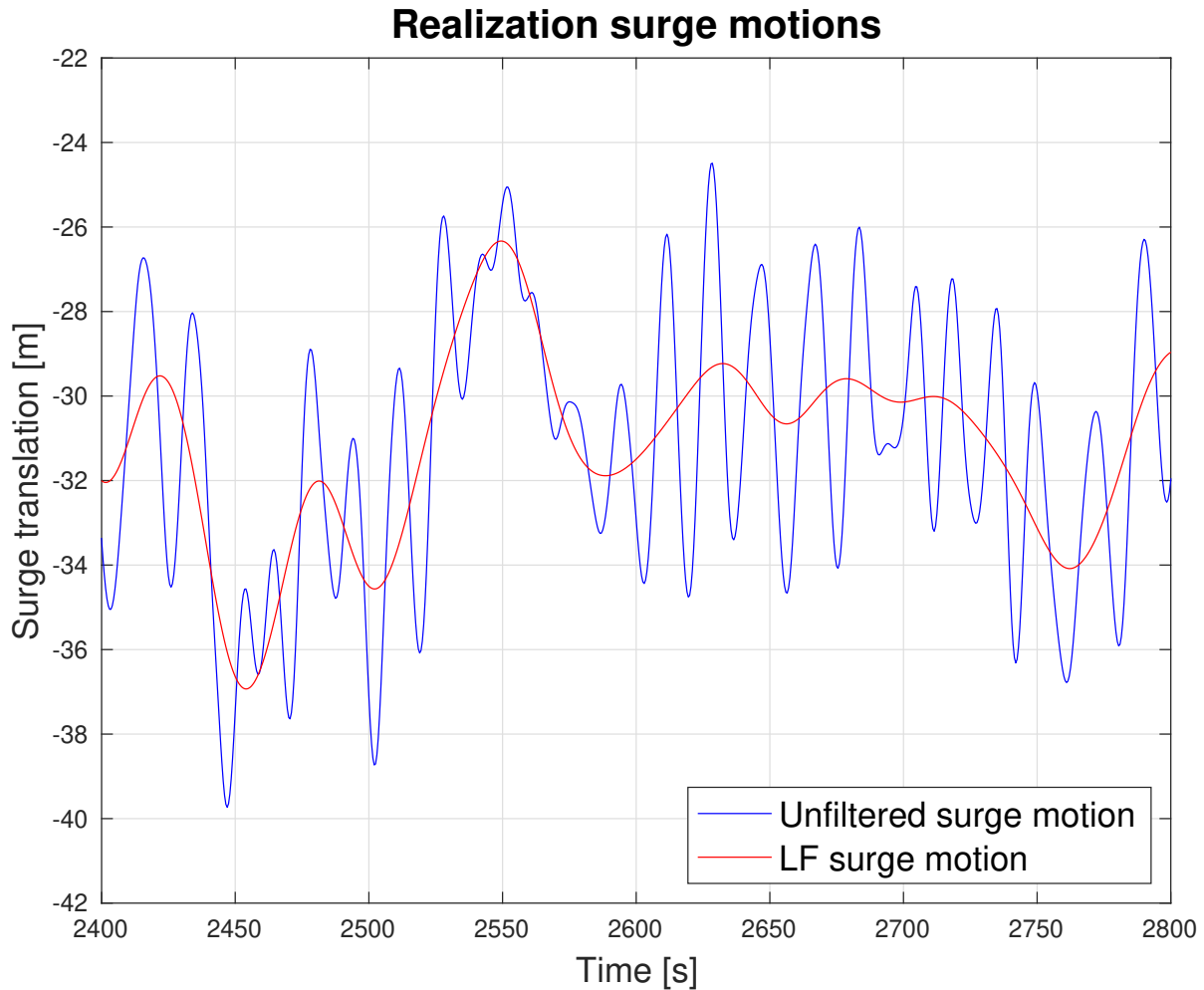


Figure 8.8: Selection of surge motion for arbitrary base case C_D realization

Statistics for low frequency surge motions in Figure 8.7 indicate the same motion pattern as described for the low frequency sway motions. Thus, the model has largest absolute surge translations for the cases where quadratic current coefficients are included which is due to the above mentioned effect of LF and WF waves working in unison. A zoomed realization of an arbitrary surge motion is depicted in Figure 8.8, where the LF surge motion is displayed together with the realization. Evaluating the unfiltered and LF filtered surge motions, there are clear correlations to the energy peaks in the PSD for surge translational motions shown in Figure 8.9.

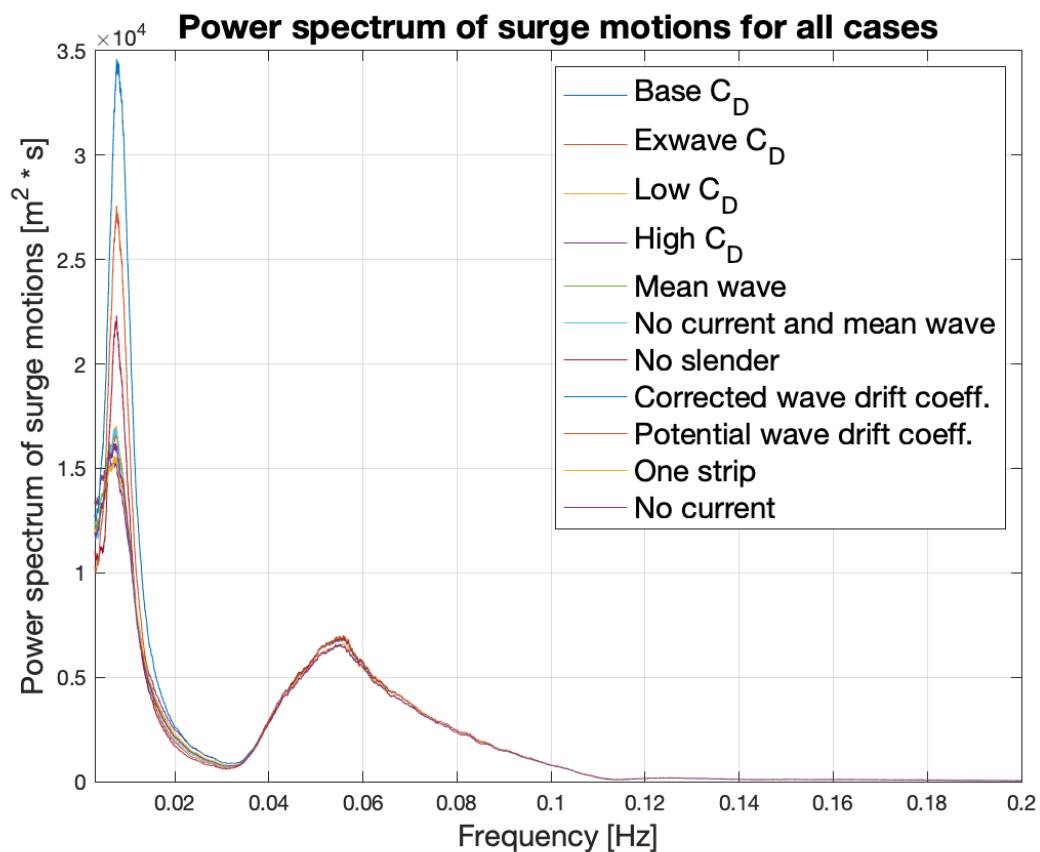


Figure 8.9: Power spectrum of surge motions for all cases

8.2 Forces

In Chapter 6 the most heavily loaded mooring line was found to be mooring line number 3, therefore the presented results is based on this mooring line. Figure 8.10 and 8.11 is an arbitrary force realization for corrected wave drift coefficient case and base C_D case respectively.

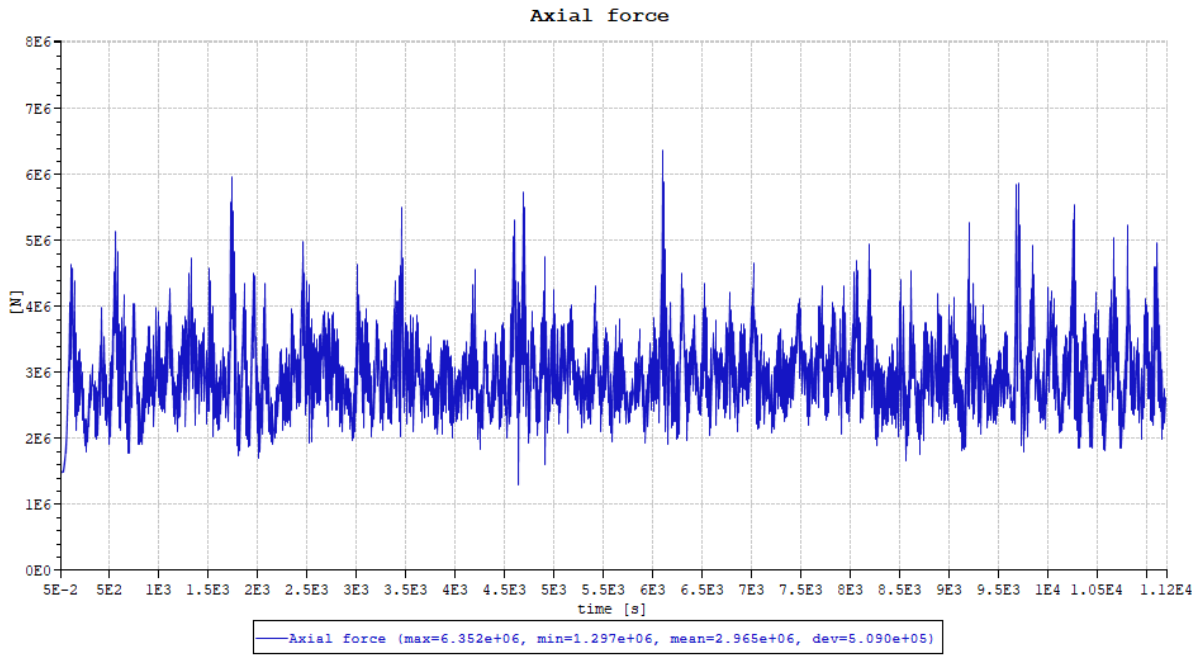


Figure 8.10: Realization of corrected wave drift coeff. axial force

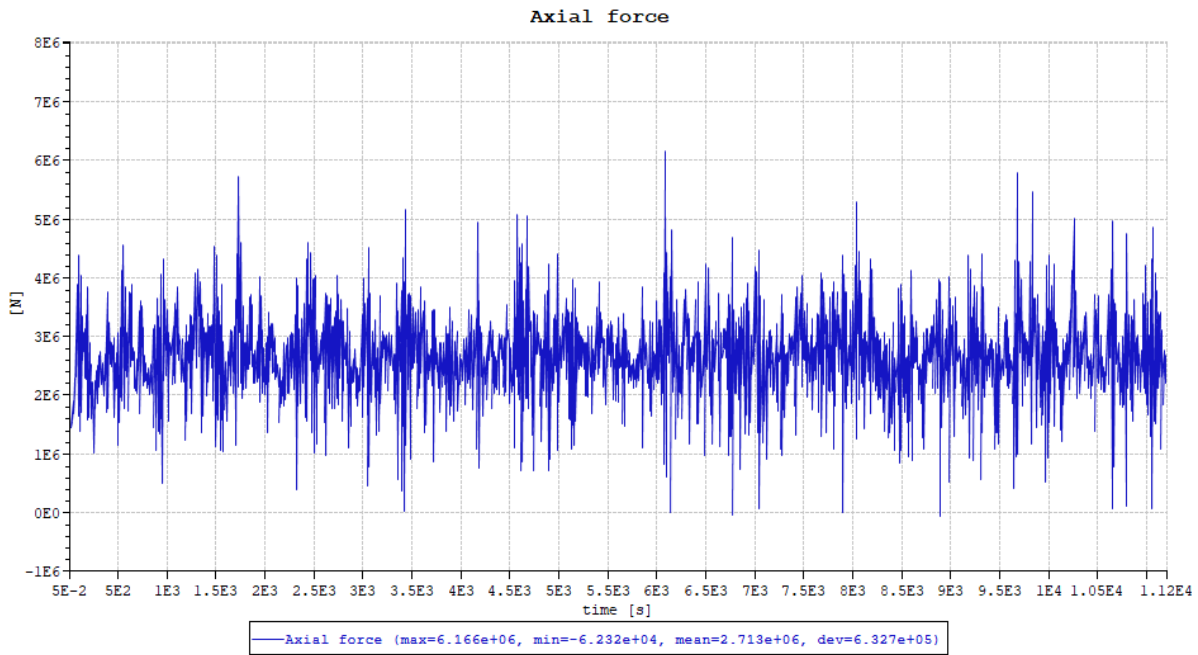


Figure 8.11: Realization of base case C_D axial force

Similar to the realizations of the motions, the forces show close correlation between the majority of the maximum forces in the presented realizations. However, there is a larger discrepancy in the realization for the base case C_D which has significantly more fluctuating mooring line tension than the other case. Statistics for the forces are presented in Table 8.1, showing a mean value for the cases with quadratic current coefficients in the same order of magnitude as the high C_D case. The highest maximum tension occurs for

the corrected current coefficient case, with close to 4% larger tension than the case with one strip.

Extreme forces all simulations						
Simulation	T_{MPM}	Mean	StD	Max	Min	Dim
Slender base C_D	5819.7	2715.4	729.6	7790.3	0	[kN]
Slender EXWAVE C_D	5831.4	2728.9	724.1	7762.5	0	[kN]
Slender low C_D	5645.8	2673.1	717.6	7577.0	0	[kN]
Slender high C_D	6262.9	2925.3	656.6	7985.4	0	[kN]
Slender one strip	6051.3	2841.7	724.9	7998.0	0	[kN]
Slender no current	5485.5	2622.1	696.9	7351.1	0	[kN]
Slender mean wave	5768.0	2734.9	695.2	7654.1	0	[kN]
Slender no current & mean wave	5479.0	2623.7	700.6	7386.0	0	[kN]
Slender no slender	5346.5	2480.2	718.4	7306.7	0	[kN]
With correction	5490.6	2954.4	487.5	8326.6	1297.2	[kN]
Without correction	4979.4	2826.1	413.7	7338.8	1296.3	[kN]

Table 8.1: Results of design load for all simulations

An observation to pinpoint is the larger deviation between T_{MPM} and max measured tension for the cases with current coefficients instead of slender elements. The standard deviation for these cases are less than 25% compared to the other standard deviations. This is clearly seen from the probability distribution function of the most probable maximum values presented in Figure 8.12. The narrow distributions for the two cases based on current coefficients is in great contrast to the other cases presented.

Evaluating the sensitivity of drag coefficients between the different cases seen in Figure 8.13. The power spectrum of low frequency forces shows a small variation in magnitude between the different cases, where the viscous force contribution is not shown to be significant. Hence, these effects are assumed to be dominant for more slender structures with a higher λ/D and H/D ratio according to force classification clarified in Section 4.8. H/D for the columns are between 1.5-3 which is in the lower range of mass dominating forces, and the classification of when viscous forces dominate is approximately above 10. In addition, the wave length calculated based on formulas for infinite water depth in (Faltinsen, 1990), are found to be 517. This result in a λ/D in the range between 20-32, dependent on the defined diameter of the columns. From (Pettersen, 2007), the λ/D range where drag forces dominate are above 90. Therefore these effects may be easier to evaluate and subtract for a structure with more slender columns.

However, focusing on the simulated cases with slender elements, the high C_D case and the one strip case have larger energy contributions from the filtered low frequency forces presented in Figure 8.13. In terms of T_{MPM} , the case with high C_D obtains a slightly higher value than the one strip case. These two are the only simulations with results above 6000kN, with the rest of simulations with values below 5820kN.

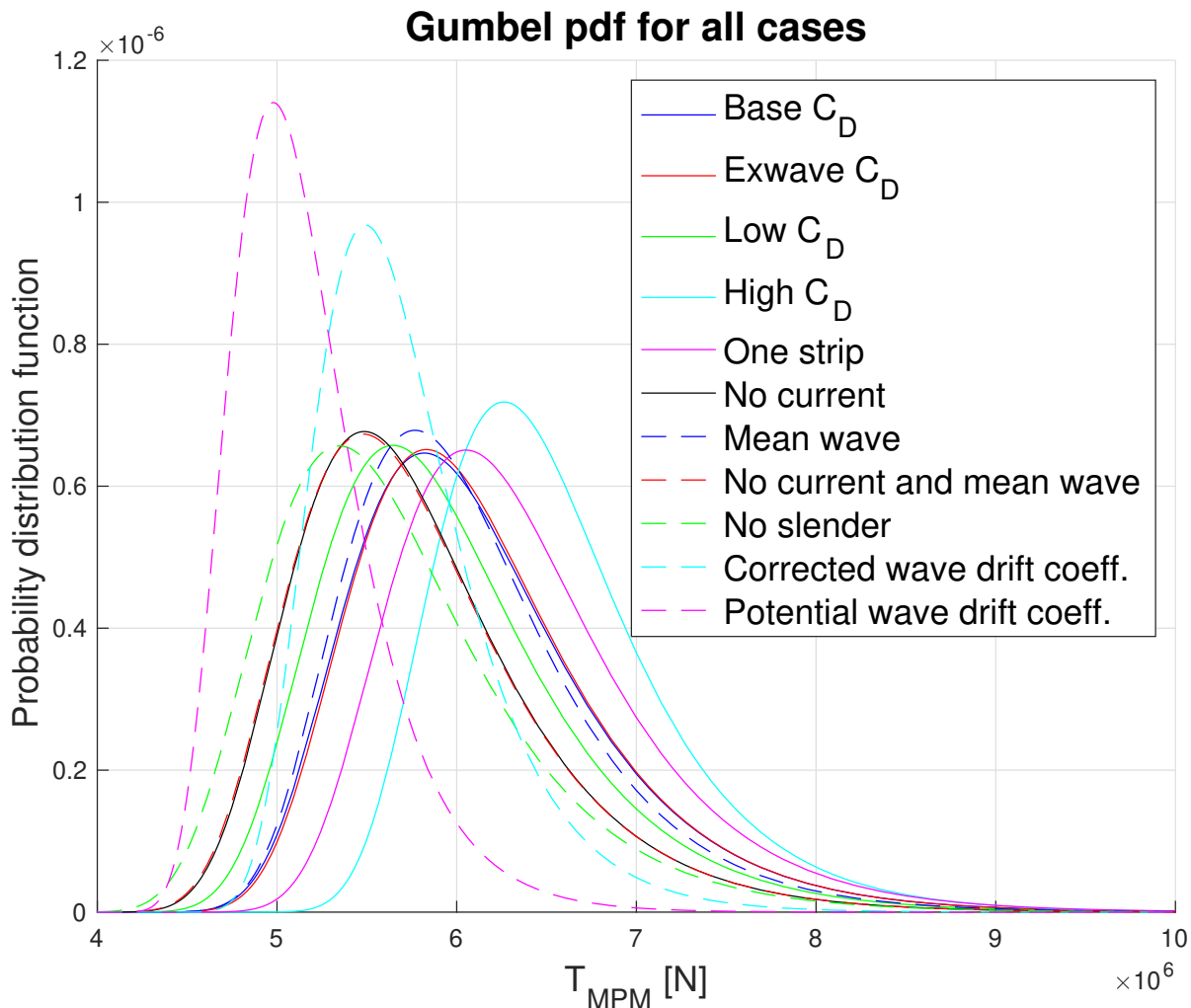


Figure 8.12: Gumbel distribution of T_{MPM}

Comparing the cases with base C_D and EXWAVE C_D , the difference in calculated T_{MPM} and contribution in terms of low frequency motions, are almost non-existent. Both mean and standard deviation of the two cases are close to identical, indicating drag force on the semi-submersible is not particularly sensitive to the change in drag coefficients for the two cases. Further comparison to the case with low C_D shows close to non discrepancy when the LF force contribution is compared. However, T_{MPM} for low C_D gives slightly lower most probable maximum tension and similar for the standard deviation.

High C_D was presented above as the case resulting in the highest T_{MPM} . Although, the standard deviation for the case is lower than all the other cases based on slender modelling without current coefficients. There is reason to believe that the significantly higher drag coefficients, results in higher forces on the semi-submersible and more viscous hull damping. This results in large forces in addition to a lower standard deviation from the added damping. Compared to the standard deviation for motions in the same case, both LF sway and LF surge motions are smaller compared to the other cases. This is presented in Figure 8.6 and 8.7. Even though the standard deviation in Table 8.1 for the high C_D case is the smallest of all the cases without current coefficient, mean drift motions for the semi-submersible are largest for the same case.

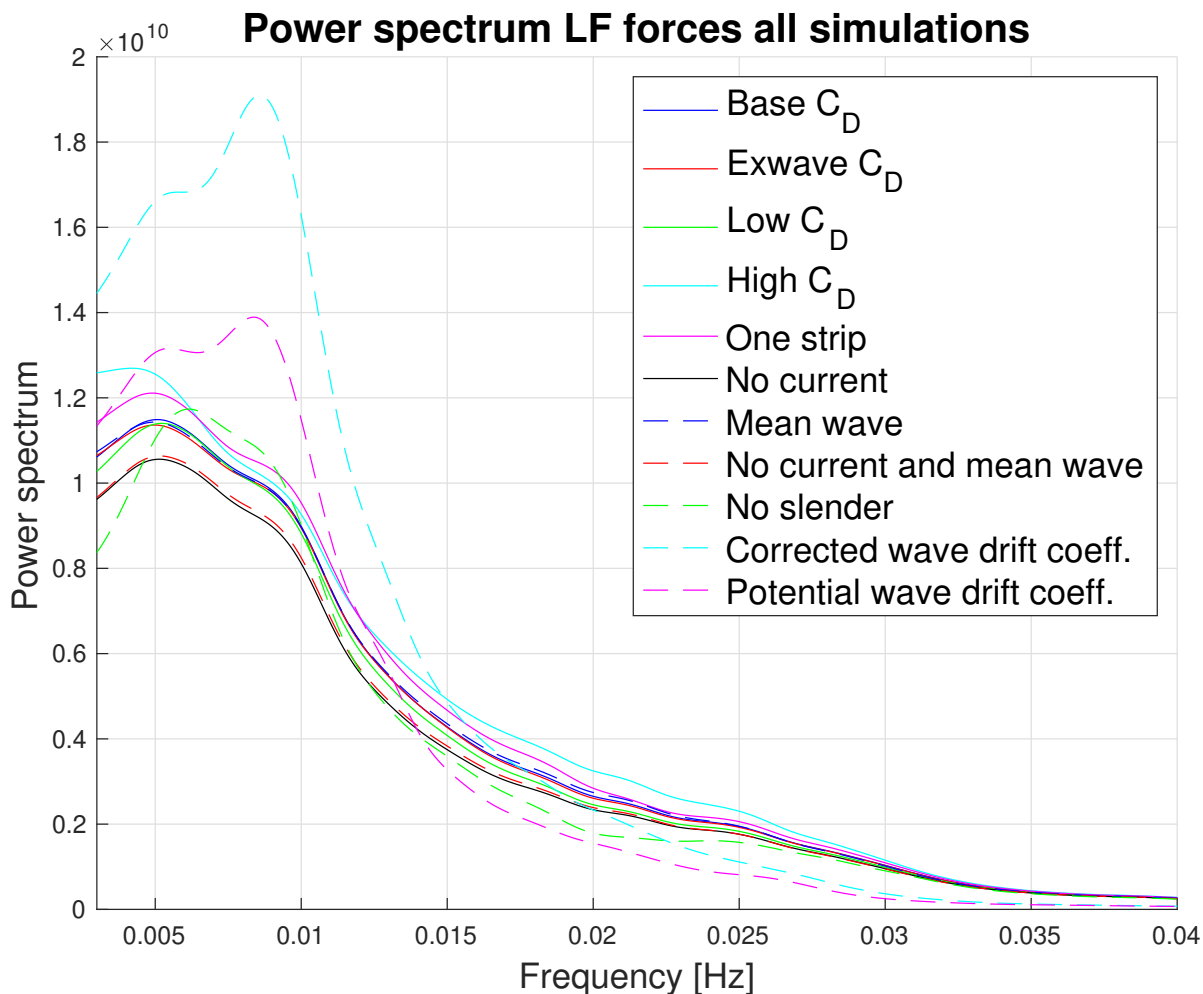


Figure 8.13: Power spectrum of the low frequency force contribution

For both base case C_D and mean wave case, the drag coefficients are the same. The difference between the cases are how the contribution from the waves are calculated. Base case C_D is as mentioned before, calculated by including second order waves with integration of wave forces to wave surface. On the other hand, the mean wave case are calculated with wave force calculation to mean surface level. This results in a higher standard deviation and higher T_{MPM} for the case with integration of wave forces to wave surface. The difference is not insubstantial, but not significant in any way and by comparing the LF energy contribution for the two cases are almost impossible. This indicates that wave-current interaction and cross-flow over the pontoons do not contribute to an identifiable level to the total force in the mooring line.

For the simulations with no current, no current and mean wave and no slender elements, the forces were expected to be smaller in magnitude than the other cases where current was included. The distinction between the case with no current and no current and mean wave, show close to none disagreement in the results both in terms of T_{MPM} and StD. When the LF force contributions for the three cases are compared, the no slender case has slightly more energy concentrated in the range between 0.005-0.01Hz. Which is expected when the case is disregarding viscous hull damping which can be up to 1/3 of the total damping for surge direction (Larsen K., Vigesdal T., Bjørkli R., Dalane D.,

2018).

The calculated PSD for the forces is shown Figure 8.14, where it is noticeable that the load models based on current coefficients are deviating from slender modelling. The obtained results do not correspond to the expected forces according to recent studies within the field of viscous drift forces (DNV GL, 2017b). Non-normalities in the obtained force pattern indicate that there may be something wrong in the calculation of forces for the two cases based on current coefficients.

The deviation in motions for the different cases are not inconsistent, but for forces the obtained results are not coinciding with results from earlier studies within the field of slow drift motions. However, as the forces do not show the correlation to the obtained motions there is reason to doubt the obtained results for the motions as well as the forces that are calculated. It will require further studies with the model to investigate possible errors or shortcomings for this type of calculations.

In order to determine the cause of the abnormal results, one must first differentiate the difference between the load models. As stated in Section 4.11 the difference between load modelling with current forces calculated with current coefficients (potential and corrected wave drift coeff.) and slender element method is

- (a) How the submerged section is calculated
- (b) How the current contribution is chosen

The main difference in (a) between the two are: slender modelling calculates the second order wave contribution of the actual wave surface elevation while load models based on current coefficients calculates the forces based on the mean water level. Therefore, it does not consider the cross-flow principle which can occur for a semi-submersible, neither does it consider the second order wave contribution of wave forces to wave surface. Although, as stated in Section 4.11, the correction formula is supposed to account for viscous effects and hence cross-flow principle and current interaction effects. In addition, the obtained forces for the slender model with mean water level shows good correspondence with forces for base case C_D . Based on the arguments above, the calculation method of the kinematics in wave zone seem not to be the fault in the power spectrum for the forces presented in Figure 8.14.

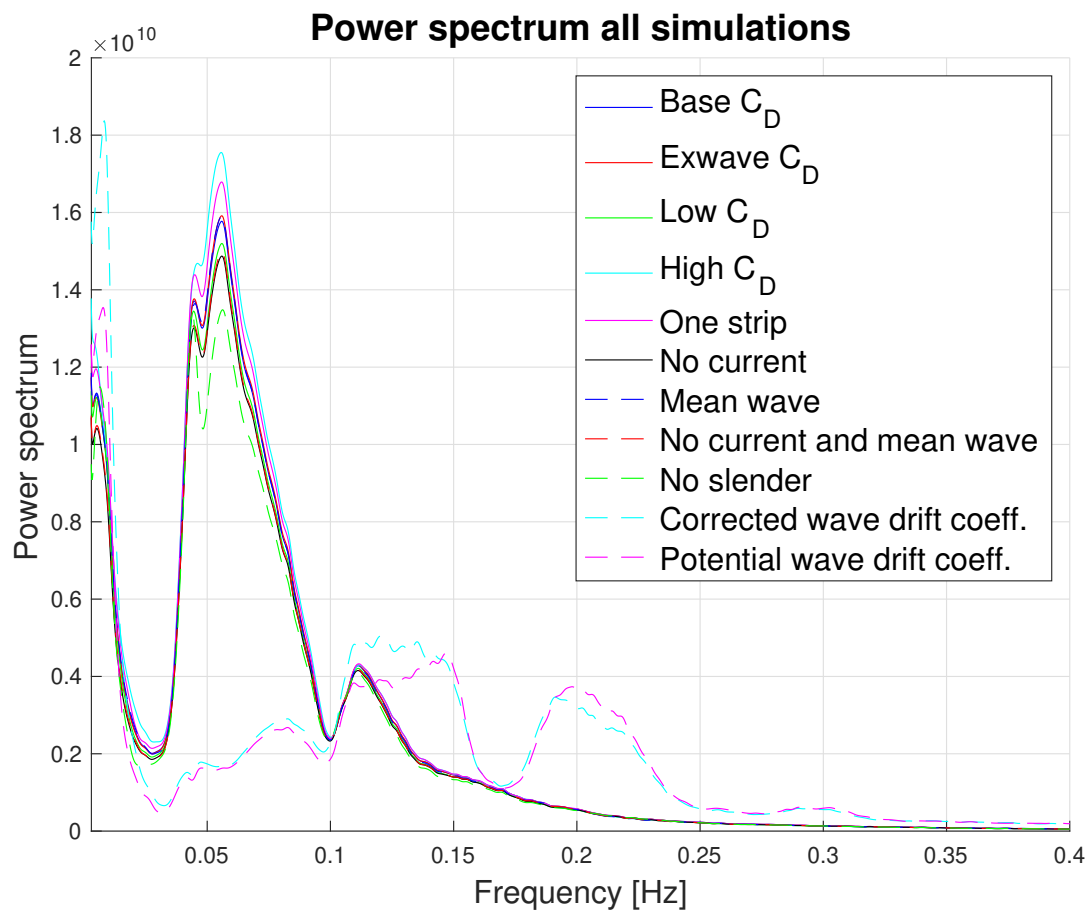


Figure 8.14: Power spectrum of the low frequency force contribution

Therefore the only other difference is how the load model accounts for the current contributions. However, it is difficult to ascertain the fault in current calculation which are explained in Section 4.11.

Chapter 9

Further work

Ideas and proposals for future work are presented in this chapter.

When designing for the maximum tension in a mooring line the peak in the H_s-T_p contour plot may not give the largest tension in the lines. A thorough check of the points along the contour line should be checked with simulations for 10-20 seeds over a 3 hour sea state.

To check the same set of analysis for a semi-submersible with smaller columns is of interest to investigate how this affect the viscous contribution on the maximum line tension. The viscous effects are believed to give larger contribution for semi-submersibles with smaller columns.

With regard to slender elements in this thesis there were only tested with the number of strips presented in Chapter 7, except from the slender case with one strip per element. This gave large mooring line tensions and it is therefore of interest to investigate effect from number of strips per slender element. An indication from the number of strips tested in this thesis show that the simulations may be sensitive to the number of strips.

The damping in surge direction is about 30%, while the recommended damping for semi-submersibles in extreme sea states are in the range between 40-70% (Larsen K., Vigesdal T., Bjørkli R., Dalane D., 2018). This affects both motions and forces for the model, and a correction of the damping level for the model should be included for further analysis.

To further mature the understanding of characteristics for the load model related to current coefficients, subjects that may be of relevance to explore and do further considerations with respect to are:

- How the load model determines forces for the given environmental condition
- The correspondence between calculated motions and forces for the semi-submersible or similar semi-submersibles
- How the obtained forces are related to the calculations of the kinematics in wave zone
- Marine growth and its impact on the mooring line and viscous hull drag

When designing the mooring lines, the cross-sectional area is constant within the whole mooring line. In reality, this is not the case and transition components may have more critical breaking strength than the chain utilized in the calculations. In addition, fatigue damage is also important to mention and can reduce the breaking strength of the chain components.

The effect of different anchor types are neglected in the thesis. Therefore, it is of interest to see the how a displaced or tilted anchor affects the motion of a semi-submersible.

Chapter 10

Conclusion

A design is presented which was able to comply with offshore regulations, utilizing the SIMA software. An extra partial safety factor of 20% between SIMO and RIFLEX was not sufficient enough to satisfy the design equation in DNVGL-OS-E301.

Three different load models for calculation of maximum axial force in mooring lines have been investigated. Two of the methods are based on wave drift forces from Newman's approximation, by utilizing quadratic current coefficients as input for calculation of the current forces. The last method calculate the viscous loads on the semi-submersible through the drag term in Morison's equation.

The sensitivity of drag coefficients between the different cases conducted are shown to give small variations in the contribution to T_{MPM} . In addition, the power spectrum of low frequency forces shows a small variation in magnitude between the different cases, where the viscous force contribution is not shown to be significant. The low contribution from viscous forces is attributed to H/D for the columns, which are between 1.5-3 corresponding to the lower range of mass dominating forces.

The translational motions of the semi-submersible in sway direction are in average over 20% higher than the translational motions in surge direction. This is a result from the difference in shape between the two directions with pontoons along the surge direction.

The deviation in motions for the different cases are not inconsistent, but for forces the obtained results are not coinciding with results from earlier studies within the field of slow drift motions. However, as the forces do not show the correlation to the obtained motions there is reason to doubt the obtained results for the motions as well as the forces that are calculated. The reason is believed to be due to a fault in how the current forces are calculated.

Viscous effects are highlighted and discussed, but in no circumstance proven to dominate the forces for the simulated semi-submersible in the chosen environmental condition.

Bibliography

- Bastos de Araujo, J., Diniz Machado, R., and Jose de Medeiros Junior, C. (2004). High holding power torpedo pile: Results for the first long term application.
- Bluewater (2019). What is an fpso? <https://www.bluewater.com/fleet-operations/what-is-an-fpso/>. (Accessed on 05/11/2019).
- Bridon (2013). *Oil and Gas catalogue*. Edition 6.
- Burns, G. E. (1983). Calculating viscous drift of a tension leg platform. *OMAE*.
- Chakrabarti, S. K. (1984). Steady drift force on vertical cylinder - viscous vs. potential. *Applied Ocean Research*, 6(2):73 – 82.
- Chakrabarti, S. K. (2005). *Handbook of offshore engineering*, volume 2. Elsevier Ltd.
- DNV GL (2017a). Environmental conditions and environmental loads. Technical report, DNV GL, <https://rules.dnvgl.com/docs/pdf/DNVGL/RP/2017-08/DNVGL-RP-C205.pdf>. (Accessed on 13/05/2019).
- DNV GL (2017b). Handbook on low-frequency wave forces and response - guidelines and recommendations. Technical Report 1, DNV GL, Confidential. EXWAVE JIP Wave Forces on Floating Units in Extreme Seas.
- DNV GL (2018). Position mooring. Technical report, DNV GL, <https://rules.dnvgl.com/docs/pdf/DNVGL/OS/2018-07/DNVGL-OS-E301.pdf>. (Accessed on 23/11/2018).
- Faltinsen, O. (1990). *Sea loads on ships and offshore structures*, volume 1. Cambridge university press.
- Faj, H. (1990). *Dynamic Positioning Systems: Principles, Design, and Applications*. ÉDITIONS TECHNIP.
- Ferretti, C. Berta, M. (1980). Viscous effect contribution to the drift forces on floating structures. *International Symposium on Ocean Engineering and Shiphandling*.
- Fonseca, N., Trygve Stansberg, C., Larsen, K., Bjørkli, R., Vigesimal, T., and Dalane, O. (2018). Low frequency excitation and damping of four modus in severe seastates with current.
- Greco, M. (2012). Tmr 4215: Sea loads, lecture notes.

- Hildebrandt, A., Sparboom, U., and Oumeraci, H. (2009). Wave forces on groups of slender cylinders in comparison to an isolated cylinder due to non-breaking waves. In *Coastal Engineering 2008*, pages 3770–3781. World Scientific Publishing Co. Pte. Ltd.
- ISO (2013). Petroleum and natural gas industries - specific requirements for offshore structures - part 7: Stationkeeping systems for floating offshore structures and mobile units. Technical report, International Standard Organization.
- Kvitrud, A. (2014). Lessons learned from norwegian mooring line failures 2010–2013. *OMAE2014-23095*.
- Larsen, C. M. (2014). Marine dynamics tmr 4182. *Dept. of Marin Techn. NTNU, Trondheim, Norway*.
- Larsen, K. (2015). Static equilibrium of a mooring line.
- Larsen, K. (2018). Lecture notes marine operations tmr 4225.
- Larsen K., Vigesimal T., Bjørkli R., Dalane D. (2018). Mooring of semi submersibles in extreme sea states: Simplified models for wave drift forces and low frequency damping.
- Lavis, J. (2018). Shallow, mid to ultra deepwater definitions. <https://drillers.com/shallow-mid-to-ultra-deepwater-definitions/>. (Accessed on 05/10/2019).
- Leira, B. J. (2014). Stochastic theory of sealoads, tmr 4235. *Dept. of Marin Techn. NTNU, Trondheim, Norway*.
- Lie, H., Gao, Z., and Moan, T. (2007). Mooring line damping estimation by a simplified dynamic model. *Proceedings of the International Conference on Offshore Mechanics and Arctic Engineering - OMAE*, 1.
- Lie, H. and Kaasen, K. (2008). Viscous drift forces on semis in irregular seas: A frequency domain approach. *Proceedings of the International Conference on Offshore Mechanics and Arctic Engineering - OMAE*, 1. OMAE2008-57313.
- Lied, M. R. (2018). Design of mooring systems in extreme sea states with focus on viscous drift force modelling.
- Maruo, H. (1960). The drift of a body floating in waves. *Journal of Ship Research*, 4.
- Morison *et al* (1950). The force exerted by surface waves on piles - onepetro. <https://www.onepetro.org/journal-paper/SPE-950149-G>. (Accessed on 04/02/2019).
- Newman, J. N. (1967). The drift force and moment on ships in waves. *Journal of ship research*. 11(1):51-60.
- Ommani B., Fonseca N., Stansberg C. T. (2017). Simulation of low frequency motions in severe seastates accounting for wave-current interaction effects.
- Orcina Ltd (2019). Chain: Axial and bending stiffness. <https://www.orcina.com/webhelp/OrcaFlex/Content/html/Chain,Axialandbendingstiffness.htm>. (Accessed on 05/13/2019).

- Ormberg, H. and Larsen, K. (1998). Coupled analysis of floater motion and mooring dynamics for a turret-moored ship. *Applied Ocean Research*, 20:55–67.
- Palm (2016). Torpedo anchors. <https://www.offshoreengineering.com/education/mooring-engineering/292-torpedo-anchors>. (Accessed on 05/10/2019).
- Pettersen, B. (2007). Marin teknikk 3: hydrodynamikk. *Dept. of Marin Techn. NTNU, Trondheim, Norway*.
- Pinkster, J. (1980). Low frequency second order wave exciting forces on floating structures.
- Ramnäs Bruk (2015). *Ramnäs Bruk Product Catalogue*. Product catalogue for chain.
- Ruinen, R. (2004). Stevmanta v/a installation, a case history. International Mooring Seminar 2004 November 29, 2004 – New Orleans.
- SINTEF Ocean (2018a). *RIFLEX 4.14.0 User Guide*.
- SINTEF Ocean (2018b). *SIMO 4.14.0 User Guide*.
- Sprenger, F., Hermundstad, E. M., Roger Hoff, J., Fathi, D., and Selvik, (2017). Comparative study of motions and drift forces in waves and current.
- SPT Offshore (2019). Suction piles for mooring. <http://www.sptoffshore.com/en/solutions/floating-facilities/suction-piles-for-moorings>. (Accessed on 05/08/2019).
- Stansberg, C., Hoff, J. R., Hermundstad, E. M., and Baarholm, R. (2013). Wave drift forces and responses in current. *Proceedings of the International Conference on Offshore Mechanics and Arctic Engineering - OMAE*, 1.
- Stansberg, C. T. (1997). Linear and nonlinear system identification in model testing. *International Conference on "Nonlinear Aspects of Physical Model Tests*.
- Stansberg, C. T. (2001). Data interpretation and system identification in hydrodynamic model testing. *Proceedings of the Eleventh (2001) International Offshore and Polar Engineering Conferenc*.
- Stansberg, C. T., Kaasen, K. E., Abrahamsen, B. C., Nestegård, A., Shao, Y., and Larsen, K. (2015). Challenges in wave force modelling for mooring design in high seas.
- Statoil (2004). Heidrun metocean design basis. Technical Report 2, Corporate Statoil, Confidential.
- Statoil (2015). Confidential. Technical Report 1, Corporate Statoil, Confidential.
- The Nautical Institute (2011). What is dynamic positioning? <https://web.archive.org/web/20130125101320/http://www.nautinst.org/en/dynamic-positioning/what-is-dynamic-positioning/index.cfm>. (Accessed on 05/11/2019).
- Vryhof, A. (2017). Anchor products. <http://www.vryhof.com/products/anchors>. (Accessed on 05/08/2019).

- Wang, L.-z., Kanmin, S., Li, L.-l., and Guo, Z. (2014). Integrated analysis of drag embedment anchor installation. *Ocean Engineering*, 88:149–163.
- Wang, R. (2016). Design of mooring systems in extreme seastates with focus on viscous drift force modelling. MA thesis.
- Yang, L., Falkenberg, E., and Nestegård, A. (2018). Analysis of semi-submersible under combined high waves and current conditions compared with model tests. *Proceedings of the ASME 2018 37th International Conference on Ocean, Offshore and Arctic Engineering*.
- Yang, L., Falkenberg, E., Nestegård, A., and Birknes-Berg, J. (2017). Viscous drift force and motion analysis of semi-submersible in storm sea states compared with model tests.
- Yuan et al (2017). Real-time method for calculating retardation functions. *Journal of Marine Science and Technology*, Vol. 25, No. 6, pp. 715-721 (2017).

Appendices

Calculation parameters and results

A Properties of the Semi-submersible

Hydrostatic Properties and Natural Periods				
		Wamit Model	DSME	Difference (%)
Loading Condition	-	Survival	Survival	
Draught	m	19.15	19.15	0.00 %
Displacement	Te	54770	54520.6	0.46 %
Waterplane Area	m ²	1203	1190	1.10 %
KG	m	26.77	26.9	-0.49 %
LCG	m	0.00	0	0.00 %
KB	m	6.78	-	-
LCB	m	0.00	0.00	0.00 %
GM _T	m	1.06	1.00	5.27 %
GM _L	m	2.08	2.00	3.87 %
T ₀ heave	sec	22.4	23	-2.80 %
T ₀ roll	sec	95.4	-	-
T ₀ pitch	sec	70.1	-	-
rx _{wl}	m	33.700	33.700	0.00 %
ry _{wl}	m	34.800	34.800	0.00 %
rzz _{wl}	m	37.400	37.400	0.00 %

Table 3 Hydrostatics of Cat D from Wamit and DSME_Survival Draught

Figure A1: Hydrostatic properties and natural periods for the semi-submersible

B Iterative design process

Stainless chain, diameter	90	92	95	97	100	102	105	157
Diameter [millimeter]	90	92	95	97	100	102	105	157
Break load [kN]	8167	8497	9001	9343	9864	10217	10754	21234
Break load [Te]	832,80	866,45	917,84	952,72	1005,84	1041,84	1096,60	2165,25
Pre tension u/ safety [kN]	816,7	849,7	900,1	934,3	986,4	1021,7	1075,4	2123,4
Weight in air [kg/m]	162	169	181	188	200	208	221	493
Weight in air [N/m]	1588,69	1657,33	1775,01	1843,66	1961,34	2039,79	2167,28	4834,70
Weight in water [N/m]	1382,16	1441,88	1544,26	1603,98	1706,37	1774,62	1885,53	4206,19
Ballast [N]	1,18E+07	1,24E+07	1,30E+07	1,35E+07	1,37E+07	1,40E+07	1,58E+07	3,25E+07
E-modulus	5,2250E+10	5,220E+10	5,2125E+10	5,2075E+10	5,20E+10	5,1950E+10	5,1875E+10	5,0575E+10
Max allowed line length	2507,4	2504,7	2493,7	2493,0	2485,5	2481,4	2472,2	2355,4
ULS Check								
Tabulated break load	8,17E+06	8,50E+06	9,00E+06	9,34E+06	9,86E+06	1,02E+07	1,08E+07	2,12E+07
Max simulated load SIMO	4,16E+06	4,17E+06	4,20E+06	4,23E+06	4,25E+06	4,24E+06	4,31E+06	4,81E+06
Environmental load	3,34E+06	3,32E+06	3,30E+06	3,30E+06	3,26E+06	3,22E+06	3,23E+06	2,69E+06
OK? [positive if OK]	-6,32E+05	-2,97E+05	1,81E+05	4,83E+05	1,00E+06	1,41E+06	1,84E+06	1,21E+07
Suspended line length - S [m]	1432,6	1404,3	1361,8	1341,0	1303,2	1276,5	1247,7	882,9
Total line length [m]	1932,6	1904,3	1861,8	1841,0	1803,2	1776,5	1747,7	1382,9
Maks drift off x [m]	66,1	65,6	65,6	65	64,6	66,9	63,5	57,5
Maks drift off y [m]	95,8	94,9	93,5	91,6	90,4	95,7	87,3	73,8
ALS1 check								
Tabulated break load	8,17E+06	8,50E+06	9,00E+06	9,34E+06	9,86E+06	1,02E+07	1,08E+07	2,12E+07
Max simulated load SIMO	5,41E+06	5,43E+06	5,47E+06	5,49E+06	5,52E+06	5,54E+06	5,57E+06	5,95E+06
Environmental load	4,59E+06	4,58E+06	4,57E+06	4,56E+06	4,53E+06	4,52E+06	4,49E+06	3,83E+06
OK? [positive if OK]	1,74E+05	5,26E+05	1,05E+06	1,41E+06	1,97E+06	2,35E+06	2,93E+06	1,46E+07
Maks drift off x [m]	74,4	74,1	73,8	73,3	72,7	72,4	71,7	66
Maks drift off y [m]	105,1	104,2	102,8	101,3	99,7	98,7	96,6	82,7
ULS Extreme								
Tabulated break load	8,17E+06	8,50E+06	9,00E+06	9,34E+06	9,86E+06	1,02E+07	1,08E+07	2,12E+07
Max simulated load SIMO	4,60E+06	4,61E+06	4,63E+06	4,65E+06	4,70E+06	4,68E+06	4,70E+06	5,20E+06
Environmental load	3,78E+06	3,76E+06	3,73E+06	3,72E+06	3,71E+06	3,66E+06	3,62E+06	3,08E+06
OK? [positive if OK]	2,27E+06	2,60E+06	3,09E+06	3,41E+06	3,88E+06	4,26E+06	4,79E+06	1,48E+07
Line in water - S [m]	1506,5	1476,5	1429,8	1406,0	1370,5	1341,0	1303,7	918,0
Total line length [m]	2006,5	1976,5	1929,8	1906,0	1870,5	1841,0	1803,7	1418,0
Maks drift off x [m]	68,1	67,8	67,3	66,8	66,2	66,9	64,9	59,4
Maks drift off y [m]	99,8	98,9	97,5	94,1	94,6	93,4	91,4	77

Figure B1: Test of different chain dimensions with corresponding results from design checks

C Decay tests

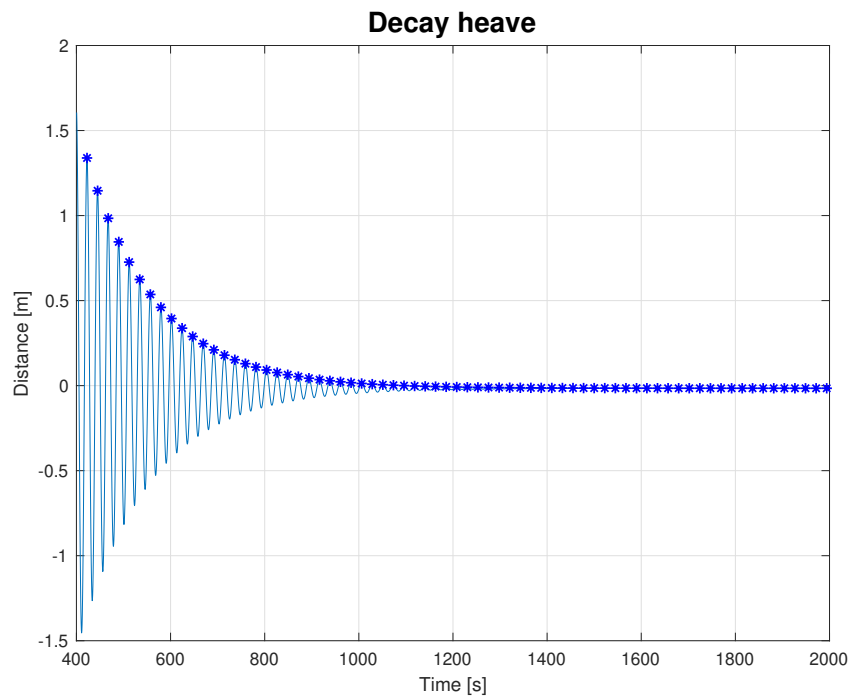


Figure C1: Decay test heave

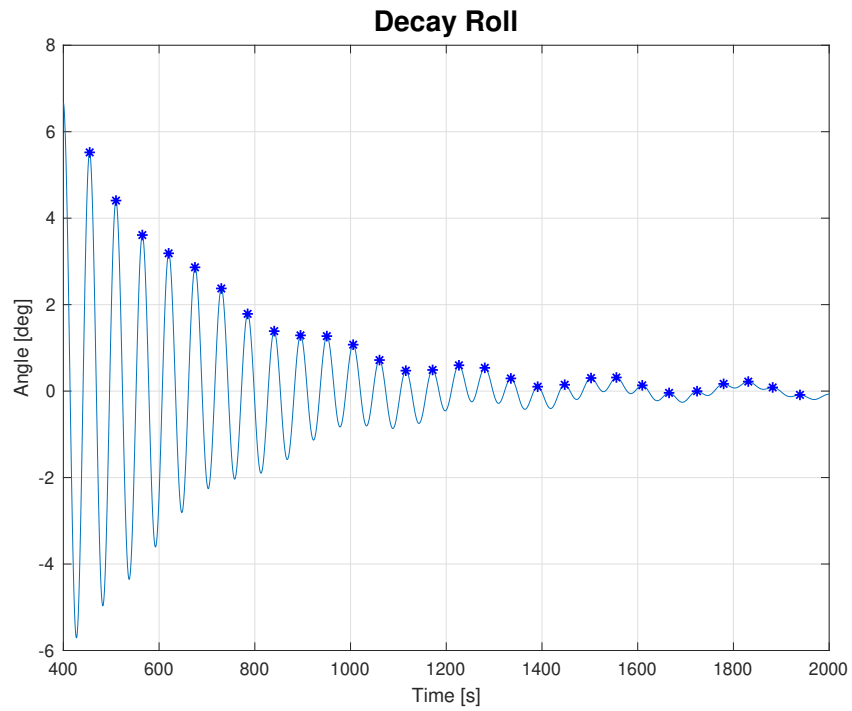


Figure C2: Decays test roll

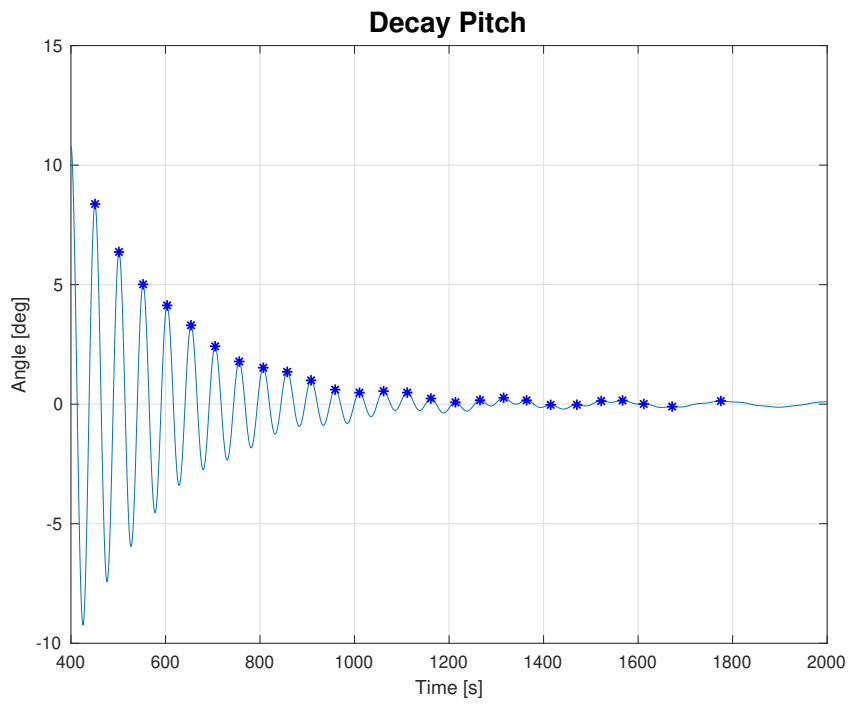


Figure C3: Decay test pitch

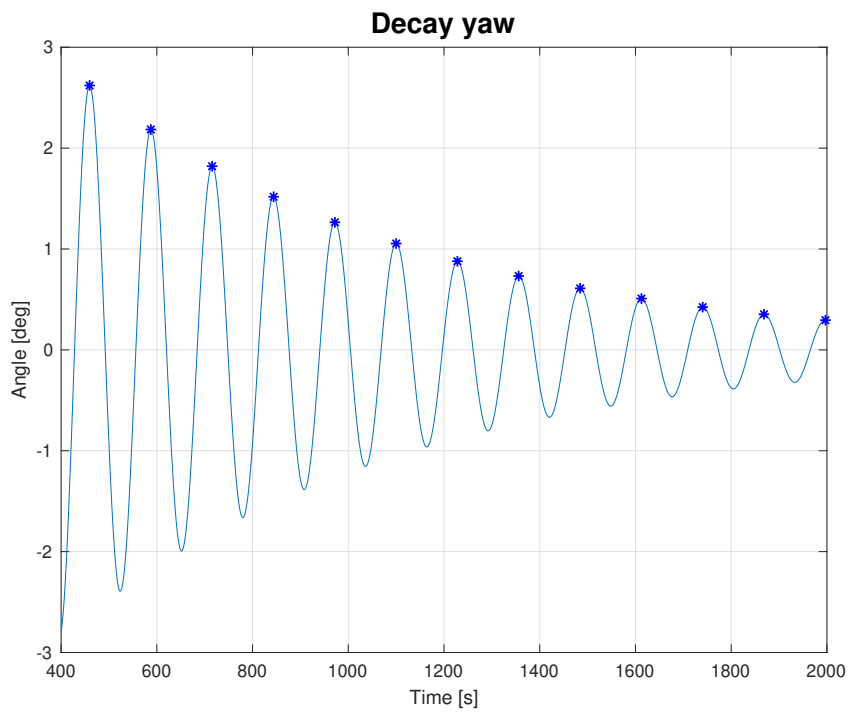


Figure C4: Decay test yaw

D Quadratic current coefficients

No	Direct...	C21	C22	C23	C24	C25	C26
1	0.0	4.0862e+05	-11962	0.0	0.0	0.0	24223
2	10.0	4.4472e+05	1.7577e+05	0.0	0.0	0.0	-2.4592e+06
3	20.0	4.9707e+05	3.3665e+05	0.0	0.0	0.0	-3.8902e+06
4	30.0	4.7014e+05	5.3753e+05	0.0	0.0	0.0	-5.8217e+06
5	40.0	4.0593e+05	7.1667e+05	0.0	0.0	0.0	-6.2881e+06
6	50.0	3.1277e+05	9.3014e+05	0.0	0.0	0.0	-8.1986e+06
7	60.0	2.3371e+05	1.0506e+06	0.0	0.0	0.0	-8.8099e+06
8	70.0	1.316e+05	1.0527e+06	0.0	0.0	0.0	-6.9693e+06
9	80.0	86852	9.29e+05	0.0	0.0	0.0	-3.2862e+06
10	90.0	5272.0	8.1937e+05	0.0	0.0	0.0	-32840
11	100.0	-61346	8.7795e+05	0.0	0.0	0.0	5.1465e+06
12	110.0	-1.3292e+05	1.0173e+06	0.0	0.0	0.0	7.3783e+06
13	120.0	-2.1288e+05	1.0275e+06	0.0	0.0	0.0	8.2057e+06
14	130.0	-2.9688e+05	9.443e+05	0.0	0.0	0.0	8.8506e+06
15	140.0	-4.0198e+05	7.4718e+05	0.0	0.0	0.0	6.1335e+06
16	150.0	-4.553e+05	5.6837e+05	0.0	0.0	0.0	6.0572e+06
17	160.0	-4.6547e+05	4.0376e+05	0.0	0.0	0.0	4.9032e+06
18	170.0	-4.5019e+05	1.8875e+05	0.0	0.0	0.0	2.4268e+06
19	180.0	-4.0124e+05	11425	0.0	0.0	0.0	-1.6149e+05
20	190.0	-4.4486e+05	-1.7224e+05	0.0	0.0	0.0	-3.163e+06
21	200.0	-4.8807e+05	-3.5197e+05	0.0	0.0	0.0	-3.8496e+06
22	210.0	-4.6244e+05	-5.4439e+05	0.0	0.0	0.0	-5.5294e+06
23	220.0	-4.0386e+05	-7.5476e+05	0.0	0.0	0.0	-7.1748e+06
24	230.0	-3.015e+05	-9.7263e+05	0.0	0.0	0.0	-1.0489e+07
25	240.0	-1.8761e+05	-1.0527e+06	0.0	0.0	0.0	-1.0778e+07
26	250.0	-1.3056e+05	-1.0743e+06	0.0	0.0	0.0	-9.047e+06
27	260.0	-64712	-9.5663e+05	0.0	0.0	0.0	-6.2937e+06
28	270.0	7694.3	-8.2514e+05	0.0	0.0	0.0	-1.486e+06
29	280.0	88558	-9.0347e+05	0.0	0.0	0.0	4.4007e+06
30	290.0	1.6335e+05	-1.0313e+06	0.0	0.0	0.0	7.82e+06
31	300.0	2.2908e+05	-1.041e+06	0.0	0.0	0.0	1.0255e+07
32	310.0	3.2144e+05	-9.5723e+05	0.0	0.0	0.0	9.0625e+06
33	320.0	4.0024e+05	-7.4031e+05	0.0	0.0	0.0	5.7756e+06
34	330.0	4.6526e+05	-5.4624e+05	0.0	0.0	0.0	5.3346e+06
35	340.0	4.9832e+05	-3.5993e+05	0.0	0.0	0.0	3.8818e+06
36	350.0	4.7242e+05	-1.9346e+05	0.0	0.0	0.0	2.5667e+06
37	360.0	4.0862e+05	-11962	0.0	0.0	0.0	24223

Figure D1: Quadratic current coefficients for the semi-submersible

E Wave drift coefficients

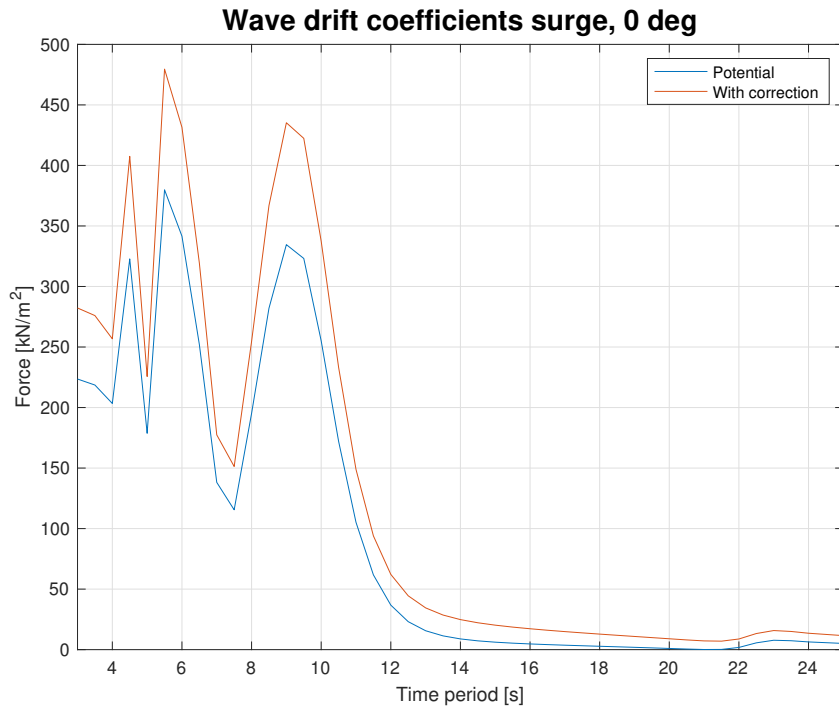


Figure E1: Corrected wave drift coefficients surge 0 deg

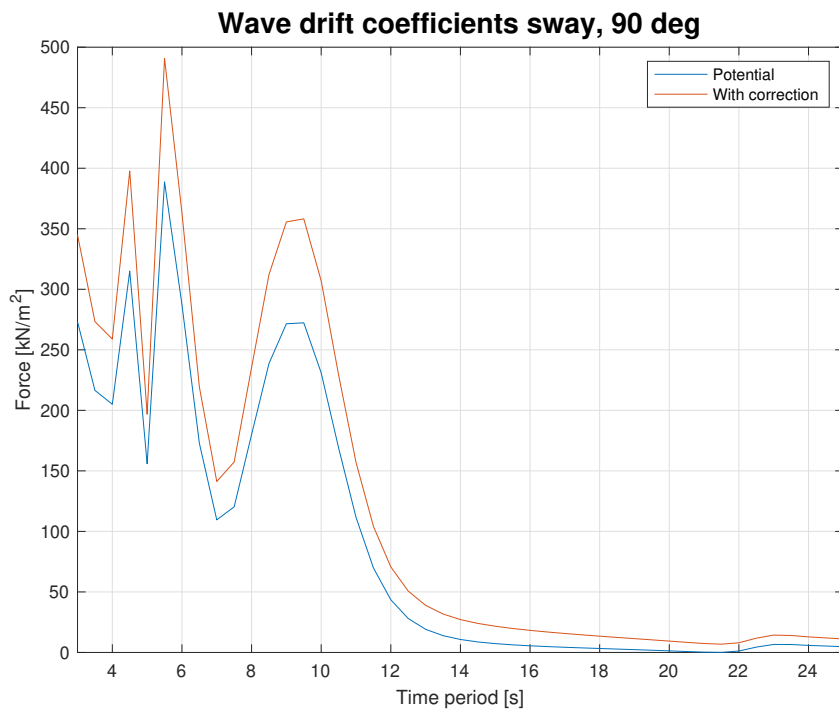


Figure E2: Corrected wave drift coefficients sway 90 deg

Matlab codes

F wave_drift_coeff.m

```

1  clc
2  clear all
3
4  %% Directions
5  filename = '/Users/Martin/OneDrive - NTNU/Master/Sima/Test/
   wave_drift_coeff.txt';
6  delimiter = ' ';
7  startRow = 12;
8  endRow = 18;
9
10 formatSpec = '%f%f*s*s*s*s*s*s*s%[\n\r]';
11 fileID = fopen(filename,'r');
12 dataArray = textscan(fileID, formatSpec, endRow-startRow+1,
   'Delimiter', delimiter, 'MultipleDelimsAsOne', true, '
   TextType', 'string', 'HeaderLines', startRow-1, '
   ReturnOnError', false, 'EndOfLine', '\r\n');
13 fclose(fileID);
14 directions = table(dataArray{1:end-1}, 'VariableNames', {'
   VarName1','VarName2'});
15 clearvars filename delimiter startRow endRow formatSpec
   fileID dataArray ans;
16
17 directions = table2array(directions);
18
19 %% Frequencies
20 filename = '/Users/Martin/OneDrive - NTNU/Master/Sima/Test/
   wave_drift_coeff.txt';
21 delimiter = ' ';
22 startRow = 23;
23 endRow = 68;
24
25 formatSpec = '%f%f*s*s*s*s*s*s*s%[\n\r]';
26 fileID = fopen(filename,'r');
27 dataArray = textscan(fileID, formatSpec, endRow-startRow+1,
   'Delimiter', delimiter, 'MultipleDelimsAsOne', true, '
   TextType', 'string', 'HeaderLines', startRow-1, '
   ReturnOnError', false, 'EndOfLine', '\r\n');
28 fclose(fileID);
29 frequencies = table(dataArray{1:end-1}, 'VariableNames', {'
   VarName1','VarName2'});
30 clearvars filename delimiter startRow endRow formatSpec
   fileID dataArray ans;

```

```
31
32 frequencies = table2array(frequencies);
33
34 %% Surge
35 filename = '/Users/Martin/OneDrive - NTNU/Master/Sima/Test/
    wave_drift_coeff.txt';
36 delimiter = ' ';
37 startRow = 72;
38 endRow = 393;
39
40 formatSpec = '%f%f%f*s*s*s*s*s%[\n\r]';
41
42 fileID = fopen(filename,'r');
43
44 dataArray = textscan(fileID, formatSpec, endRow-startRow+1,
    'Delimiter', delimiter, 'MultipleDelimsAsOne', true, '
    TextType', 'string', 'HeaderLines', startRow-1, '
    ReturnOnError', false, 'EndOfLine', '\r\n');
45 fclose(fileID);
46 surge = table(dataArray{1:end-1}, 'VariableNames', {'
    VarName1','VarName2','VarName3'});
47 clearvars filename delimiter startRow endRow formatSpec
    fileID dataArray ans;
48
49 surge = table2array(surge);
50
51 %% Sway
52 filename = '/Users/Martin/OneDrive - NTNU/Master/Sima/Test/
    wave_drift_coeff.txt';
53 delimiter = ' ';
54 startRow = 397;
55 endRow = 718;
56
57 formatSpec = '%f%f%f*s*s*s*s*s%[\n\r]';
58
59 fileID = fopen(filename,'r');
60
61 dataArray = textscan(fileID, formatSpec, endRow-startRow+1,
    'Delimiter', delimiter, 'MultipleDelimsAsOne', true, '
    TextType', 'string', 'HeaderLines', startRow-1, '
    ReturnOnError', false, 'EndOfLine', '\r\n');
62 fclose(fileID);
63 sway = table(dataArray{1:end-1}, 'VariableNames', {'VarName1
    ','VarName2','VarName3'});
64 clearvars filename delimiter startRow endRow formatSpec
    fileID dataArray ans;
65
```

```

66 sway = table2array(sway);
67
68 %%
69 z = zeros(46,1);
70 first_col = [z+1; z+2; z+3; z+4; z+5; z+6; z+7];
71 step = 1:46;
72 step = step';
73 second_col = repmat(step,7,1);
74 dir = [z; z+15; z+30; z+45; z+60; z+75; z+90];
75 theta = 135; % Wave direction
76 Cp = 0.25; % Wave current interaction
77 theta_rel = 0; % Relative angle between waves and
    current
78 Uc = 1.05; % Current vel
79 G = 10; % Do not ask.
80 omega = frequencies(:,2); % 2pi/T
81 omega = repmat(omega,7,1);
82 %T = [30 28 26 24:-.5:3]';
83 %omegacheck = (2*pi)./T;
84 lambda = (2*pi*G)./(omega.^2); % Wave length
85 k = 2*pi./lambda; % Wave number
86 Awp = 1202; % Total water plane area
87 D0 = sqrt(Awp/pi); %
88 Dsum = 4*D0; %
89
90 Bprime = k.*exp(-1.25*(k*D0).^2);
91 B = Bprime * Dsum; %
92
93 format shortE
94 fDx = surge(:,3).*(1+Cp*Uc.*cosd(theta_rel))...
95     + B.*(G*Uc.*cosd(theta_rel)).*cosd(dir);
96 fDy = sway(:,3).*(1+Cp*Uc.*cosd(theta_rel))...
97     + B.*(G*Uc.*cosd(theta_rel)).*sind(dir);
98
99 fDx = [first_col second_col fDx];
100 fDy = [first_col second_col fDy];
101
102 l = 1:322;
103
104 % surge with frequencies
105 % figure(1)
106 % plot(omega(1:46),surge(1:46,3),omega(1:46),fDx(1:46,3))
107 % hold off
108 %
109 % figure(2)
110 % plot(omega(277:322),sway(277:322,3),omega(277:322),fDy
    (277:322,3))

```

```

111
112 deg0 = 1:46;
113 deg45 = 139:184;
114 deg90 = 277:322;
115
116 % surge with periods, 0 deg
117 figure(10)
118 period = 2*pi./omega;
119 plot(period(deg0),surge(deg0,3),period(deg0),fDx(deg0,3))
120 grid on
121 title('Wave drift coefficients surge, 0 deg','FontSize',16)
122 axis([3 25 0 500])
123 ylabel('Force [kN/m^2]')
124 xlabel('Time period [s]')
125 legend({'Potential','With correction'},'Location','northeast
        ')
126 %print('wdc_surge_0', '-depsc')
127
128 % surge with periods, 45 deg
129 figure(11)
130 period = 2*pi./omega;
131 plot(period(deg45),surge(deg45,3),period(deg45),fDx(deg45,3)
        )
132 grid on
133 title('Wave drift coefficients surge, 45 deg','FontSize',16)
134 axis([3 25 0 500])
135 ylabel('Force [kN/m^2]')
136 xlabel('Time period [s]')
137 legend({'Potential','With correction'},'Location','northeast
        ')
138 %print('wdc_surge_45', '-depsc')
139
140 % Sway with periods, 45 deg
141 figure(12)
142 plot(period(deg45),sway(deg45,3),'',period(deg45),fDy(deg45
        ,3))
143 grid on
144 title('Wave drift coefficients sway, 45 deg','FontSize',16)
145 axis([3 25 0 500])
146 ylabel('Force [kN/m^2]')
147 xlabel('Time period [s]')
148 legend({'Potential','With correction'},'Location','northeast
        ')
149 %print('wdc_sway_45', '-depsc')
150
151 % Sway with periods, 90 deg
152 figure(13)

```

```
153 plot(period(deg90),sway(deg90,3),' ',period(deg90),fDy(deg90
    ,3))
154 grid on
155 title('Wave drift coefficients sway, 90 deg','FontSize',16)
156 axis([3 25 0 500])
157 ylabel('Force [kN/m^2]')
158 xlabel('Time period [s]')
159 legend({'Potential','With correction'},'Location','northeast
    ')
160 %print('wdc_sway_90', '-depsc')
161
162
163 %% Write to file, write_to.txt
164
165 % filename = 'write_to_sway.txt' % Change between surge and
    sway
166 % fid = fopen(filename,'w')
167 % fclose(fid)
168 %
169 % fid = fopen(filename,'r+')
170 % fDx = fDx';
171 % fDy = fDy';
172 %
173 % % fprintf(fid,' %i \t %i \t%.9e\n',fDx); %
174 % % fprintf(fid,' %i %i %.9e\n',fDx)
175 %
176 % fprintf(fid,' %i %i %.9e\n',fDy); % change between
    surge and sway
```